Dynamic Modelling and Nonlinear Control of Vortex-Coupled Delta Wing Systems

Mehrdad Pakmehr

A Thesis
in
The Department
of
Mechanical and Industrial Engineering

Presented in Partial Fulfillment of the Requirements
For the Degree of Master of Applied Science at
Concordia University
Montreal, Quebec, Canada

Sep. 15, 2005

Your file Votre référence
ISBN: 0-494-10269-1
Our file Notre référence
ISBN: 0-494-10269-1

Abstract

Dynamic Modelling and Nonlinear Control of Vortex-Coupled Delta Wing Systems

Mehrdad Pakmehr

The first part of this thesis proposes a control-oriented vortex-coupled nonlinear retarded state space representation of free-to-roll motion of a delta wing. Linear, nonlinear and neural network based parameter identification methods have been used to approximate the rolling moment coefficient. Various experimental results validate the proposed model.

In the second part, fast vortex-coupled delta wing roll dynamics with state delay in is controlled using a robust adaptive output feedback control law. The controller has been tested against modelling uncertainties in rolling moment coefficient. The controller is shown to render the delta wing vortex-coupled roll dynamics globally practically stable. Heuristic design process and parameter selection methods have been proposed for easier implementation of this control algorithm. The results of the numerical simulation demonstrate the applicability of this controller for different initial conditions.

The third part proposes a combinatory control strategy combined of a modified state feedback stabilizing controller, as the internal loop, and a robust adaptive sliding tracking controller. The robust adaptive tracking controller utilizes a special gaussian radial basis function network for online estimation of unknown nonlinearity. To show the capability of the proposed combinatory control structure, it has been implemented to the delta wing dynamics to follow a complex reference trajectory. Implementing the

proposed combined control structure enhanced the tracking performance in comparison to the controller without internal loop. Adding two more control inputs enhanced the tracking controller performance. The Heuristic design process and parameter selection methods have been proposed for easier implementation of tracking control and combined control structure.

Acknowledgments

This thesis was carried out in the Control and Information System Laboratory (CIS) at Concordia University, Montreal, Canada. I am grateful for having the opportunity to be a part of CIS research team.

I would like to thank my supervisor, Dr. Brandon Gordon, who not only helped me from the scientific point of view, by showing me the way whenever I was lost and giving me ideas that were the key to solve my problems, but also in teaching me the philosophy of science and control engineering. A supervisor that posses understanding of both the science and its philosophy and who supports his students throughout all the ups and downs of their student life, is rare to find and I am really happy that I had this opportunity to work under his supervision.

I also would like to thank my co-supervisor, Dr. C. A. Rabbath, who supported me during this period by giving me guidelines, ideas and encouragement and helped me to improve my work.

I also would like to acknowledge Dr. X. Z. Huang from NRC-CNRC for providing us with his experimental data.

I would like to thank my parents, to whom I have dedicated this thesis. Without their support this work was impossible. I will always be in debt for their never ending love, support and encouragements.

To My Parents

Table of Contents

List of Figures

Nomenclature

C_l	rolling moment coefficient
f_c	bearing friction coefficient
s_w	wing element area
b_w	wing span
c_w	wing chord
t	time at observation
τ	time at step onset
T^*	release time
T	time period of decay (time delay) in delta wing model
c	a constant in delta wing model equal to π / T^*
X_{vb}	non-dimensional vortex breakdown location
X_s	static term in X_{vb}
u_∞	free stream velocity
I_w	moment of inertia
ρ	air density
q	dynamic air pressure
α	angle of attack
ϕ	roll angle
$\dot{\phi}$	roll rate
λ_0	half apex angle

Γ	circulation or vortex strength
Γ_c	critical circulation
Λ	effective sweep back angle
Λ_e	empirically obtained value of the sweep back angle
σ	body axis inclination
ε_d	damping coefficient in modified delta wing model
ε_{SMA}	constant in first order filters related to SMA input, (6^{th} order delta wing model)
x	vector of the plant states
$\aleph$	vector of vortex breakdown locations: $[X_{vbl}, X_{vbr}]$
I_n	$n \times n$ identity matrix
M^T	transpose of matrix M
M^+	pseudo-inverse of matrix M
$\lambda_{\max}[M](\lambda_{\min}[M])$	denote the maximum (minimum) eigen values of M
$M > 0$	indicates that M is positive definite symmetric (p.d.s.).
$\|x\|$	denote the Euclidian norm of $x \in \Re^n$
$G(\delta) := \{x \in \Re^n \mid \|x\| \le \delta\}$	closed ball in $\Re^n$ of radius δ cantered at $x = 0$
η	length of the retardation in RFDE model
x_t	function in RDFE defined by: $x_t(\theta) = x(t+\theta),\ \theta \in [-\eta, 0]$
$c_1 = c_1([-\eta,0], \Re^n)$	the Banach space of all continuous functions which map the real interval $[-\eta,0]$ into $\Re^n$ equipped with the sup norm

	$\|x_t\| = \sup_{\tau\in[-\eta,0]} \|x(t+\tau)\|$
A_0, B_0, C_0, D_0	system matrices of retarded dynamical model
H_0	matrix in matching condition
$L(.)$	lumped uncertainties and nonlinearities
ς, ϑ	constants in assumption 1, related to the bounds of the uncertainty
Δ, Γ_u	design parameters in equation (32) of Chapter 4
d, e	constant elements in output matrix C_0
P_0, Q_0	positive definite symmetric matrices in Lyapunov equation of Chapter 4
$T(s)$	rational function matrix (Chapter 4)
y	output of the system in RFDE form
μ_0	constant gain in state feedback controller
μ_d	adaptive gain in adaptive output feedback controller
$u_\rho(.)$	output (state) feedback control with constant gain
$u_\rho^d(.)$	output feedback control with adaptive gain
A, M	constants in reference model, for defining its complexity
$s(t)$	error metric in tracking controller
s_Δ	continuous function used in adaptation law
ε	boundary layer widths in sliding controller
λ	positive constant in error metric

$m(t)$	modulation function in tracking controller
Ψ	positive constant in the modulation function representing the width of the transition region between $\overline{A}$ and $\overline{A}_d$ sets
X_0	vector of centers in the modulation function
W	vector of weights in the modulation function
N	number of neurons in RBF network
σ_l, σ_r	radial basis functions (RBF) widths
ξ_l, ξ_r	centers in RBF nodes (input weights)
w_i	output weights in RBF neural network
k_a	constant in adaptive law
k_d	PD control gain
k_{sl}	sliding control gain
$u_{pd}(t)$	PD control input
$u_{sl}(t)$	sliding control input
$u_{ad}(t)$	adaptive control input
ρ_{vbl}, ρ_{vbr}	constant coefficients in the left and right vortex breakdown control inputs

Subscripts

w	wing (i.e. delta wing)
q	quasi-steady term

s	static term
u	unsteady term
vb	vortex breakdown
l	left vortex
r	right vortex

Abbreviations

IAR	institute for aerospace research
DRDC	defence research and development Canada
ISS	internal state space
NIR	nonlinear indicial response
AOA	angle of attack
SISO	single input single output
MIMO	multi input multi output
SMA	shape memory alloy
MEMS	micro electromechanical systems
RBF	radial basis function
NN	neural network
ANN	artificial neural network
UAV	unmanned aerial vehicle
IC	initial condition
RFDE	retarded functional differential equation

1 . Introduction

1.1 Motivation

The main objective of the project, started in Defence Research and Development Canada (DRDC), is to develop novel flight control systems that can be embedded in the structure of a delta wing to provide sufficient control authority through boundary layer and vortex manipulation under subsonic flight conditions. This project aims to increase our understanding of the issues surrounding subsonic active flow control. Another objective of the project is to develop control schemes that take into account the characteristics of the flow and the distributed nature of the micro-actuators and sensors. A part of the second objective is the subject and motivation of the present thesis.

In the context of guidance and control of precision weapons, the new concept of flight control of a weapon system by manipulation of the flow structure is studied in this project with respect to a subsonic delta wing system. This enables the use of the empirical and mathematical flow models available in this project, which are ideal for control system design.

The concept of flight control by manipulation of the flow structure is based on the idea that if forebody vortices can be manipulated to generate lifting forces through perturbation of the flow at the nose of a missile then a means exists to control flight without resorting to conventional canards or fins.

The design of a flight control system using actuation on the flow around a wing is a very challenging problem that requires fundamental research work, numerical simulation validation and, preferably, wind tunnel tests for the proof of concepts. Underlying any active control system design is a model of the flow. The model may have been obtained mathematically, with simplifying assumptions to render the problem tractable, with flight data. Flight control system design strongly depends on wind tunnel testing for a given airframe. Consequently, the dynamics of the missile system are bound to be uncertain. The control scheme, then, not only has to cope with a highly nonlinear, coupled behavior of the boundary layer with changing aerodynamic configurations, but also with uncertain dynamic coefficients. From a control perspective, one approach to tackle this challenging problem is to develop a robust adaptive control scheme that achieves closed-loop stability through on-line identification and scheduling. This can be achieved by judicious selection of the 1) flight envelope where the missile's aerodynamic behavior is, to some extent, predictable, 2) trim points, and 3) actuator and sensor dynamics. Computational speed of the algorithms will be of prime importance given the real-time control requirements of the missile.

1.2 Research Objectives

The objective of this thesis is three-fold: In the first part of the thesis, a control-oriented dynamic model of a high performance 65-degree delta wing is proposed. This model can be directly implemented for nonlinear control purposes of vortex-coupled delta wing dynamics subject to delay. The proposed model relies on the nonlinear indicial response method, in conjunction with internal state-space (NIRISS) representation. This model proposes a control-oriented vortex-based nonlinear state space form of the roll

motion of a delta wing in high angle of attack flight condition. The relationships among the vortex breakdown location, rolling moment coefficient and roll angle is developed using a state-space model. Linear, nonlinear and neural network based parameter identification methods are applied to approximate the uncertainties of the nonlinear dynamic model, such as rolling moment coefficient. Experimental results are utilized to verify the model.

In the second part, we investigate the applicability of the adaptive stabilizing control approach presented in [66], for 4^{th} order delta wing vortex-coupled roll dynamics with state delay as the first application of this method in delta wing vortex-coupled system control. We will test the controller against modelling uncertainties in rolling moment coefficient and also left and right vortex breakdown locations as time varying uncertainties. The parameter of this adaptive controller is updated robustly when the bounds of these uncertainties are unknown. The heuristic design process and parameter selection methods are proposed for easier implementation of this control algorithm. It should be noted that we are applying this control scheme to a fast and high performance delta wing dynamics in high angle of attack (AOA) and near-stall flight condition.

In the third part, we propose a combinatory control structure to control the available high performance delta wing retarded dynamic system. The controller is a combination of robust state feedback controller as the internal loop of the combinatory controller and a sliding adaptive tracking controller which uses a special gaussian RBF neural network as the online estimator of the unknown nonlinearity. This controller is applied to the vortex-coupled roll dynamics of the delta wing to track a complex reference trajectory. This complex trajectory is chosen to show the ability of the proposed

combinatory controller to control the delta wing for complicated manoeuvres since delta wings are high performance aerial vehicles which are flying in high angle of attack flight condition with subsonic or supersonic speeds.

The combinatory control input also is applied to 4^{th} order delta wing vortex-coupled roll dynamics with state delay, and 6^{th} order delta wing vortex-coupled roll dynamics with state delay and SMA micro-actuator dynamics, to check the effect of perturbations as inputs to the vortex breakdown dynamics. The heuristic design process and parameter selection methods are proposed for easier implementation of the controllers with and without internal loop.

1.3 Literature Review

A non-linear indicial response (NIR) method, in conjunction with internal state-space (ISS) representation (NIRISS) has been used in [10], [11] to describe the vortex breakdown location over a delta wing. It has been found that for a delta wing, its leading edge primary vortex behaviour has a dominant effect on its air loads [10], [11]. Consequently, the related air loads applied to the surface of the delta wing and the delta wing attitude can be calculated in terms of the primary vortex breakdown location. In [10], [11], a mathematical model for the case of free-to-roll motion has been presented.

Several methods can be found in the literature for the simulation and modelling of vortex breakdown over delta wing and high performance aircraft dynamics and also vortical flows. These methods include computational, neural-network and mathematical methods. Several methods can also be found for the modelling of nonlinear flight dynamics and system identification of nonlinear systems. In [12], a parabolic distribution for the chord wise axial circulation distribution over slender delta wing has been

proposed. Leading-edge vortex breakdown locations have been predicted on the basis of a critical value of the circulation. In [13], a method has been proposed to predict the normal force coefficient acting on a delta wing under static or dynamic conditions. In [14], the three dimensional, Reynolds-averaged, Navier-Stokes (RANS) equations have been used to numerically simulate nonsteady vertical flow about a 65-deg sweep delta wing at 30-deg angle of attack. In [15], a conceptual model of the breakdown of a delta-wing vortex as a symmetry-breaking subcritical bifurcation from an asymmetric unburst vortex to a helically symmetric translating spiral burst form has been presented.

In [16], a specific neural network based model for the identification of non-linear systems has been proposed. This neural network structure is able to identify a non-linear state space model of the plant. Ref [17] investigates the identification of nonlinear systems by neural networks. As the identification methods, Feedforward Neural Networks (FNN) Radial Basis Function Neural Networks (RBFNN) Runge-Kutta Neural Networks (RKNN) and Adaptive Neuro-Fuzzy Inference Systems (ANFIS) based identification mechanisms have been studied. In [18], wavelet-based neural network (WNN) has been introduced for adaptive nonlinear system identification. Ref [19] presents a stable, on-line identification scheme for multivariable nonlinear dynamic system. Growing Gaussian Radial Basis Function (GRBF) network with all its parameters being adaptable has been used to approximate an unknown nonlinear system. In [20], the suitability of non-linear system identification modelling air vehicles of complex configuration has been argued. The approach has been demonstrated through a laboratory test rig. Extensive time and frequency-domain model-validation tests have been employed in order to instil confidence in the estimated model.

One of the methods which have been used for modelling the uncertain aerodynamics and nonlinear flight dynamics of high performance aircraft and delta wings is nonlinear indicial response (NIR) method initiated by Tobak and his colleagues [35]. This approach represents aerodynamic responses, such as force, moment, etc., due to an arbitrary motion input as a summation of nonlinear responses to a series of "step" motions leading up to step onset. Three new important concepts were introduced in this approach: (1) a nonlinear indicial response functional, (2) a generalized superposition integral and (3) under conditions where Frechet differentiability is lost, i.e. at a critical state, a splitting of the integral plus a transient term is proposed [10].

In [21]-[28], the nonlinear indicial response (NIR) method has been applied for modelling the uncertain aerodynamics and nonlinear flight dynamics in different situations. Ref. [29] demonstrates the use of a time-domain Volterra kernel identification method which uses physically realizable inputs, and minimizes or eliminates the need for analytical assumptions.

In [30], the state-space representation of aerodynamic forces and moments for unsteady aircraft motion has been proposed. In [31], simplification of the equations of motion of an aircraft, in a way that incorporates aeroelastic effects, to facilitate the development of reliable time-domain dynamic models, has been accomplished. In [32], the state-space representation of an aerodynamic vortex lattice model has been considered from a classical and system identification perspective. Ref. [33] presents an alternative to traditional single frequency forced-oscillation testing by utilizing Schroeder sweeps to efficiently obtain the frequency response of the unsteady aerodynamic model. In [34], a short theoretical study of aircraft aerodynamic model equations with unsteady

effects has been presented. The aerodynamic forces and moments have been expressed in terms of indicial functions or internal state variables. In [35], basic concepts involved in the mathematical modelling of the aerodynamic response of an aircraft to arbitrary manoeuvres have been reviewed. The original formulation of an aerodynamic response in terms of nonlinear functionals has been shown to be compatible with a derivation based on the use of nonlinear functional expansions. In [36], the mathematical modelling of the aerodynamic response of an aircraft to arbitrary manoeuvres has been reviewed. Bryan's original formulation, linear aerodynamic indicial functions, and superposition have been considered. Ref. [37] is a review of aerodynamic mathematical modelling for aircraft motions at high angles of attack. The mathematical model serves to define a set of characteristic motions from whose known aerodynamic responses the aerodynamic response to an arbitrary high angle-of-attack flight manoeuvre can be predicted. In [38], dynamic wind-tunnel test results of a 65-degree swept delta wing has been reviewed and examined in light of the NIR theory, the existence of critical states with respect to roll angle has been reported. In [39], critical-state transients for a rolling 65-degree delta wing have been investigated.

Most of these modelling papers and methods are presented to build mathematical models out of experimental data, which are not usable directly for control purposes.

Controlling delta wing, as a high performance missile or a UAV, has been investigated recently. Several theoretical and experimental studies have been conducted. Most of these researches involve study of wing rock phenomenon, wing flutter and limit cycles. In Ref. [48], a research on the active control of aeroelastic structures has been done which has been resulted in a new model for the control of delta wing flutter. Control

of wing-rock motion has been investigated extensively in the literature [49-59]. In Ref. [49], based on the variable structure model reference adaptive control theory, a new control system for the control of wing-rock motion of slender delta wings, using only roll angle measurement, has been designed. In Ref. [50], adaptive control of feedback linearizable systems is applied to designing the control of wing rock motion with the extension of the technique to include tracking. In Ref. [51], based on a nonlinear model, an adaptive control law for wing-rock control has been derived. In Ref. [52], control of the nonlinear wing rock motion of slender delta wings using a nonlinear H_∞ robust method has been presented. In Ref. [53], a theoretical analysis has been conducted to determine the optimal control input for wing-rock suppression through a Hamiltonian formulation. In Ref. [54], a model-error control synthesis approach has been used in conjunction with a variable structure controller to suppress the wing-rock motion of a slender delta wing. In Ref. [55], fuzzy logic-based roll controllers have been designed to control wing-rock motion of a delta wing. In Ref. [56], a variable universe fuzzy control design approach is utilized to improve both tracking precision and robustness of fuzzy PD control for aircraft wing rock control. In Ref. [57], an RNN adaptive control system has been developed for a wing-rock motion system. In Ref. [58], dynamic recurrent RBF network control methodology has been proposed to control the wing rock motion. In the proposed neural control structure, the recurrent dynamic RBF network performs identification process in order to approximate the unknown nonlinearities of the physical system. In Ref. [59], control of the non-linear wing rock motion of slender delta wing configurations using a new non-linear suboptimal control technique, is discussed.

In Ref. [60] a robust adaptive tracking control strategy has been proposed and applied for vortex-coupled delta wing roll dynamics, without delay, with parameter uncertainty in the rolling moment coefficient. The robust adaptive tracking neuro-controller employs a network of Gaussian Radial Basis Functions (RBF) to adaptively compensate for the rolling moment coefficient. In Ref. [70], an on-line learning neuro-control scheme that incorporates a growing radial basis function network (GRBFN) is proposed for a nonlinear aircraft controller design. Ref. [71] is concerned with the development of an adaptive control scheme applicable to strict feedback plants with time-varying structure belonging to a class of feedback linearizable plants. In Ref. [72], an indirect adaptive control system approach is proposed and demonstrated via nonlinear six-degree-of-freedom simulations of a tailless fighter aircraft. Ref. [73] presents a direct adaptive reconfigurable flight control approach and demonstrates its effectiveness via an application to an advanced tailless fighter aircraft. An on-line neural network has been used to adaptively regulate the error between the desired response model and the actual vehicle response. Ref. [74] illustrates the application of an adaptive flight control and guidance architecture to various unmanned aerial vehicles and weapons delivery platforms.

The delay effect on the stability of systems with delays in the state and/or input, is a problem of recurring interest since the presence of delay may induce complex behaviours (oscillations, instability) for the (closed-loop) schemes. Furthermore, a chaotic behaviour may appear if the delayed state is a nonlinear function [61]. The study of time-delay systems has received considerable attention over the past years. In the control theory literature, the problem of control and stabilization of uncertain nonlinear

time-delay systems has been dealt via a number of different techniques, mostly sliding and adaptive control approaches. In Ref. [62], the output tracking control problem for a class of non-linear time delay systems with some unknown constant parameters is addressed. Such a problem is solved in the case that the non-linear time delay system has full delay relative degree and stable internal dynamics. Ref. [63], investigates the issue of the internal stability of nonlinear delay systems controlled with a feedback law that performs exact input–output, linearization and delay cancellation. Ref. [64], considers the sliding mode control of uncertain systems with single or multiple, constant or time-varying state-delays, submitted to additive perturbations. In Ref. [65] a control strategy combined of a modified output feedback stabilizing controller and a robust adaptive tracking controller, which employs a network of Gaussian Radial Basis Functions (RBF) to adaptively compensate for the rolling moment coefficient, has been presented, and applied to the vortex-coupled roll dynamics of delta wing subject to state delay and SMA actuator dynamics.

Any of the papers presented in this review does not present a control strategy to control the retarded delta wing dynamics to follow a complex reference trajectory. Robust adaptive tracking control of retarded systems with unknown time-varying nonlinearity is still an unsolved problem in adaptive control field.

1.4 Thesis Contribution and the Outline of the Thesis

We first review some background material including delta wing dynamics and vortex breakdown phenomena, adaptive neural controllers, delay systems, retarded dynamical systems and also practical stability notion in *Chapter two*. In *Chapter three*, a control-oriented dynamic model of a high performance 65-degree delta wing is proposed

which can be directly implemented for nonlinear control purposes of vortex-coupled delta wing dynamics subject to delay. The relationships among the vortex breakdown location, rolling moment coefficient and roll angle are developed using a nonlinear state-space model. Linear, nonlinear and neural network based parameter identification methods are applied to approximate the rolling moment coefficient as unknown nonlinearity. Experimental results from NRC-CNRC are utilized to verify the model. In *Chapter four*, the applicability of the adaptive stabilizing control approach presented in [66], to the 4^{th} order delta wing vortex-coupled roll dynamics with state delay is investigated, as the first application of this method in delta wing vortex-coupled system control. The controller is tested against modelling uncertainties in rolling moment coefficient and also left and right vortex breakdown locations as time varying uncertainties. The parameter of this adaptive controller is updated robustly when the bounds of these uncertainties are unknown. The heuristic design process and parameter selection methods are proposed for easier implementation of this control algorithm. In *Chapter five*, a combinatory control structure is proposed to control the available high performance delta wing retarded dynamic system. The controller is a combination of a robust state feedback controller as the internal loop of the combinatory controller and a sliding adaptive tracking controller which uses a special gaussian RBF neural network, developed for the delta wing vortex-coupled dynamics, as the online estimator of the unknown nonlinearity (C_l). This controller is applied to the vortex-coupled roll dynamics of the delta wing to track a complex reference trajectory. The combinatory control input is also applied to 4^{th} order delta wing vortex-coupled roll dynamics with state delay, and 6^{th} order delta wing vortex-coupled roll dynamics with state delay and SMA micro-actuator dynamics, to check the

effect of perturbations as inputs to the vortex breakdown dynamics. The heuristic design process and parameter selection methods are proposed for easier implementation of the controllers with and without internal loop. In *Chapter six*, conclusions and future directions for the research are presented. In *Appendix A*, we present the definitions and the properties which are the fundamentals for the controller proposed in Chapter 4. In *Appendix B*, we present theories and proofs of the theories which are presented and utilized in Chapter 4.

2 . Background Material

2.1 A Review on Delta Wing Dynamics

2.1.1 What is Delta Wing?

A *delta wing* is a wing whose shape when viewed from above looks like a triangle, often with its tip cut off. It sweeps sharply back from the fuselage with the angle between the leading edge (the front) of the wing often as high as 60 degrees and the angle between the fuselage and the trailing edge of the wing at around 90 degrees. Often delta-wing airplanes lack horizontal stabilizers. Delta wings actually perform poorly at low speeds and often are *unstable* (i.e., they do not stay in level flight on their own). Their primary advantage is efficiency in high-speed flight [1].

2.1.2 Basic Aerodynamics of Delta Wings

Delta wings (Deltas) are symmetrical triangular wings designed to fly at subsonic or supersonic speeds. At supersonic speeds the leading-edge can be subsonic, sonic or supersonic, depending on the relation between sweep angle and speed.

Leading edges are generally linear, although there are cases of more complex geometries, such as the ogive delta (Concorde SST), the gothic delta, the cranked delta

(Lockheed CL-823), the double delta (SAAB Viggen), delta plus canards (North American XB-70 and others).

Almost all delta wings fall into the category of low aspect-ratio wings. Their aspect-ratio is defined by $AR = 4/tan(D)$, where D is the leading edge sweep angle (this lead to AR less than 3 in most cases; about 1.8 in the case of Concorde). Wing thickness is generally small.

The problem is to find the aerodynamic properties of the wing (C_L, C_d, C_m, C_p distribution, etc.), along with the lateral and longitudinal stability characteristics of the wings at different operation points.

The technical literature on deltas is huge, and it is safe to say that all speeds and sweep angles have been investigated (experimental, theoretical and computational research).

2.1.2.1 Delta Wing in Subsonic Flow

Flows past delta wings are severely compounded by the leading edge separation, by the roll-up structure of the concentrated vortices, and by the lateral and longitudinal instability that is consequent to large sweeps, high-angle of attack, and sharp maneuvers. Although the aerodynamics of the delta wing is nonlinear, most of the research has relied for a long time on linearized small perturbation theory (shortly reviewed below). Computational methods (ex. vortex lattice methods, panel codes) have proved tremendously effective at low speeds and unsteady flows.

2.1.2.1.1 Linearized Theory

Linearized theory for the slender body with small angle of attack leads to a very simple conclusion: lift is produced in the conical flow created by the streamwise variation

of span b(x). There is one singularity at the apex of the delta, where the theoretical pressure would be infinite.

The expression for the lift coefficient is $C_L = 2\alpha$, that is correct only for very low aspect-ratios (AR=1). The corresponding induced drag coefficient is $C_D = C_L\alpha/2$, that is just half the value that is expected at angle of attack α. The center of pressure is found at 2/3 chord from the pointed leading-edge, where the pressure is also singular.

2.1.2.1.2 Fuselage Effects

The effect of a fuselage can also be estimated by a more general formulation that gives a lift coefficient in the wing-body configuration is lower that the wing-alone. Lifting surface theory (for ex., vortex lattice method) is a better approach to the prediction of the basic coefficients. There are also methods for arrowhead wings and wings in yawed flow.

2.1.2.2 Delta Wings in Supersonic Flow

Delta wings are appropriate plan forms to fly at supersonic and hypersonic speeds, therefore there has been a long time interest in investigating the effects of high Mach numbers. The principle of independence allows investigating separately wings with subsonic and supersonic leading edges (e.g. for which the normal Mach number is below or above the speed of sound).

2.1.2.2.1 Separation Characteristics

In general, wings with subsonic leading edges are characterized by leading edge separation; wings with supersonic leading edge are characterized a Prandtl-Meyer expansion. The main parameters of the wing problem are sweep, free stream Mach

number, angle of attack and wing thickness. The effects of all these parameters can be collapsed in one single plane alfan-Machn, where the occurrence of subsonic or supersonic flow can be diagnosed as function of the parameters.

2.1.2.2.2 Delta Wing with Subsonic Leading-Edge

The wing is inside the Mach cone if the sweep angle is greater than the Mach angle, thus yielding leading-edges that are fully subsonic (Figure 1). Linearized theory leads again to simplified expressions for the main aerodynamic characteristics, which are quite powerful to describe the operation of the wing.

The lift coefficient depends on the aspect-ratio, according to en expression that is fairly approximate for incidences less than 5 degrees. According to the theory, the strong leading edge suction gives rise to a *leading edge thrust* that decreases the amount of drag (in practice only a small amount of this suction can be realized.)

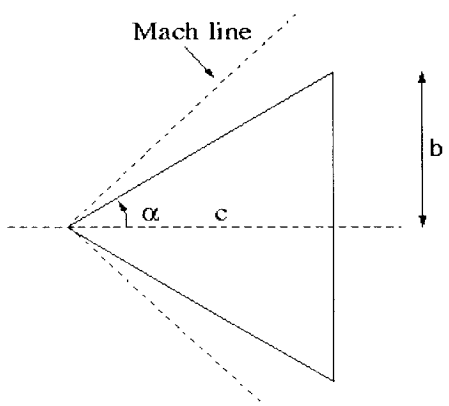

Figure 1. Delta wing with subsonic leading-edge [2]

2.1.2.2.3 Delta Wing with Supersonic Leading-Edge

The leading-edge is inside the Mach cone, by virtue of the comparatively larger sweep angle (Figure 2), in such a case there is no interaction of flows between upper and lower surface.

The pressure jump at any given point on the wind surface has a definite expression, which is constant along lines through the wing vertex (*conical flow*). By integration of the pressure jump one finds that the lift coefficient is independent from the sweep angle, and the lift-curve slope is also independent from the angle of attack for as long as the leading edge is supersonic.

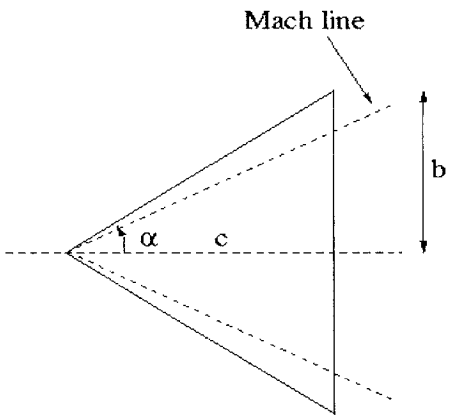

Figure 2. Delta wing with supersonic leading-edge [2]

2.1.2.3 Flow Separation on Highly Swept Wings

Real cases of flow past slender delta wings (wings of small aspect-ratios) are almost certainly separated, and to a great extent. Separation starts from the leading-edge and produces a series of vortical regions that have a conical shape growing stream wise. The angle of attack at which these vortices appear depends on the slenderness.

Separation is at the leading-edge when the leading edge is sharp, and leads to performances largely independent from the Reynolds number. The presence of the leading-edge vortices is the cause of a number of phenomena:

- The lift coefficient is larger than that predicted with linearized theory. This is due to the *suction* effect of the separation vortices. The difference between the linear value of the lift and its actual value is called *vortex lift*.

- The leading-edge vortices induce a field of *low pressure* on the suction side of the wing. The increased suction is a reason for increased lift (point above).
- Stall occurs at a large angle of attack, because of the vortex instability, leading to vortex burst. When the vortex core bursts the suction effect disappears. As vortex burst far behind the trailing edge, the burst has little or no effect; vortex burst on the wing itself will reduce the vortex lift.
- The vortex pattern behind the delta wing depends on the slenderness, because slenderness, together with angle of attack, is what decides the vortex burst.
- Vortex asymmetry appears on very slender wings at lower and lower angles of attack, because the vortex finds less physical limits for development, therefore becoming soon unstable.

Flow separation characteristics depend on speed (Mach number), wing sweep, angle of attack and wing thickness.

Wings with subsonic leading edge are dominated by leading edge separation. Secondary separation appears at moderate to high angles of attack (Figure 3). Wings with supersonic leading edges are characterized by a Prandtl-Meyer expansion behind the bow shock and by an attached leading edge flow (Figure 4).

For more information about delta wing aerodynamics, refer to [2].

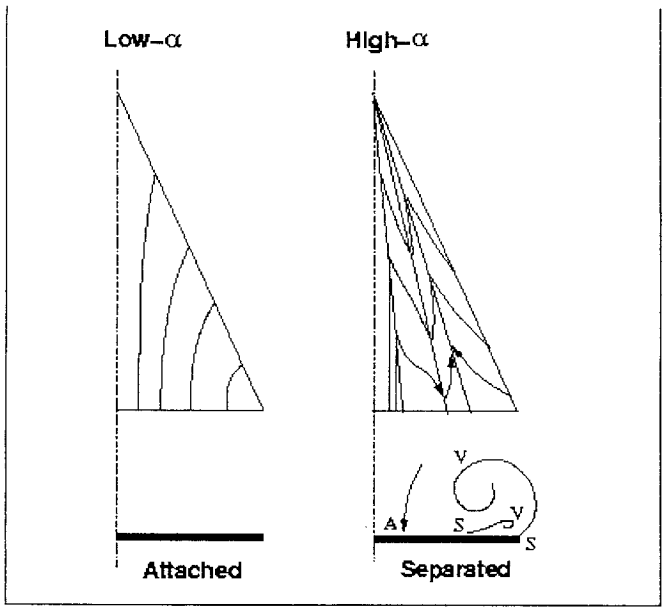

Figure 3. Flow separation on delta wing with *subsonic* leading edge. A = attachment; S = separation; V = vortex. , [2]

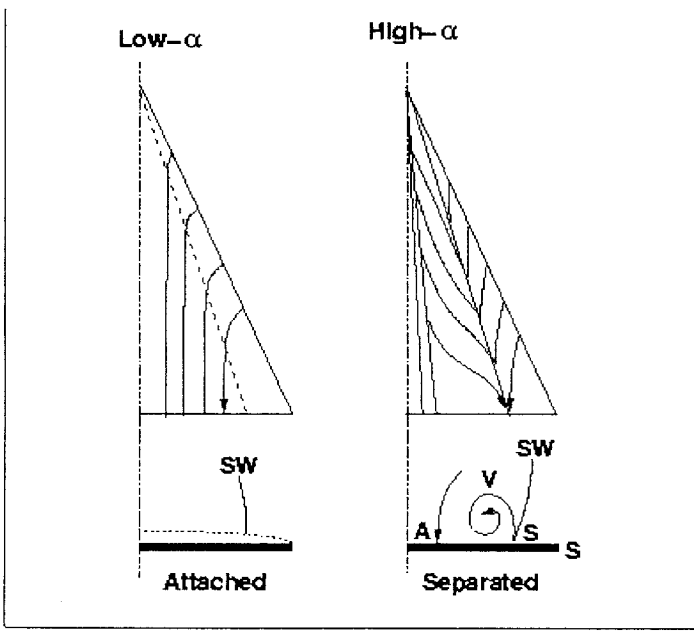

Figure 4. Flow separation on delta wing with *supersonic* leading edge. SW = shock wave, [2]

2.1.3 High Angle of Attack Aerodynamics

2.1.3.1 Airfoil Flows

All airfoils stall past a critical angle of attack (angle corresponding to the maximum lift). The (static) stall characteristics depend on the design (thickness, leading edge radius, camber, trailing edge angle) and conditions of operation (ground, out of ground, etc.). Figure 5, shows representation of stall of airfoils.

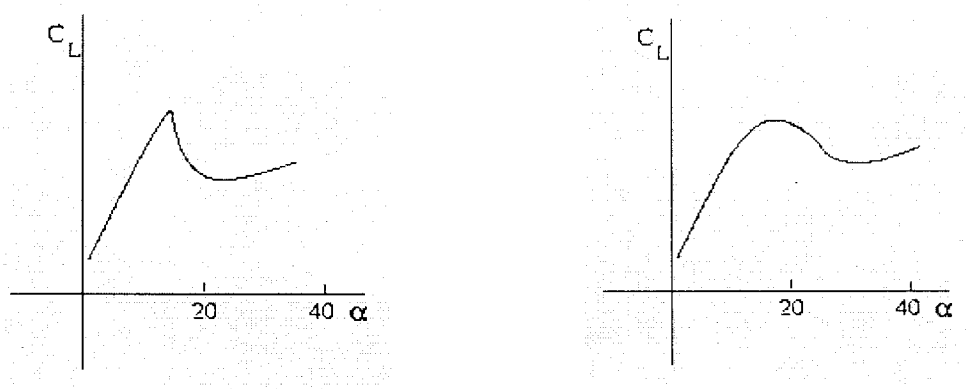

Figure 5. Static stall on airfoil [2]

2.1.3.2 Wing Rock

Wing rock is a rolling oscillation due to loss of damping at high angles of attack. This often leads to loss of control. Two particularly important cases are the highly swept wing and the slender body wing rock (for ex. forebody-delta wing).

2.1.3.3 Breakdown of Symmetric Flow

One of the features of high angle of attack flows is the appearance of asymmetrical patters and thus non symmetrical loads (rolling moment, yawing moment, side force, etc.).

Figure 6 shows how the breakdown in the symmetry flow on a wing-body

combination can be tackled. By using a spiral trip on the fuselage both yaw and rolling moments can be greatly improved at high angles of attack.

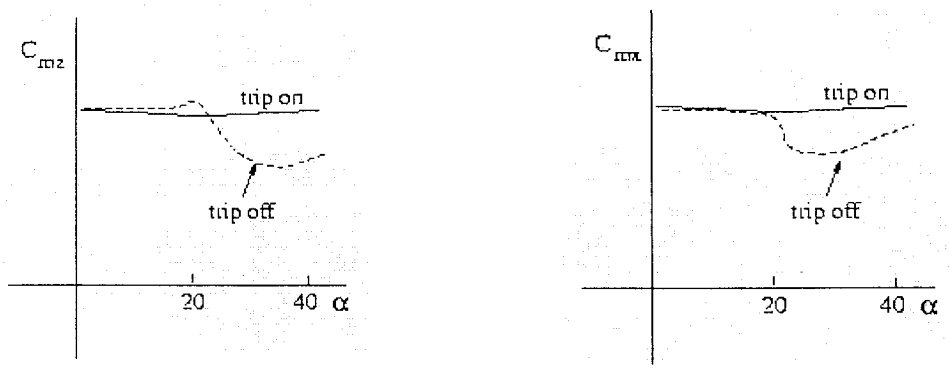

Figure 6. Yawing and rolling moment on wing-body combination [2].

An extreme case of high angle of attack aerodynamics is the atmospheric entry of the Space Shuttle (about 40 deg at hypersonic speeds M > 20).

2.1.3.4 Separation Characteristics

High-alpha effects are particularly pronounced on delta wings, on which they have been studied for a wide range of aspect-ratio, Reynolds and Mach numbers. Three cases are of special interest: leading edge separation; separation with shock; shock-induced separation.

For more information about high angle of attack aerodynamics, refer to [3].

2.1.4 Vortex Shifting Concept using MEMS

The concept of using small actuators (micro-millimeter scale) to provide large control forces for a large-scale system (meters scale) is of great interest in recent decades.

This was theorized by using fluid separation phenomenon, vortex symmetry, and vortex dynamics on a delta wing aircraft [4].

It has been known that the ensuing leading edge vortex flow is extremely sensitive at the separation location of the free shear layer on a swept aerodynamic planform. Sharp leading edges have a natural boundary condition of separation at the sharp edges. For round leading edges, the genesis location of the free shear layer is a complex curved line that runs along the leading edge from the apex to the wing tip. Changing the surface boundary condition in quasi-steady state (i.e., expanding surface curvature) near the separation line can cause a global change to the developing vortex. In general, delta wing leading edges create symmetric pairs of primary and secondary vortices [4].

The controlled separation of the thin boundary layer at the synthesis location of the vortex pairs on a delta wing aircraft will allow the manipulation of pressure field about the aircraft. By using micro actuators along the round leading edges to create vortex shifts, a resulting loading change about the aircraft would occur. Although at first glance this appears to be the mere adoption of vortex flap with MEMS, however, the difference lies in the fact that the vortex being controlled is not "trapped" at the leading edge. The round leading edge allows the manipulation of the vortex pairs on the entire leeward side of the aerodynamic surfaces.

The length scale of the micro actuators will need to be compatible with the boundary layer thickness. It was speculated from the beginning that the boundary thickness would be the key to the flap/vortex interaction. The boundary thickness was estimated to be between 100s of microns to 1-2 millimeter, depending on the length scale

of the aircraft and the Reynolds number. Figure 7, shows that pairs of vortex system increase size and strength with increasing AOA [4].

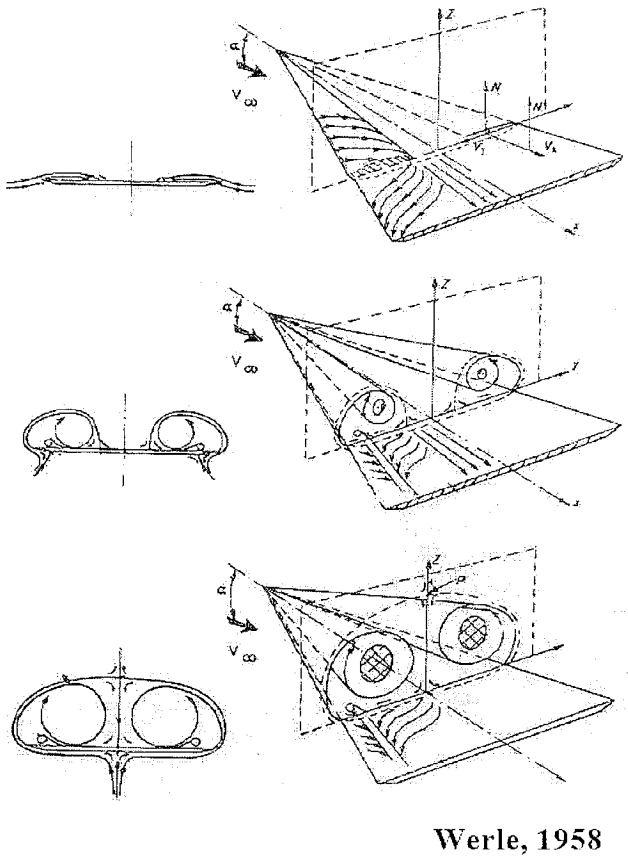

Figure 7. Typical evolution of primary vortex pairs with increasing AOA on delta wings [4].

Thus, it was hypothesized that the vortex shifting mechanisms can be used to replace or supplement conventional surfaces at high angles of attack where the latter became ineffective due to trailing edge separation of the potential flow.

2.2 A Review of Nonlinear Adaptive Neural Control Scheme

Over the last four decades, adaptive control has evolved as a powerful methodology for designing feedback controllers of nonlinear systems. However, most of these studies assume that the system nonlinearities are known *a priori,* which is generally

not applicable in the real world. To overcome this drawback, from 1990s, there has been a tremendous amount of activity in applying Neural Networks (NNs) for adaptive control. With their ability to approximate nonlinear functions, neuro-controllers can fulfill the control objectives by canceling or learning the unknown nonlinearities of the systems to be controlled. NNs are especially suitable for the adaptive flight control applications where the system dynamics are dominated by the unknown nonlinearities. Moreover, among different choices of network structures, Radial Basis Function Network (RBFN) has shown its potential for on-line identification and control, and hence arouses much interest [5].

2.2.1 Adaptive Control of Nonlinear Systems Using Neural Networks

Adaptive control was motivated by the problem of designing autopilots for aircraft operating at a wide range of speeds and altitudes in 1950s. However, it was only in the 1960s, when Lyapunov's stability theory was firmly established, that the convergence of the proposed adaptive control schemes could be mathematically proven. Following this, in 1970s, complete proofs of stability for several adaptive schemes appeared. Further, in the late 1970s and early 1980s, state space based proofs of stability for model reference adaptive schemes appeared in the works of Narendra, Lin, Valavani and Morse. Surveys of the applications of adaptive control are given in books edited by Narendra and Monopoli and Unbehauen. Those early results on stability dealt with the ideal case of exact plant model (no modelling errors). Since then, a considerable amount of adaptive control research has been devoted to the development of robust adaptive control systems, where closed-loop stability properties are retained in the presence of not

only a large parametric uncertainty, but also of modelling errors. In the 1970s and 1980s, there also has been a great deal of interest in the use of state feedback to exactly linearize the input-output behavior of nonlinear control systems. The theory of linearization by exact feedback was developed through the efforts of several researchers, such as Singh and Rugh, Isidori, Krener, Gori-Giorgi and Monaco. All these efforts in research and development has given substantial innovations and the fundamental issues of adaptive control for linear systems, such as selection of controller structures, development of adaptive law, etc., have been well established. These results have been reported in several books dealing with the design and analysis of adaptive systems [5].

Although it is known that most practical systems are inherently nonlinear, adaptive control of such systems was not seriously considered until the advances in geometric nonlinear systems theory, such as feedback linearization, were made. With these achievements, in the last ten years, adaptive control has evolved as a rigorous control strategy for a reasonably large class of nonlinear systems. Many remarkable results and new design tools, such as backstepping procedure, feedback linearization techniques, have appeared in both Lyapunov and estimation based schemes. Some of these methods are briefly reviewed in [5].

2.2.2 An Overview of Neural Networks in Adaptive Control

Artificial Neural Networks (ANNs) have emerged over the last three decades as one of the most vigorous and exciting fields of modem science, because of their powerful ability to learn, to generalize, and to adapt to unknown nonlinearities. In the last decade,

almost independent from the adaptive nonlinear control research, a tremendous amount of activity in neurocontrol approach has been carried out.

Generally, for adaptive control purposes neural networks are used as approximation models of unknown nonlinearities. The input/output response of neural network models is modified by adjusting the values of its parameters. Although it is true that polynomials, trigonometric series, splines, and orthogonal functions can also be used as function approximator, neural networks have been found to be particularly useful for controlling highly uncertain, nonlinear, and complex systems.

Neural control strategies can be broadly classified into off-line and on-line schemes based on how the parameters of the network are tuned. When the neural controller operates in an on-line mode, it has no *a priori* knowledge of the system to be controlled, and the parameters of the network are updated during control system operation, preferably in real-time. However, in the off-line control, the network's parameters are determined from the known training pairs, and then those parameters are fixed for control purposes.

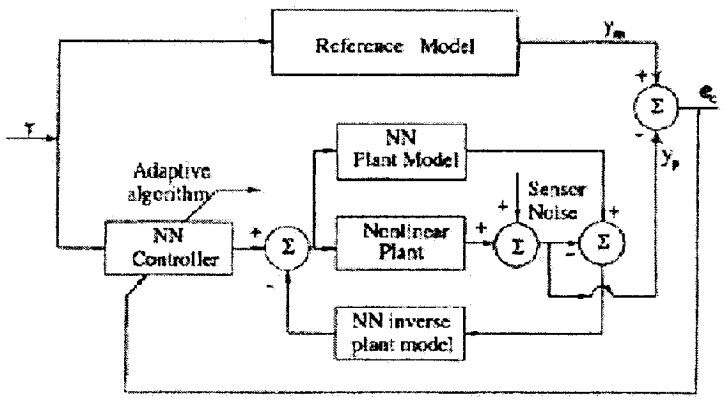

Figure 8. Adaptive inverse control system [5]

Though the role of neural networks in the on-line and/or off-line learning are to learn some underlying functions related to the system, the methodologies differ by the way in which they are utilized. They range from learning the inverse dynamics of the system without any guarantee of stability, the feedback linearization strategy to the direct adaptive control that guarantees stability of the overall systems. Figure 8, shows a schematic of adaptive inverse control system. In [6], Agarwal has given a comprehensive classification of the neural-network-based control schemes proposed in the literature. In Agarwal's work, the NN based control schemes are classified into two main categories; one is called "neural network only as an aid", where the neural networks are used to relieve the complex diagnostics, tedious modelling, unwieldy tuning, or excessive computational effort in conventional control schemes. The other class comprises schemes where a neural network is used as a controller and is updated using available input signals. The data pairs for adjusting the network are obtained either from the real plant, or using a model simulation. It can be seen from the literature that neural network based adaptive control covers a very broad area, and in this section we introduce some of the popular control strategies [5].

2.2.2.1 Neural Flight Control Systems Advantages

The implementation of on-line neurocontrollers in the autopilot control laws for high performance aircraft has the following advantages: first, it can avoid the pre-computation, storing, and interpolation between thousands of feedback gains of a typical flight control system. Second, it has the ability to compensate for nonlinearities and model uncertainties. Last, through on-line learning ability, the designed controller avoids

the time-consuming gain recalculation following any modification to the aircraft or its control system during the operative life [5].

2.3 A Review on Time Delay Systems, Stability and Control

Time-delay systems (TDS) are also called systems with aftereffect or dead-time, hereditary systems, equations with deviating argument or differential-difference equations. They belong to the class of functional differential equations (FDEs) which are infinite dimensional, as opposed to ordinary differential equations (ODEs). Four points may give a possible explanation of motivation for a continuous interest and development in TDS:

(1) Aftereffect is an applied problem: it is well known that, together with the increasing expectations of dynamic performances, engineers need their models to behave more like the real process. Many processes include aftereffect phenomena in their inner dynamics.

(2) Delay systems are still resistant to many "classical controllers"; one could think that the simplest approach would consist in replacing them by some finite-dimensional approximations. Unfortunately, ignoring effects which are adequately represented by FDEs is not a general alternative: in the best situation (constant and known delays), it leads to the same degree of complexity in the control design. In worst cases (time-varying delays, for instance), it is potentially disastrous in terms of stability and oscillations.

(3) Delay properties are also surprising since several studies have shown that voluntary introduction of delays can also benefit the control (for instance, for ODEs: damping and stabilization, delayed resonators, time-delay controllers and observers,

nonlinear limit cycle control, and deadbeat control; for FDEs: finite-spectrum assignment [7].

(4) In spite of their complexity, TDS however often appear as simple infinite-dimensional models in the very complex area of partial differential equations (PDE):

Delays are known to have complex effects on stability. To deal with stability problem of TDS, there are four general methods which have been widely used: 1- The characteristic roots of retarded and neutral linear FDEs; 2- The Krasovskii-type approach; 3- The Razumikhin-type approach, control Lyapunov functions and input-to-state stability; 4- Input–output stability [7].

During the last 10 years, many studies were devoted to the control of TDS. These control methods can be categorized as follows: 1- Optimal control and the Bellman equation; 2- Sliding mode control; 3- Time delay control; 4- Adaptive control.

2.4 Retarded Functional Differential Equations

A retarded functional differential equation (RDTE) describes a system where the rate of change of state is determined by the present and past states of the system.

Suppose that $h > 0$ is a given number with understanding that h may be $+\infty$, and $\Re^n$ is an n-dimensional linear vectorspace over the reals with norm $|.|$. Let c_1 denote the vector space of continuous and bounded functions mapping the interval $[-h,0]$ into $\Re^n$. With the norm $\|.\|$ given by

$$\|\Phi\| = \sup_{\theta\in[-h,0]}|\Phi(\theta)|, \quad \Phi \in c_1 \tag{2-1}$$

c_1 is a Banach space.

Definition: The relation

$$\dot{x} = f(t, x_t) \tag{2-2}$$

is called RFDE where $f : \Re \times c_1 \to \Re^n$ is a given function, the overdot represents the right hand derivative with respect to t and the function $x_t \in c_1$ is defined by

$$x_t(\theta) = x(t+\theta),\ \theta \in [-h, 0] \tag{2-3}$$

Definition: The function $x : \Re \to \Re^n$ is a solution of the RFDE (2-2) with the initial condition

$$x_\sigma = \Phi;\ \sigma \in \Re,\ \Phi \in c_1 \tag{2-4}$$

if there exist a scalar $\delta > 0$ such that $x_t \in c_1$ and x satisfies (2-2) and (2-4) for all $t \in [\sigma, \sigma + \delta]$.

For more information about RFDE refer to [8].

2.5 Practical Stability Notion

Complete stability is a more desirable feature in applications than asymptotic stability. Sometimes even instability may be good enough. Since the desired state of a system may be mathematically unstable but the system may oscillate sufficiently near this state so that its performance is considered acceptable. For example, an aircraft or a missile may oscillate around a mathematically unstable course yet its performance may be acceptable. Many problems fall into this category including the travel of a space vehicle between two points and some problems in chemical processes. To deal with such situations, the notion of *practical stability* is more useful, which we present it below [9].

Definition: The system (2-5)

$$\dot{x} = f(t,x),\ x(t_0) = x_0,\ t_0 \geq 0 \tag{2-5}$$

is said to be *practically stable* if, given (λ, A) with $0 < \lambda < A$, we have $|x_0| < \lambda$ implies $|x(t)| < A,\ t \geq t_0$ for some $t_0 \in \Re$.

For more information about practical stability refer to [9].

3 . Control-Oriented Modelling and Identification of Delta Wing Vortex-Coupled Roll Dynamics

3.1 Introduction

In order to reach the desired roll angle in a prescribed time and improve the efficiency and other dynamic behaviour, control algorithms must be designed. As the start up for control algorithms design, the objective of this chapter is to develop the state space model for designing control algorithms to be applied to the vortex-coupled roll dynamics of a 65-degree delta wing. The proposed model, in fact, integrates the vortex breakdown location on the delta wing surface into the delta wing roll dynamics for control purposes. In order to implement the controllers more efficiently, different methods have been applied to approximate the uncertain parameters of the system.

In this chapter, a control-oriented dynamic model of a high performance 65-degree delta wing is proposed which can be directly implemented for nonlinear control purposes of vortex-coupled delta wing dynamics subject to delay. The proposed model relies on the NIRISS method and represents a control-oriented vortex-based nonlinear state space form of the roll motion of a delta wing in high angle of attack flight condition. The relationships among the vortex breakdown location, rolling moment coefficient and

roll angle are developed using a state-space model. The model, in fact, integrates the vortex breakdown location on the delta wing surface into the delta wing roll dynamics for control synthesis. Linear, nonlinear and neural network based parameter identification methods are applied to approximate the uncertainties of the nonlinear dynamic model, such as rolling moment coefficient. The experimental results are utilized to verify the model.

The experimental data available form Huang [10], in fact can be categorized into 4 different types as indicated in table 1, the main characteristics for these categories are the initial roll angle and the trim point.

Category No.	**Initial Roll Angle (release angle)**	**Trim (attractor or equilibrium) Point**
1	positive	positive
2	positive	zero or (near to zero)
3	negative	zero or (near to zero)
4	negative	negative

Table 1. Different categories of available experimental data

In our verification we have used 3 categories to show the credibility of the proposed model. There are four key features in the proposed model:

1- Time delay (T); significant time lags in the vortex breakdown motions relative to the body motions strongly influence the dynamic forces and moments [14];

2 -Uncertainty and nonlinearity due to the rolling moment coefficient (C_l) and vortex breakdown locations (X_{vbl}, X_{vbr}) [40];

3 -Assuming C_l as a function of (X_{vbl}, X_{vbr}): $C_l = f(X_{vbl}, X_{vbr})$ [40];

4 -The model has multiple equilibrium points [38, 41], so we use different

experimental datasets for the proposed C_l equation in the model.

3.2 Description of Experimental Facilities

A comprehensive experimental study has been conducted to understand the flow physics and to obtain a mathematical model in the non-linear region as described in [10], [11]. A 65-degree delta wing model was used to simulate the free-to-roll experiments conducted at the Institute for Aerospace Research (IAR) 2m x 3m and WL/SARL 7 ft x 10 ft wind tunnels. The experimental apparatus and model with MEMS actuators are shown in Figures 9 to 14. Figure 9 shows 65-degree delta wing model. Figure 10 shows the IAR's wind tunnel facility. Figure 11 shows the half model experimental set-up. Figure 12 shows the conceptual design of full wing model experimental set-up. Figure 13 shows the flow pattern with and without vortex flap. Figure 14 shows leading-edge vortex flap, servo motors and mechanical actuator have been used in experiments.

Experiments carried out in IAR shows that taking the flow over delta wing at high incidence, there may exist primary, secondary and tertiary vortices over the wing. The presence of leading-edge vortices and particularly their breakdown is the main cause of airloads' nonlinearities and time dependence. Generally, the effect of secondary and tertiary vortices on airloads is second order to that of the primary ones on the airloads. Therefore, as a first order approximation, the presence of the secondary and tertiary vortices is ignored [10].

In the experiments, the delta wing model (Figure 9) was released from an initial roll angle with zero initial angular velocity and allowed to roll freely about its axis. The system bearings introduced an approximately constant friction torque of about

$0.0461[kg.m]$ regardless of the angular velocity and load, while the moment of inertia of the moving system was $I_w = 0.00311[kg.m.s^2]$.

Observations in different experiments showed that, at a free stream velocity of $u_\infty = 91.44[m/s]$ the 65-degree delta wing configuration have multiple stable trim points in roll (depending on σ) [10].

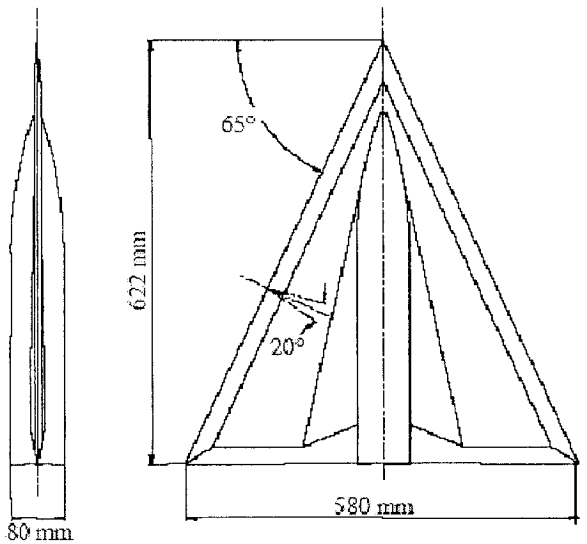

Figure 9. 65-degree delta wing model [10].

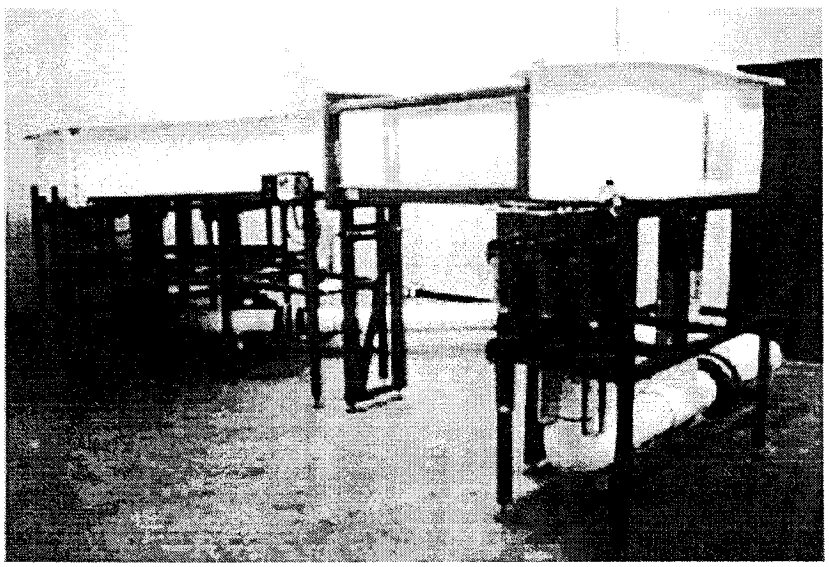

Figure 10. IAR wind tunnel facility [47].

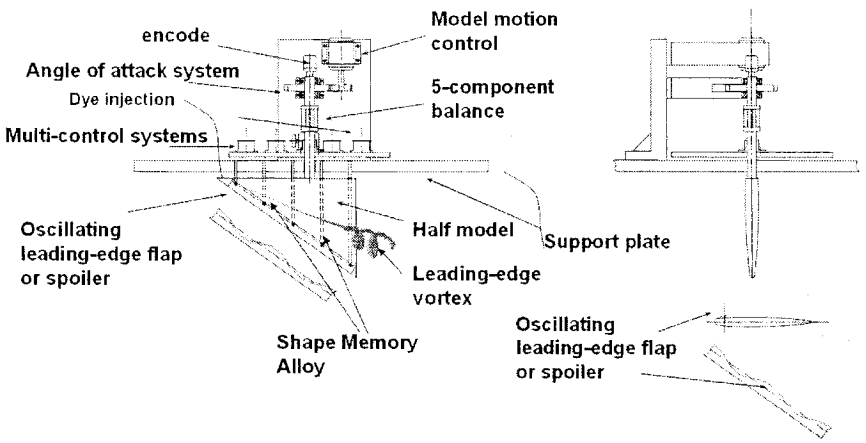

Figure 11. Half-model experimental set-up [47].

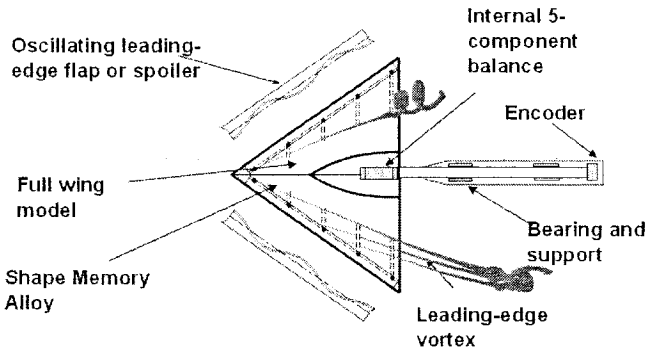

Figure 12. Conceptual design of full wing experimental set-up [47].

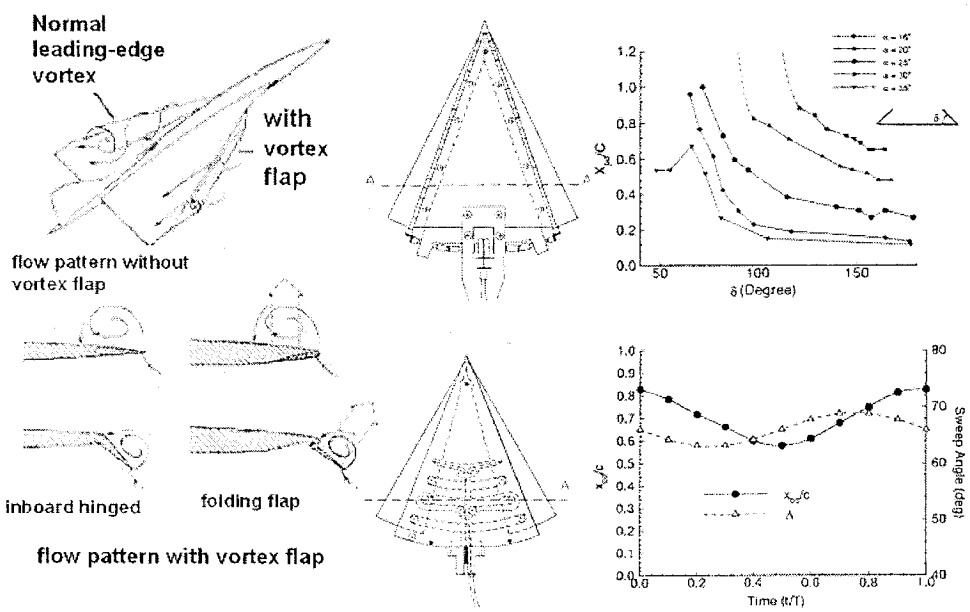

Figure 13. Leading/trailing edge flaps, and flow pattern over delta wing with and without vortex flap [47].

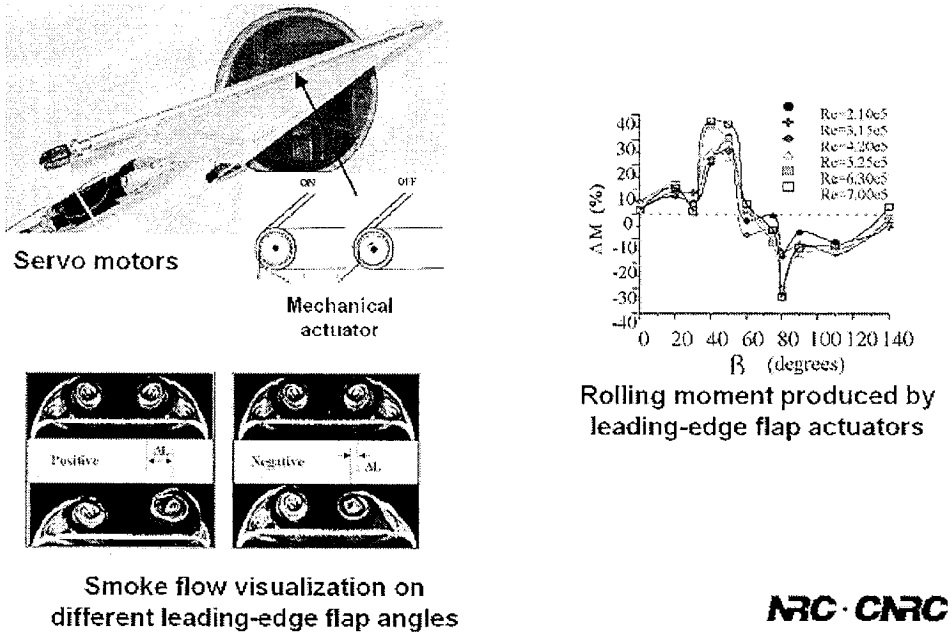

Figure 14. Leading edge vortex flap, servo motors and mechanical actuators [47].

3.3 State Space Formulation of System

For control purposes and also numerical simulations of delta wing highly nonlinear roll dynamics in high angle of attack flight condition, it is necessary to develop an appropriate mathematical model; in this section we will propose a nonlinear vortex-coupled state space model subject to delay. Using the approach presented in [30], we will define the vector of kinematic parameters as the system input:

$$H = (\alpha, \beta, A_{l\&r}, B_{l\&r}, C_{0l\&r}, \Lambda_{l\&r}, \Gamma_{cl\&r}, \Gamma_{l\&r}, X_{sl\&r}, u) \tag{3-1}$$

As in delta wing case, the rate of change of states are determined by the present and past states of the system, so the system dynamics should be described by a retarded functional differential equation (RFDE) [8], so the state space mathematical formulation will be

$$\left.\begin{aligned} \frac{dx}{dt} &= f(x_t, \aleph, H) \\ y &= g(x) \\ \aleph &= \xi(x, H) \end{aligned}\right\} \; x \in \Re^n,\ u \in \Re^m,\ y \in \Re^p,\ \aleph \in \Re^s \tag{3-2}$$

where y is the output vector, $\aleph$ is the vector of vortex breakdown locations and the function $x_t \in c_1$ is defined [8] as follows:

$$x_t(\theta) = x(t+\theta),\ \theta \in [-\eta, 0],\ \eta \le T \tag{3-3}$$

The initial condition will be defined as follows:

$$x_{t_0}(\theta) = \nu(\theta)\ ,\quad \theta \in [-\eta, 0] \tag{3-4}$$

c_1 denotes the vector space of continuous and bounded function mapping the interval $[-\eta, 0]$ into $\Re^n$. With the norm $\|.\|$ given by

$$\|\Phi\| = \sup_{\theta \in [-\eta, 0]} |\Phi(\theta)|,\quad \Phi \in c_1 \tag{3-5}$$

c_1 is a Banach space. η is the length of retardation. As η is finite, i.e. delay is bounded, so the norm in (5) is equivalent to $\max_{\theta \in [-\eta, 0]} |\Phi(\theta)|$.

3.3.1 Derivation of State Space Formulation

The procedure of developing the state space formulation of the nonlinear delta wing vortex-coupled roll dynamics is illustrated in Figure 15.

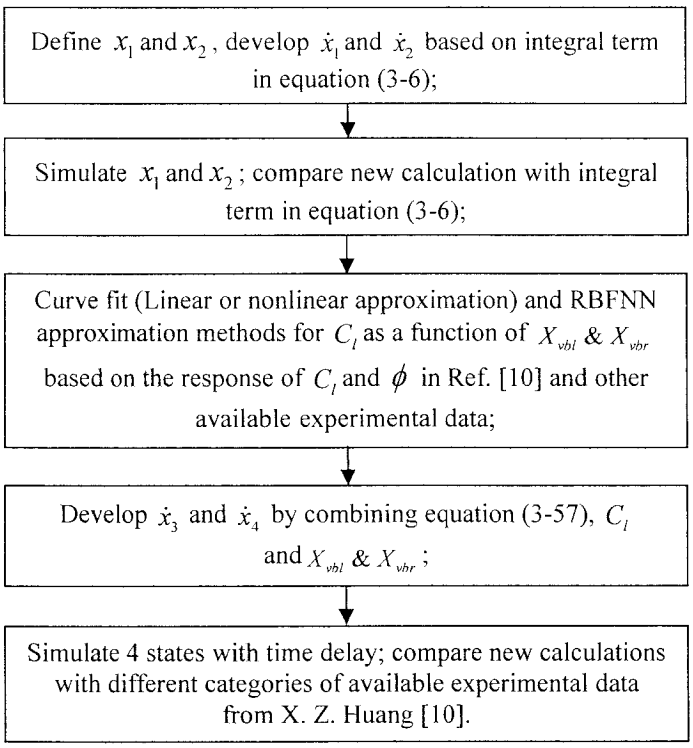

Figure 15. Procedure of developing the state space formulation

Dimensionless Vortex breakdown location of free-to-roll motion over a delta wing is given as [10]:

$$X_{vb}(t) = X_s(\phi(t)) + X_q(\dot{\phi}(t))X_s(\phi(t)) + \int_{t-T}^{t} X_u(t-\tau)\dot{\phi}(\tau)d\tau \qquad (3\text{-}6)$$

where the first term represents the static value at time t, and the second and third terms reflect the quasi-steady and unsteady effects.

Two vortices, the left and the right vortex, over the delta wing need to be considered, thus, two vortex breakdown locations, X_{vbl} and X_{vbr}, which are representing the left and right vortex breakdown positions subsequently, are to be calculated as:

$$X_{vbl}(t) = X_{sl}(\phi(t)) + X_q(\dot{\phi}(t))X_{sl}(\phi(t)) + \int_{t-T}^{t} X_u(t-\tau)\dot{\phi}(\tau)d\tau \qquad (3\text{-}7)$$

$$X_{vbr}(t) = X_{sr}(\phi(t)) + X_q(\dot{\phi}(t))X_{sr}(\phi(t)) - \int_{t-T}^{t} X_u(t-\tau)\dot{\phi}(\tau)d\tau \qquad (3\text{-}8)$$

The difference between X_{vbl} and X_{vbr} are the static terms X_{sl} and X_{sr}. The dynamic terms have the same formulation, but opposite sign.

Figure 16 shows a schematic representation of vortex breakdown locations on the delta wing and its effect on the rolling moment.

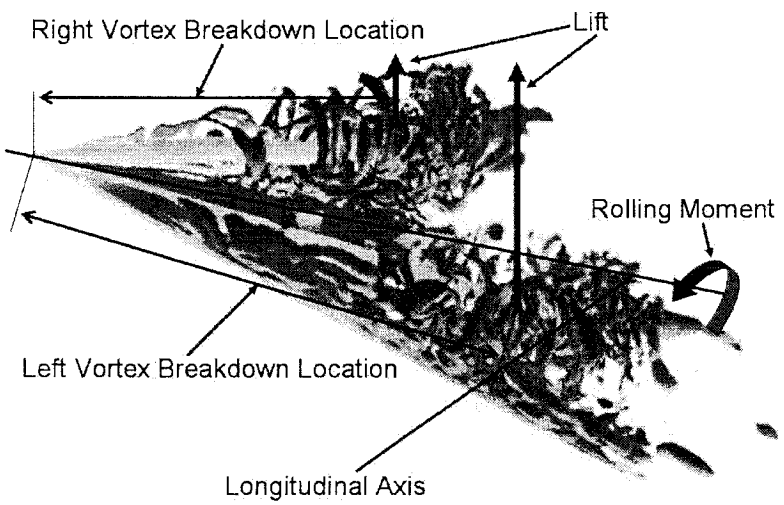

Figure 16. Schematic illustration of vortex breakdown on the delta wing surface

The static term X_s is assumed to be in parabolic form [10], [11]:

$$\Gamma = C_0 + BX - AX^2 \qquad (3\text{-}9)$$

where Γ depends on Leading Edge sweep angle and parameters A, B and C_0 are defined in [10] are experimentally obtained values. Using the formulation in [10], A and B for the left and right vortices are as follows:

$$Al = 1.1\sin(\alpha(t))\sin(\Lambda l(t)),\ Bl = 4 \cdot Al \qquad (3\text{-}10)$$

$$Ar = 1.1\sin(\alpha(t))\sin(\Lambda r(t)),\ Br = 4 \cdot Ar \tag{3-11}$$

where effective leading edge sweep angle of the right and left halves of delta wing are:

$$\Lambda l(t) = \lambda_0 - \text{atan}(\tan(\sigma)\sin(\phi(t))) \tag{3-12}$$

$$\Lambda r(t) = \lambda_0 + \text{atan}(\tan(\sigma)\sin(\phi(t))) \tag{3-13}$$

where λ_0 and σ are half apex angle and structure angle. Critical circulation:

$$\Gamma cl(t) = 0.8\cos[4(\Lambda l(t) - \Lambda_e)] \tag{3-14}$$

$$\Gamma cr(t) = 0.8\cos[4(\Lambda r(t) - \Lambda_e)] \tag{3-15}$$

where, Λ_e is obtained by experiments.

$$\Lambda_e = 20/57.3\ [rad] \tag{3-16}$$

The non-dimensional circulation at trailing edge (non-dimensional chord $X = 1$) is used to determine the distributions of circulation in chord wise in parabolic form [10].

$$\Gamma l(t) = 5.11(\Lambda l(t) + \frac{2.65}{57.3})(\alpha(t) - \frac{3.5}{57.3}) \tag{3-17}$$

$$C_0 l = \Gamma l - Bl + Al \tag{3-18}$$

$$\Gamma r(t) = 5.11(\Lambda r(t) + \frac{2.65}{57.3})(\alpha(t) - \frac{3.5}{57.3}) \tag{3-19}$$

$$C_0 r = \Gamma r - Br + Ar \tag{3-20}$$

The solution of static term X_s is determined as follows [10], which is one possible method of determining X_s.

If $(Bl)^2 + 4 \cdot Al \cdot C_0 l - 4 \cdot Al \cdot \Gamma cl$ is greater than or equal to 0, then:

$$Xsl(t) = \frac{Bl - \sqrt{|(Bl)^2 + 4AlC_{0}l - 4Al\Gamma cl|}}{2Al} \tag{3-21}$$

Otherwise:

$$Xsl(t) = \frac{Bl + \sqrt{|(Bl)^2 + 4AlC_{0}l - 4Al\Gamma cl|}}{2Al} \tag{3-22}$$

If $(Br)^2 + 4 \cdot Ar \cdot C_{0}r - 4 \cdot Ar \cdot \Gamma cr$ is greater than or equal to 0, then:

$$Xsr(t) = \frac{Br - \sqrt{|(Br)^2 + 4ArC_{0}r - 4Ar\Gamma cr|}}{2Ar} \tag{3-23}$$

Otherwise:

$$Xsr(t) = \frac{Br + \sqrt{|(Br)^2 + 4ArC_{0}r - 4Ar\Gamma cr|}}{2Ar} \tag{3-24}$$

In order to develop the *state equations*, let us first consider the integral term, which is the dynamic term in the model of vortex breakdown location (equation (3-6)), Let

$$In = \int_{t-T}^{t} X_{u}(t-\tau)\dot{\phi}(\tau)d\tau \tag{3-25}$$

$$a(t) = 1.65/\tan(\alpha(t)) \tag{3-26}$$

$$c = \pi / T^{*} \tag{3-27}$$

T^{*}, in fact is a function [10] of roll rate ($\dot{\phi}$), but in this research we will assume T^{*} is a constant and equal to T:

$$T^{*} = T \tag{3-28}$$

$X_u(t-\tau)$ can be obtained from equation (12) in [10]:

$$X_u(t-\tau)=\frac{1.65}{\tan\alpha(t)}\sin(\frac{\pi(t-\tau)}{T^*}) \tag{3-29}$$

Using (3-26) and (3-27), equation (3-29) is simplified as follows:

$$X_u(t-\tau)=a(t)\ \sin(c(t-\tau)) \tag{3-30}$$

Expanding (3-30), equation (3-31) is obtained:

$$X_u(t-\tau)=a(t)\ \sin(ct)\cos(c\tau)-a(t)\cos(ct)\sin(c\tau) \tag{3-31}$$

Substitute (3-31) for $X_u(t-\tau)$ in (3-25), the integral term can then be represented as:

$$In=a(t)\sin(ct)\underbrace{\int_{t-T}^{t}\cos(c\tau)\dot{\phi}(\tau)d\tau}_{z_1(t)}-a(t)\cos(ct)\underbrace{\int_{t-T}^{t}\sin(c\tau)\dot{\phi}(\tau)d\tau}_{z_2(t)} \tag{3-32}$$

That is

$$In=a(t)[\sin(ct)z_1(t)-\cos(ct)z_2(t)] \tag{3-33}$$

In (3-33), let

$$x_1(t)=\sin(ct)z_1(t)-\cos(ct)z_2(t) \tag{3-34}$$

Then differentiating $x_1(t)$ with regard to t, following holds

$$\dot{x}_1(t)=\sin(ct)\dot{z}_1(t)-\cos(ct)\dot{z}_2(t)+c\underbrace{(\cos(ct)z_1(t)+\sin(ct)z_2(t))}_{x_2(t)} \tag{3-35}$$

In (3-35), let

$$x_2(t)=\cos(ct)z_1(t)+\sin(ct)z_2(t) \tag{3-36}$$

Combining (3-34) and (3-36), following holds

$$x_{VBD}(t) = \begin{cases} x_1(t) = \sin(ct)z_1(t) - \cos(ct)z_2(t) \\ x_2(t) = \cos(ct)z_1(t) + \sin(ct)z_2(t) \end{cases} \tag{3-37}$$

$(x_{VBD}(t))$ is the vector of vortex breakdown related states. Rewriting (3-37), in matrix form

$$(x_{VBD}(t)) = R(z(t)) \tag{3-38}$$

$$(z(t)) = R^{-1}(x_{VBD}(t)) \tag{3-39}$$

where

$$R = \begin{pmatrix} \sin(ct) & -\cos(ct) \\ \cos(ct) & \sin(ct) \end{pmatrix} \tag{3-40}$$

$$\det(R) = 1 \tag{3-41}$$

$$R^{-1} = \begin{pmatrix} \sin(ct) & \cos(ct) \\ -\cos(ct) & \sin(ct) \end{pmatrix} \tag{3-42}$$

The following integration formula will be used. Let:

$$W(t) = \int_0^t f(\tau)d\tau \tag{3-43}$$

Then, differentiating (3-43) with regard to t, following holds:

$$\frac{dW}{dt} = f(t) \tag{3-44}$$

So for the function (3-45)

$$W(t) = \int_{t-T}^{t} f(\tau)d\tau \tag{3-45}$$

The derivative is

$$\frac{dW}{dt} = f(t) - f(t-T) \tag{3-46}$$

Based on the above integration formula, differentiate $z_1(t)$ and $z_2(t)$ in (3-32) with regard to t respectively, following holds

$$\begin{cases} \dot{z}_1(t) = \cos(ct)\dot{\phi}(t) - \cos(c(t-T))\dot{\phi}(t-T) \\ \dot{z}_2(t) = \sin(ct)\dot{\phi}(t) - \sin(c(t-T))\dot{\phi}(t-T) \end{cases} \tag{3-47}$$

Using (3-56), the following states has been defined

$$x_3(t) = \phi(t) \tag{3-48}$$

$$x_4(t) = \dot{\phi}(t) \tag{3-49}$$

Writing (3-47) in matrix form, and using (3-49), following holds

$$\left(\dot{z}(t)\right) = \begin{pmatrix} \dot{z}_1(t) \\ \dot{z}_2(t) \end{pmatrix} = \underbrace{\begin{pmatrix} \cos(ct) & -\cos(ct) \\ \sin(ct) & -\sin(ct) \end{pmatrix}}_{E} \underbrace{\begin{pmatrix} x_4(t) \\ x_4(t-T) \end{pmatrix}}_{F} \tag{3-50}$$

That is

$$(\dot{z}(t)) = EF \tag{3-51}$$

Differentiate $x_1(t)$ and $x_2(t)$ in (3-37) with regard to t respectively

$$\begin{aligned} \left(\dot{x}_{VBD}(t)\right) = \begin{pmatrix} \dot{x}_1(t) \\ \dot{x}_2(t) \end{pmatrix} = & \underbrace{\begin{pmatrix} c\cos(ct) & c\sin(ct) \\ -c\sin(ct) & c\cos(ct) \end{pmatrix}}_{C} \begin{pmatrix} z_1(t) \\ z_2(t) \end{pmatrix} \\ & + \underbrace{\begin{pmatrix} \sin(ct) & -\cos(ct) \\ \cos(ct) & \sin(ct) \end{pmatrix}}_{D} \begin{pmatrix} \dot{z}_1(t) \\ \dot{z}_2(t) \end{pmatrix} \end{aligned} \tag{3-52}$$

Substitute (3-39) and (3-51) for $(z(t))$ and $(\dot{z}(t))$ in (3-52) results in:

$$(\dot{x}_{VBD}(t)) = CR^{-1}(x_{VBD}(t)) + DEF \tag{3-53}$$

That is

$$\begin{cases} \dot{x}_1(t) = [\cos(ct)\sin(c(t-T)) - \sin(ct)\cos(c(t-T))]x_4(t-T) + cx_2(t) \\ \dot{x}_2(t) = [-\cos(ct)\cos(c(t-T)) - \sin(ct)\sin(c(t-T))]x_4(t-T) - cx_1(t) + x_4(t) \end{cases} \tag{3-54}$$

Simplifying (3-54) and rewrite it, results in (3-55):

$$\dot{x}_{VBD}(t) = \begin{cases} \dot{x}_1(t) = cx_2(t) \\ \dot{x}_2(t) = -cx_1(t) + x_4(t) + x_4(t-T) \end{cases} \tag{3-55}$$

The free-to-roll system equation of motion in [10] is assumed to be:

$$I_w\ddot{\phi}(t) + f_c sign(\dot{\phi}(t)) + C_l(t)qs_w b_w = 0 \tag{3-56}$$

For the proposed model it is assumed as:

$$I_w\ddot{\phi}(t) + f_c sign(\dot{\phi}(t)) + C_l(t)qs_w b_w = h_1 u_1(t) \tag{3-57}$$

where $u_1(t)$ is input torque in the delta wing roll dynamics.

3.3.2 Summaries of State Space Formulation

3.3.2.1 Definitions of State Variables

The integral term in X_{vb} equation (3-33)

$$x_1(t) = \sin(ct)z_1(t) - \cos(ct)z_2(t)$$

A component in $\dot{x}_1(t)$ (equation (3-35))

$$x_2(t) = \cos(ct)z_1(t) + \sin(ct)z_2(t)$$

Roll angle

$$x_3(t) = \phi(t)$$

Roll angular velocity

$$x_4(t) = \dot{\phi}(t)$$

3.3.2.2 Vortex Breakdown Locations in New Form

Vortex breakdown locations in new form with control inputs and with manipulating the integral term using state variables are as follows:

$$X_{vbl}(t) = X_{Sl}(t) + X_{sl}(t)k_q(t)x_4(t) + a(t)x_1(t) + h_2u_2(t) \tag{3-58}$$

$$X_{vbr}(t) = X_{Sr}(t) + X_{sr}(t)k_q(t)x_4(t) - a(t)x_1(t) + h_3u_3(t) \tag{3-59}$$

$$\aleph = [X_{vbl}(t), X_{vbr}(t)]^T \tag{3-60}$$

where

$$k_q(t) = 0.91/\tan(\alpha(t)) \tag{3-61}$$

Angle of attack is considered as follows [10]:

$$\alpha(t) = \text{atan}(\cos(x_3(t))\tan(\sigma)) \tag{3-62}$$

Sideslip angle is $\beta = 0$. $u_2(t)$ and $u_3(t)$ are the control inputs in vortex breakdown locations equations.

3.3.2.3 State Equations in Vector Form

Implementing the model easily for control purposes, the simplified state-space model has been presented:

$$\dot{x}(t) = \begin{cases} \dot{x}_1(t) = c\,x_2(t) \\ \dot{x}_2(t) = -c\,x_1(t) + x_4(t) + x_4(t-T) \\ \dot{x}_3(t) = x_4(t) \\ \dot{x}_4(t) = -C_l(\aleph)Q - (b_w / 2u_\infty I_w) sign(x_4(t)) x_4(t) + h_1 u_1(t) / I_w \end{cases} \tag{3-63}$$

where $Q = qs_w b_w / I_w$ and $u_1(t)$ is the control input to the model. A schematic representation of the above model is shown in Figure 17.

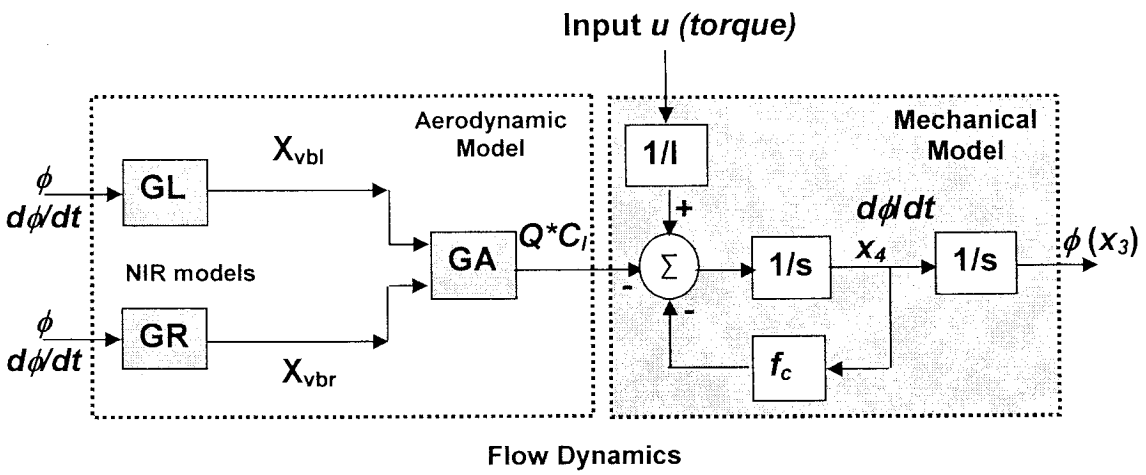

Figure 17. A schematic representation of nonlinear SISO model of free-to-roll delta wing dynamics

3.4 Model with SMA Micro-Actuators Control Inputs

Micromachined actuators have been used successfully to control leading-edge vortices of a delta wing by manipulating the thin boundary layer before flow separation [42]. It has been shown that using different distributions of MEMS actuators can increase the maximum amount of rolling moment of the delta wing from 35 % to 55% [42].

To implement the dynamics of the SMA micro-actuator dynamics in the proposed model we will assume to first order filters as follows:

$$\begin{cases} \dot{x}_5(t) = (-x_5(t) + h_2\, u_2(t)) / \varepsilon_{SMA} \\ \dot{x}_6(t) = (-x_6(t) + h_3\, u_3(t)) / \varepsilon_{SMA} \end{cases} \tag{3-64}$$

Using the data presented in [43], we will assume ε_{SMA} is equal to the time the SMA micro-actuator flaps will react to their input commands. So its range will be:

$$[\min(t_{SMA})] \le \varepsilon_{SMA} \le [\max(t_{SMA})] \tag{3-65}$$

Implementing the model easily for control synthesis, the simplified state-space model of vortex-coupled delta wing roll dynamics with delay and SMA actuator dynamics will be:

$$\dot{x}(t) = \begin{cases} \dot{x}_1(t) = c\, x_2(t) \\ \dot{x}_2(t) = -c\, x_1(t) + x_4(t) + x_4(t-T) \\ \dot{x}_3(t) = x_4(t) \\ \dot{x}_4(t) = -C_l(\aleph) Q - (b_w / 2u_\infty I_w) sign(x_4(t)) x_4(t) + h_1 u_1(t) / I_w \\ \dot{x}_5(t) = (-x_5(t) + h_2 u_2(t)) / \varepsilon_{SMA} \\ \dot{x}_6(t) = (-x_6(t) + h_3 u_3(t)) / \varepsilon_{SMA} \end{cases} \tag{3-66}$$

Vortex breakdown locations in new form, without integral term and coupled with SMA micro-actuators dynamics will be:

$$X_{vbl}(x(t)) = X_{sl}(x(t)) + X_{sl}(x(t)) k_q(t) x_4(t) + a(t) x_1(t) + x_5(t) \tag{3-67}$$

$$X_{vbr}(x(t)) = X_{sr}(x(t)) + X_{sr}(x(t)) k_q(t) x_4(t) - a(t) x_1(t) + x_6(t) \tag{3-68}$$

A schematic representation of above model is shown in Figure 18. The two inputs $u_2(t)$ and $u_3(t)$ are associated with the left and right vortex breakdown locations X_{vbl} and X_{vbr} respectively. These two inputs can be considered as perturbation inputs. Analyzing the output to $u_2(t)$ and $u_3(t)$, we know what effects the vortex breakdown locations have on the rolling motion of the delta wing.

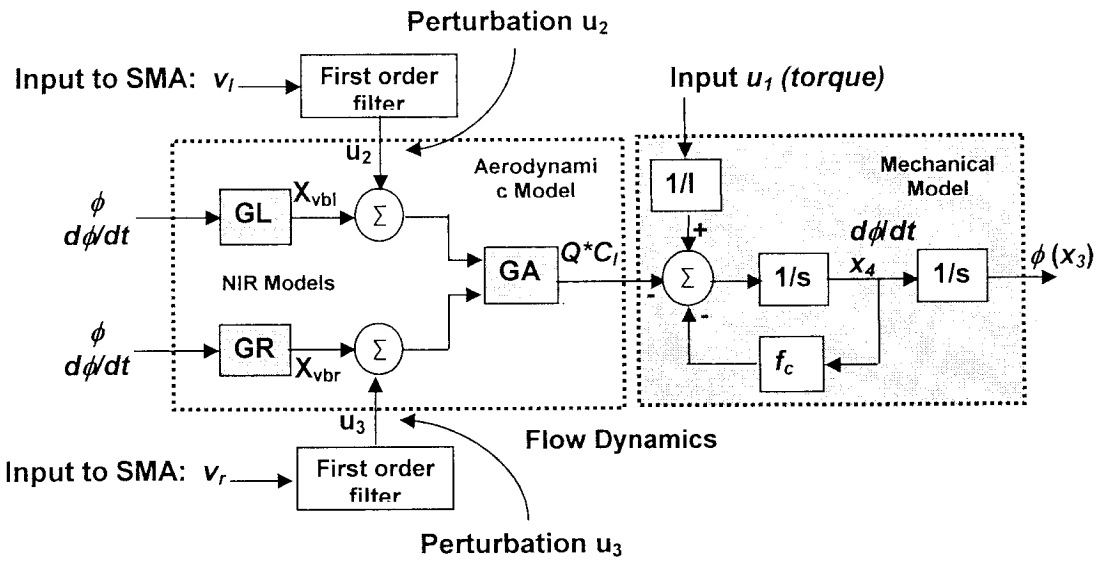

Figure 18. A schematic representation of nonlinear SISO model of free-to-roll delta wing dynamics coupled with SMA actuator dynamics

3.5 Parameters and Calculations

3.5.1 Geometries of Delta Wing

Half apex angle

$$\lambda_0 = 25/57.3\ [rad] \tag{3-69}$$

The chord c_w is normalized into 1:

$$c_w = 1 \tag{3-70}$$

Wing span

$$b_w = 2\tan(\lambda_0)c_w = 0.933 \tag{3-71}$$

Wing area

$$s_w = (0.580 \times 0.622)/2 = 0.18\ [m^2] \tag{3-72}$$

Moment of inertia

$$I_w = 0.27\,[lb.in.s^2] = 0.00311\,[kg.m.s^2] \tag{3-73}$$

3.5.2 Initial Values for Calculation

The initial values of various system parameters have been calculated using the data reported in [10] as follows:

Structure angle:

$$\sigma_0 = 30/57.3\ [rad] \tag{3-74}$$

$$\Delta\alpha = 19.8\sigma_0 - 5.2\ [\text{deg}] \tag{3-75}$$

For bevel angle of wing:

$$\sigma = \sigma_0 - (\Delta\alpha/57.3)\,[rad] \tag{3-76}$$

Sweep angle:

$$\Lambda_0 = (\pi/2) - \lambda_0\ \ [rad] \tag{3-77}$$

Release time:

$$T^* = T \in [0.1,0.2][\text{sec}] \tag{3-78}$$

Bearing friction:

$$f_c\, sign(x_4(t)) = (b_w\, x_4(t)/2u_\infty)\, sign(x_4(t)) \tag{3-79}$$

3.5.3 Aerodynamic Parameters and Their Calculations

Free stream velocity:

$$u_{\infty} = 300\ [ft/\sec] = 91.44\ [m/\sec] \tag{3-80}$$

Air density:

$$\rho = 1.2\ [kg/m^3] \tag{3-81}$$

Dynamic air pressure:

$$q = 0.5\rho u_{\infty}^{2} \tag{3-82}$$

3.6 Parameter Identification

System identification is defined as the experimental determination of values of parameters that govern the dynamics and/or nonlinear behaviour, assuming that the structure of the process model is known [44]. Since the control actions on a system depend on the accurate knowledge about the system, in this section, rolling moment coefficient (C_l), considered as an uncertain parameter in our nonlinear model, will be approximated by applying the following methods:

1- Linear Least Squares Approximation;

2- N^{th} order polynomial Approximation;

3- RBF Neural Networks Approximation;

In most of the researches has been conducted regarding delta wing roll dynamics, rolling moment coefficient has been assumed as a function of roll angle [38, 39, 45], in this research we will assume it as a function of left and right vortex breakdown locations.

3.6.1 Linear Least Squares Approximation

The rolling moment coefficient is a nonlinear function of vortex breakdown location [10], for now, a linear correlation has been assumed:

$$\Delta Xvb = X_{vbl} - X_{vbr} \tag{3-83}$$

$$C_l(X_{vbl}, X_{vbr}) = e_0 + e_1(\Delta Xvb) \tag{3-84}$$

where X_{vbl} and X_{vbr} represent the breakdown locations for the left and right vortices, e_0 and e_1 are calculated parameters using linear least square approximation of the experimental data. Figure 20 shows C_l time history, using linear approximation technique.

3.6.2 N^{th} Order Polynomial Approximation

N^{th} order polynomial curve fitting for C_l approximation as a function of vortex breakdown position, has the following form:

$$C_l(X_{vbl}, X_{vbr}) = e_0 + \sum_{i=1}^{N} e_i(X_{vbl}{}^i - X_{vbr}{}^i) \tag{3-85}$$

where X_{vbl} and X_{vbr} represent the breakdown locations for the left and right vortices, here we have done a 5^{th} order approximation and e_0, e_1, e_2, e_3, e_4 and e_5 are calculated parameters using available experimental data. Figure 27 shows C_l time history, using 5^{th} order least squares polynomial technique.

3.6.3 RBF Neural Network Approximation

Radial Basis Function (RBF) Regularization network has three desirable properties [46]: (1) The regularization network is a universal approximator; (2) Regularization network has the best approximation property; (3) The solution computed by the regularization network is optimal.

This RBF neural network in fact approximates the rolling moment coefficient as a function of vortex breakdown positions:

$$C_l = f(\aleph) \tag{3-86}$$

$$\aleph = [X_{vbl}, X_{vbr}]^T \tag{3-87}$$

For C_l approximation purpose with RBFNN, as we are using two dimensional input data, Regularization networks are utilized.

$$C_{l\lambda_R}(\aleph) = \frac{1}{\lambda_R}\sum_{i=1}^{N}[d_i - F(\aleph_i)]G(\aleph,\aleph_i) \tag{3-88}$$

$$w_i = \frac{1}{\lambda_R}[d_i - F(\aleph_i)],\ \ i = 1,2,...,N \tag{3-89}$$

$$C_{l\lambda_R}(\aleph) = \sum_{i=1}^{N} w_i G(\aleph,\aleph_i) \tag{3-90}$$

$$G(\aleph - \aleph_i) = G(\|\aleph - \aleph_i\|) \tag{3-91}$$

$G(\aleph - \aleph_i)$ is Green's function, which is only [46], depends on the Euclidian Norm of the difference vector $\aleph - \aleph_i$, in which $\aleph$ is input vector and $\aleph_i$ is the centers vector.

$$G(\aleph - \aleph_i) = \exp(-\frac{1}{2\sigma_{rbf}^2}\|\aleph - \aleph_i\|^2) \tag{3-92}$$

$$\sigma_{rbf} = \frac{d_{\max}}{\sqrt{2N}} \tag{3-93}$$

where N is the number of centers and $d_{\max}$ is the maximum distance between the chosen centers.

Matrix form of these equations has the following form:

$$d = [d_1, d_2, ..., d_N]^T \tag{3-94}$$

$$W_R = (G + \lambda_R I)^{-1} d = [w_1, w_2, ..., w_N]^T \tag{3-95}$$

$$C_{l\lambda_R} = GW_R \tag{3-96}$$

where d is the target value vector which is experimental rolling moment coefficient (C_l) in this case. The data used as reference model are in fact the experimental data from Huang [10]. λ_R, the regularization parameter, is set to 0.5 with trial and error. Figure 34 shows C_l time history, using Regularization Radial Basis neural networks approximation.

Figure 19 shows C_l time history using these three parameter identification methods. As it is apparent from this figure, RBF NN approximation is better than nonlinear polynomial curve fit and nonlinear polynomial curve fit is better than linear curve fit.

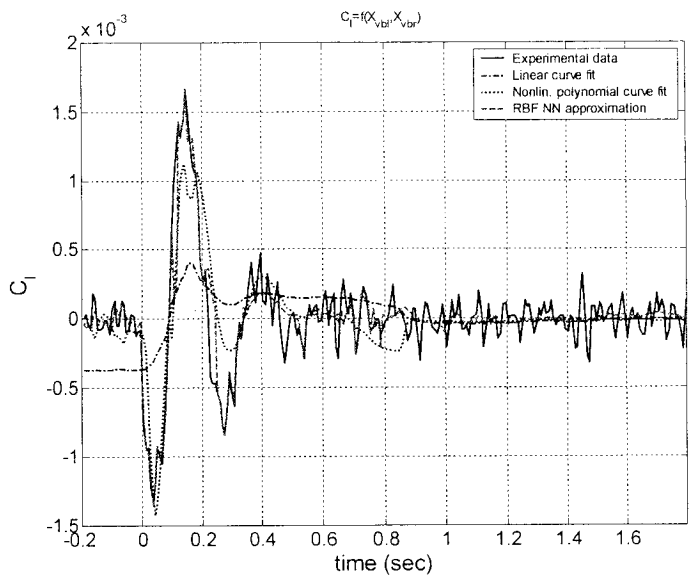

Figure 19. C_l approximation using Linear, Nonlinear polynomial and RBFNN approximation methods

3.7 Experimental Verification of Numerical Simulation

To verify that the developed nonlinear retarded state space model captures the dynamic behavior of the delta wing roll mode, simulation results are compared to delta wing free-to-roll experimental results obtained from the experimental facility at IAR. For numerical simulation the different initial conditions have been defined the same as the initial conditions of various experiments conducted by Huang [10]. For easier verification of the proposed model of free-to-roll dynamics with experimental data we assumed $u_1(t) = u_2(t) = u_3(t) = 0$ in equations (3-63), (3-58) and (3-59).

Simulation results for three different rolling moment coefficient (C_l) approximations are shown in Figures 20 - 40.

For the first simulation which has been done using linear C_l approximation, the initial conditions are: $\nu(\theta) = [x_1(\theta), x_2(\theta), x_3(\theta), x_4(\theta)]^T = [0,0,-64\,[\text{deg}],\, 0]^T$. Figure

20 shows C_l time history, using linear approximation technique. Figure 21 and 22 show the open-loop simulation and phase diagram of the plant with linear C_l approximation as the main uncertainty. Figure 23 shows state variables $x_1(t)$ and $x_2(t)$ time history obtained with the open-loop simulation and a linear C_l approximation. Figure 24 show the time history of left and right vortex breakdown locations respectively. It is apparent that the vortex breakdowns are happening on the mid-chord of the wing, as we expect it, when delta wing reaches to its trim point, in this case the trim point is almost -8-deg which near to -1-deg trim point of the experimental data. Figure 25, shows vortex breakdown locations versus roll angle. Figure 26, shows angle of attack (AOA) time history, as it is apparent the delta wing does the maneuver in the 25-deg AOA.

For the second simulation which has been done using nonlinear C_l approximation, the initial conditions are: $\nu(\theta) = [0,0,58\,[\text{deg}],\, 0]^T$. Figure 27 shows C_l time history, using 5^{th} order least squares polynomial technique. Figure 28 and 29 show the open-loop simulation and phase diagram of the plant with a nonlinear C_l approximation. Figure 30 shows state variables $x_1(t)$ and $x_2(t)$ time history obtained with open-loop simulations and a nonlinear C_l approximation. Figure 31 show the time history of left and right vortex breakdown locations respectively. It is apparent that the vortex breakdowns are happening on the mid-chord of the wing, and symmetrically so the trim point will be near zero, when delta wing reaches to its trim point, in this case the trim point is almost 1-deg which near to 0-deg trim point of the experimental data. Figure 32, shows vortex breakdown locations versus roll angle. Figure 33, shows angle of attack (AOA) time history, as it is apparent the delta wing does the maneuver in the 25-deg

AOA, in this case the jump in angle of attack is less than the first simulation. It is apparent from the figures that the delta wing free-to-roll experimental results validate the proposed nonlinear model of the delta wing. Numerical simulations of the proposed model with 5th order polynomial approximation of C_l shows superior dynamic behavior when compared with the numerical simulations using the linear C_l approximation, as expected intuitively.

For the third simulation which has been done using RBFNN for C_l approximation, the initial conditions are: $\nu(\theta) = [0,0,-38\,[\text{deg}],0]^T$. Figure 34 shows C_l time history, using Regularization Radial Basis neural networks approximation. Figure 35 and 36 show the open-loop simulation and phase diagram of the plant with utilizing RBFNN for C_l approximation. Figure 37 shows state variables $x_1(t)$ and $x_2(t)$ time history obtained with open-loop simulations and C_l approximation using RBF neural network. Figure 38 show the time history of left and right vortex breakdown locations respectively. It is apparent that the right vortex breakdown happens far beyond the trailing-edge of the wing, so the trim point will be negative; when delta wing reaches to its trim point, in this case the trim point is almost -21-deg which near to -22-deg trim point of the experimental data. Figure 39, shows vortex breakdown locations versus roll angle. Figure 40, shows angle of attack (AOA) time history, as it is apparent the delta wing does the maneuver in the 25-deg AOA, in this case the jump in angle of attack is less than the second simulation. It is apparent from the figures that the delta wing free-to-roll experimental results validate the proposed nonlinear model of the delta wing. Numerical simulations of the proposed model with RBFNN approximation of C_l shows

superior dynamic behavior when compared with the numerical simulations using the linear and nonlinear C_l approximation, as expected intuitively.

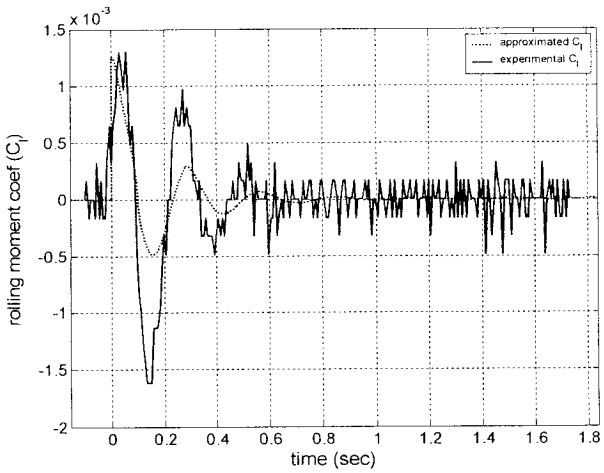

Figure 20. C_l linear approximation

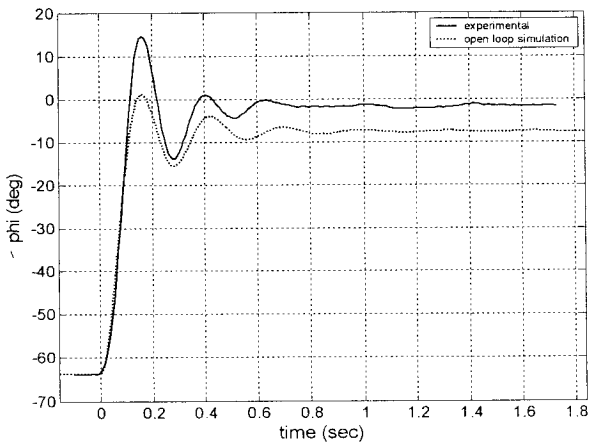

Figure 21. Open loop simulation using C_l linear approximation

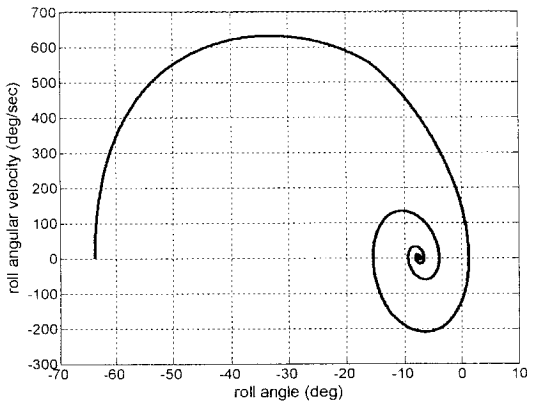

Figure 22. Phase diagram for the system with C_l linear approximation

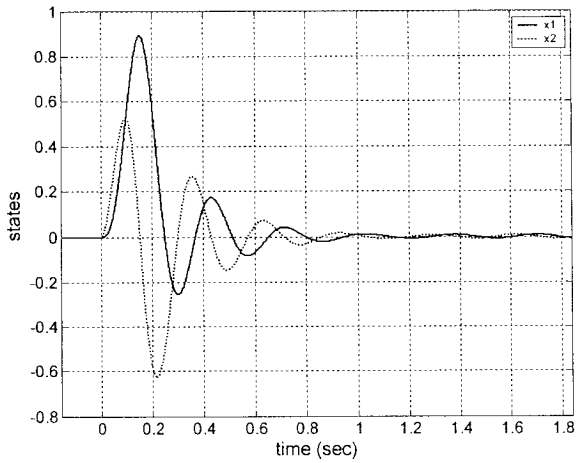

Figure 23. x_1 and x_2 state variables history with C_l linear approximation

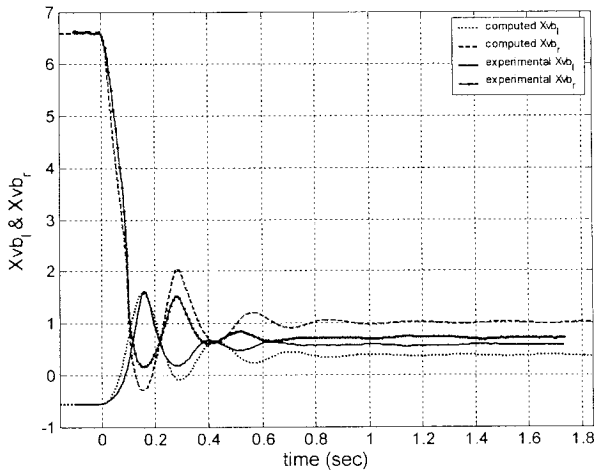

Figure 24. Left and right vortex breakdown positions time history with C_l linear approximation

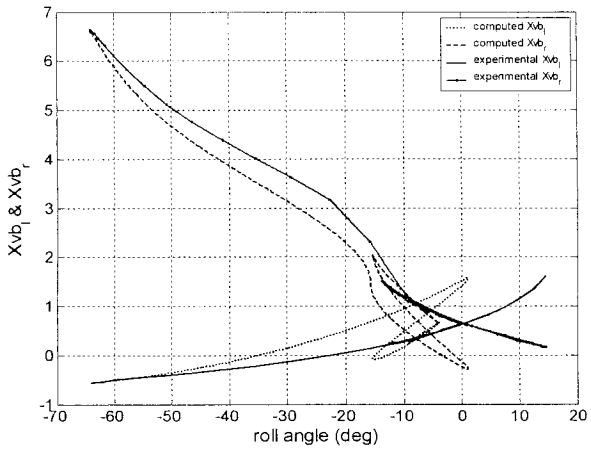

Figure 25. Left and right vortex breakdown positions vs. roll angle with C_l linear approximation

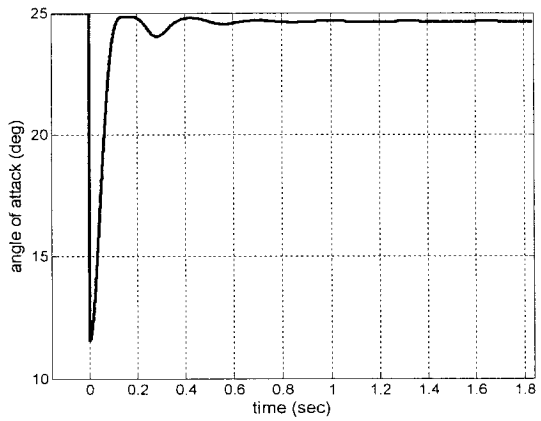

Figure 26. Angle of Attack (AOA) time history with C_l linear approximation

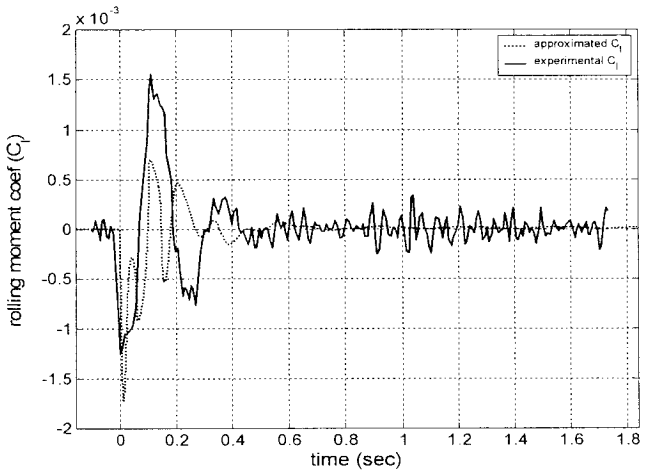

Figure 27. C_l nonlinear approximation

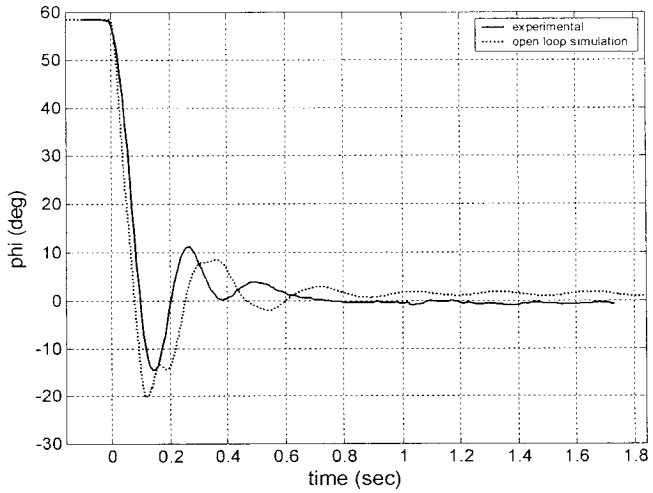

Figure 28. Open loop simulation using C_l nonlinear approximation

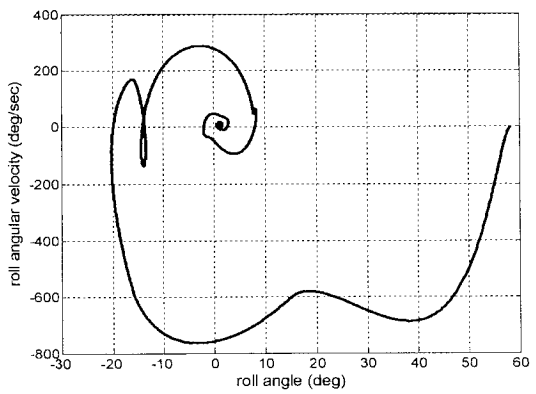

Figure 29. Phase diagram for the system with C_l nonlinear approximation

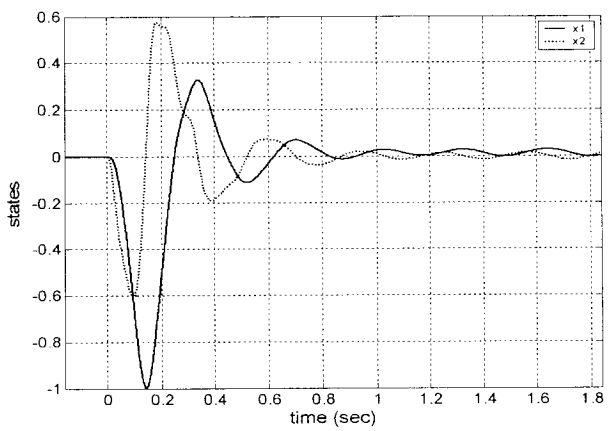

Figure 30. x_1 and x_2 state variables history with C_l nonlinear approximation

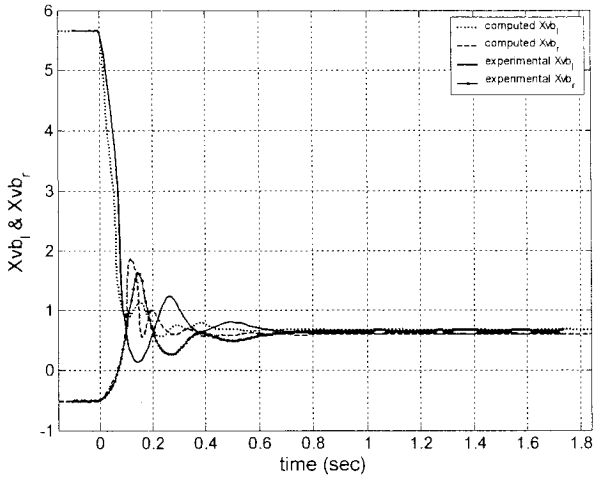

Figure 31. Left and right vortex breakdown positions time history with C_l nonlinear approximation

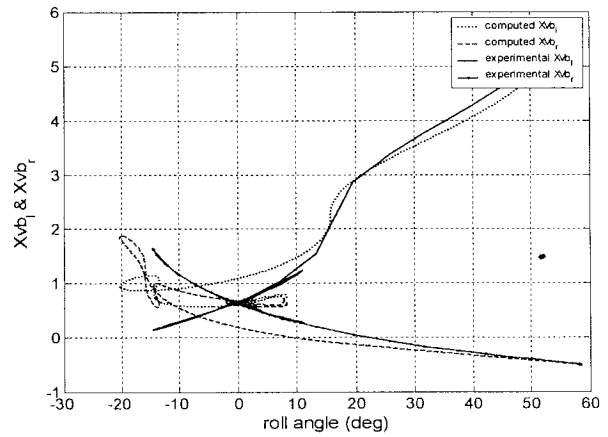

Figure 32. Left and right vortex breakdown positions vs. roll angle with C_l nonlinear approximation

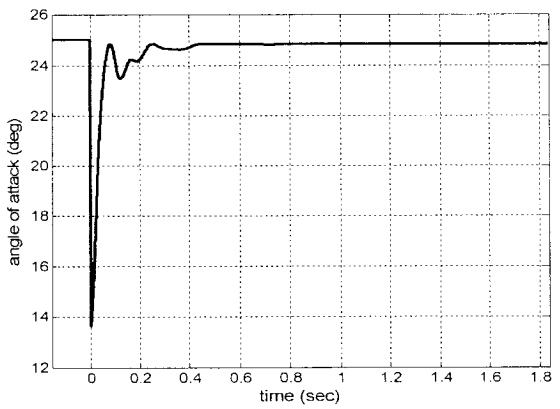

Figure 33. Angle of Attack (AOA) time history with C_l nonlinear approximation

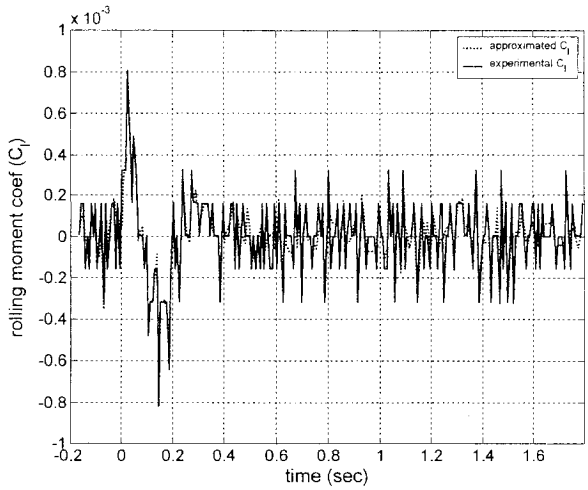

Figure 34. C_l approximation using RBFNN

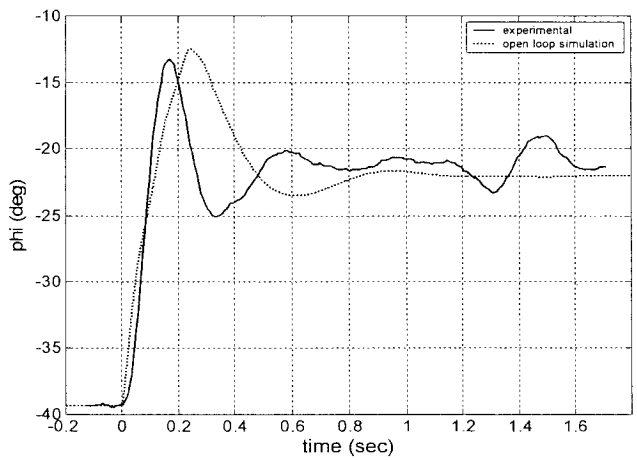

Figure 35. Open loop simulation with C_l approximation using RBFNN

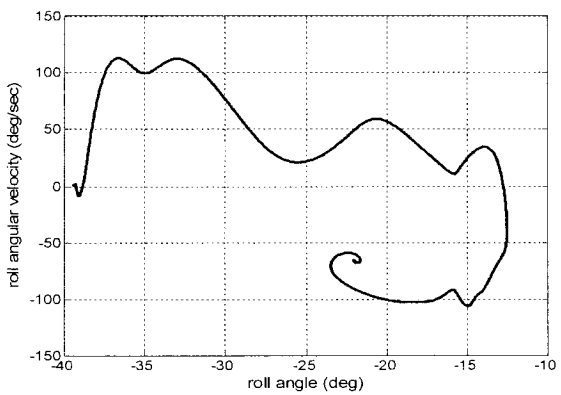

Figure 36. Phase diagram for the system with C_l approximation using RBFNN

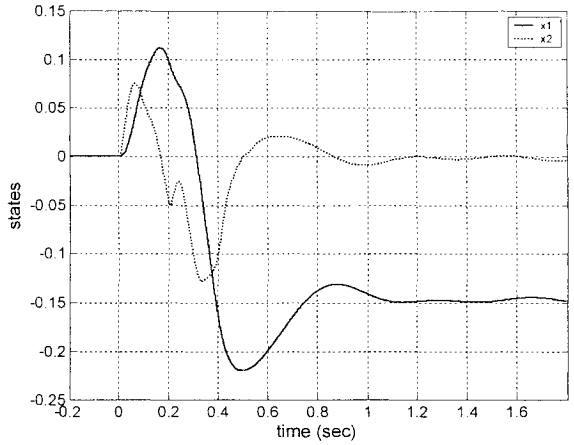

Figure 37. x_1 and x_2 state variables history for the system with C_l approximation using RBFNN

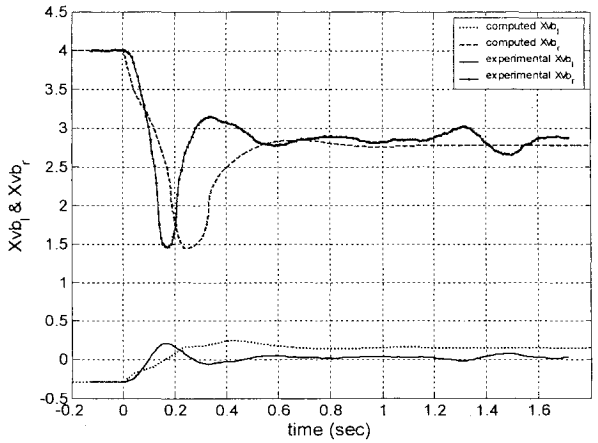

Figure 38. Left and right vortex breakdown positions time history with C_l approximation using RBFNN

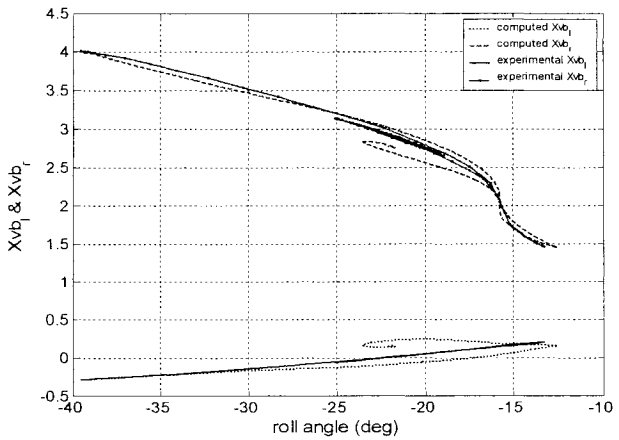

Figure 39. Left and right vortex breakdown positions vs. roll angle with C_l approximation using RBFNN

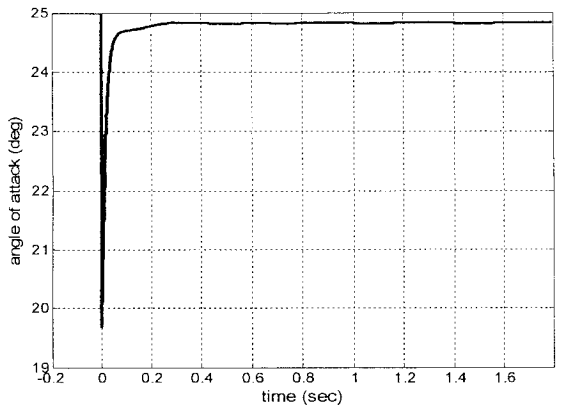

Figure 40. Angle of Attack (AOA) time history with C_l approximation using RBFNN

3.8 Summary

In this chapter a free-to-roll vortex based nonlinear retarded state-space modelling and simulation based on the work done in [10]-[11] has been proposed. The relationship among the vortex breakdown location, rolling moment coefficient and roll angle were described with state equations, which constitute a plant model in nonlinear state-space form enabling control synthesis for system with state delay. The proposed model was validated and verified with delta wing free-to-roll various experimental results. Three different methods were used for the approximation of the system uncertainty which was rolling moment coefficient ($C_l(\aleph)$). These methods are linear, nonlinear (5^{th} order polynomial) curve fitting and also Radial Basis Function Regularization Neural Networks (RBFNN). In the future, better parameter tuning is needed to increase the accuracy of the model, especially correlations for $C_l(\aleph)$. Other Neural networks (wavelet or MLP) can be utilized for this purpose. Model can be extended for the system with time-varying state delay.

4 . Robust Adaptive Stabilization of Vortex-Coupled Delta Wing Systems Subject to State Delay

4.1 Introduction

The high angle of attack flight regime often includes complex phenomena such as nonsteady flow, crossflow separation, and vortex breakdown. Modern tactical fighters fly at high angles of attack in order to take advantage of the nonlinear lift generated from vortices that form on their leeward sides. This results in a substantial improvement of an aircraft's manoeuvre and agility performance. However, at sufficiently high angle of attack, vortex asymmetries can form and induce dynamic motions such as wing rock, a sustained limit-cycle and yaw oscillation. Wing rock and other self-induced aircraft motions can be difficult to control and may result in departure from controlled flight.

In this chapter, we will investigate the applicability of the adaptive stabilizing control approach presented in [66], for 4^{th} order delta wing vortex-coupled roll dynamics with state delay as the first application of this method in delta wing vortex-coupled system control. We will test the controller against modelling uncertainties in rolling moment coefficient and also left and right vortex breakdown locations as time varying

uncertainties. The parameter of this adaptive controller is updated robustly when the bounds of these uncertainties are unknown. Heuristic design process and parameter selection methods will be proposed for easier implementation of this control algorithm. It should be noted that we are applying this control scheme to a fast and high performance delta wing dynamics in high angle of attack (AOA) and near-stall flight condition. The only application of the method has been presented in [66], for control of water-quality dynamic model with very slow dynamics, i.e. the time scale has been measured in days.

4.2 Vortex-Coupled Delta Wing Dynamics

For the control synthesis, the simplified state-space model of vortex-coupled delta wing roll dynamics which has been presented in Ref. [40] (Chapter 3) is modified by adding some damping components and also redefining the bearing friction term in the model:

$$\begin{cases} \dot{x}_1(t) = c\, x_2(t) \\ \dot{x}_2(t) = -c\, x_1(t) - \varepsilon_d\, x_2(t) + x_4(t) + x_4(t-T) \\ \dot{x}_3(t) = -\varepsilon_d\, x_3(t) + x_4(t) \\ \dot{x}_4(t) = -C_l(\aleph)(q s_w b_w / I_w) - (f_c / I_w)\, x_4(t) + (h / I_w)\, u(t) \end{cases} \tag{4-1}$$

where vortex breakdown vector is defined as follows:

$$\aleph = [X_{vbl}(t), X_{vbr}(t)]^T \tag{4-2}$$

Bearing friction has the following form:

$$f_c\, x_4(t) = (b_w / 2u_\infty)\, x_4(t) \tag{4-3}$$

A damping coefficient is selected as follows:

$$\varepsilon_d = 0.2 \tag{4-4}$$

This small positive constant is introduced into the vortex coupled model in order to make the system mildly Hurwitz. It is essentially a modelling approximation that facilitates the control design approach to follow. As this term becomes smaller the system more closely approximates the original vortex coupled model.

Vortex breakdown locations in new form, without integral term and with state variables are as follows [40]:

$$X_{vbl}(t) = X_{sl}(x(t)) + X_{sl}(x(t))k_q(t)x_4(t) + a(t)x_1(t) \tag{4-5}$$

$$X_{vbr}(t) = X_{sr}(x(t)) + X_{sr}(x(t))k_q(t)x_4(t) - a(t)x_1(t) \tag{4-6}$$

where

$$k_q(t) = 0.91/\tan(\alpha(t)) \tag{4-7}$$

$$a(t) = 1.65/\tan(\alpha(t)) \tag{4-8}$$

Angle of attack (AOA) is considered as follows [10]:

$$\alpha(t) = \arctan(\cos(\phi(t))\tan(\sigma)) \ [rad] \tag{4-9}$$

Release time:

$$T^* = T = 0.1 \ [\text{sec}] \tag{4-10}$$

Rolling moment coefficient is a nonlinear function of vortex breakdown location [10], for now, we assume it as a third order polynomial as follows:

$$C_l(\aleph) = e_0 + e_1(X_{vbl} - X_{vbr}) + e_2(X_{vbl}^{\ 2} - X_{vbr}^{\ 2}) + e_3(X_{vbl}^{\ 3} - X_{vbr}^{\ 3}) \tag{4-11}$$

where X_{vbl} and X_{vbr} represent the breakdown locations for the left and right vortices, e_0, e_1, e_2 and e_3 are parameters which have been obtained from a least squares curve fit of experimental data.

4.3 Robust Adaptive Stabilization Approach

4.3.1 Problem Statement

The adaptive control approach is applicable to state delayed systems of the form:

$$\dot{x}(t) = A_0 x(t) + D_0 x(t-\eta) + B_0[u(t) + L(x,\aleph,t)] \tag{4-12}$$

$$x_{t_0}(\theta) = \nu(\theta)\,, \quad \theta \in [-\eta, 0], \eta \le T \tag{4-13}$$

$$y(t) = C_0 x(t) \tag{4-14}$$

where $x \in c_1$ is the system state, $\aleph \in \Re^s$ is the vector of vortex breakdown locations on the wing, $u \in \Re^m$ is the control input and η is a bounded time delay. Matrices $A_0, D_0 \in \Re^{n\times n}$, $B_0 \in \Re^{n\times m}$ and $C_0 \in \Re^{P\times n}$ represent the system's nominal matrices. All the uncertainties and nonlinearities are lumped in the function $L(x,\aleph,t) : c_1 \times \Re^s \times \Re \to \Re^n$ which is continuous (known or unknown) in its arguments. It is assumed that $L(x,\aleph,t)$ is quasi-bounded and locally Lipschitz.

The system is considered as a *matched uncertain system*, i.e., the uncertainties lie in the range of nominal input matrix, and the controller has been proposed based on this fact.

The matrices, initial condition and uncertainties in delta wing dynamics can be cast into the following form:

$$A_0=\begin{bmatrix} 0 & c & 0 & 0 \\ -c & -\varepsilon_d & 0 & 1 \\ 0 & 0 & -\varepsilon_d & 1 \\ 0 & 0 & 0 & (-f_c/I_w) \end{bmatrix},\ D_0=\begin{bmatrix} 0 & 0 & 0 & 0 \\ 0 & 0 & 0 & 1 \\ 0 & 0 & 0 & 0 \\ 0 & 0 & 0 & 0 \end{bmatrix},\ B_0=\begin{bmatrix} 0 \\ 0 \\ 0 \\ (h/I_w) \end{bmatrix},\ L=C_l(\aleph)(qs_w b_w/h) \quad (4\text{-}15)$$

$$\nu(\theta)=\begin{bmatrix} 0 & 0 & \phi_0 & \dot{\phi}_0 \end{bmatrix}^T \quad (4\text{-}16)$$

$$C_0=\begin{bmatrix} 0 & 0 & d & e \end{bmatrix} \quad (4\text{-}17)$$

In this chapter we will only consider the SISO control problem. As such we introduce two output matrix parameters d and e so that proportional and derivative action can be obtained from the proposed output feedback controller. To control this system we need to use *practical stability* notion. It is obvious that, in applications, asymptotic stability is more important than stability. In fact, the desirable feature is to know the size of the region of asymptotic stability so that we can judge whether or not a given system is sufficiently stable to function properly and may be able to see how to improve its stability. On the other hand, the desired system may be unstable and yet the system may oscillate sufficiently near this state that its performance is acceptable. Thus it is clear that we need a notion of stability that is more suitable in several situations than Lyapunov stability. Such a concept is called *practical stability* [9].

The adaptive feedback control has the following form

$$\begin{aligned} u(t) &= -U[y(t),\mu(t),t] \\ \dot{\mu}(t) &= F[y(t),\mu(t),t];\ \mu(t_0)=\mu_0 \end{aligned} \quad (4\text{-}18)$$

This control strategy is developed based on measured output variables so that the resulting closed-loop system is globally practically stable.

Consider the nonlinear retarded dynamic system

$$\dot{x}(t) = f(x_t(t), u(t), t), \;\; x_{t_0}(\theta) = \nu(\theta); \;\; \theta \in [-\eta, 0] \tag{4-19}$$

where $f : c_1 \times \Re^m \times \Re \to \Re^n$ is assumed to be quasi-bounded and locally Lipschitz.

The following results are based on the definitions and properties from Ref. [66] summarized in Appendix A. It is assumed that the matrix A_0 is a Hurwitz matrix and that the retarded system considered satisfies the following assumptions:

Assumption 1

The uncertainties are matched and bounded. That is, there exist constants $\varsigma, \vartheta \in \Re_+$ such that

$$\left\| L(x_t, \aleph, t) \right\| < \varsigma + \vartheta \left\| x \right\|, \;\; \forall (x_t, \aleph, t) \in c_1 \times \Re^s \times \Re \tag{4-20}$$

Assumption 2

Note that it is assumed that there exists [66] a matrix $H_0 \in \Re^{m \times p}$ such that the rational function matrix

$$T(s) = H_0 C_0 (sI_n - A_0)^{-1} B_0 \tag{4-21}$$

is strictly positive real (SPR). Then there exist [67] positive definite symmetric matrices P_0 and Q_0 such that

$$P_0 A_0 + A_0^T P_0 = -Q_0 \tag{4-22}$$

$$B_0^T P_0 = H_0 C_0 \tag{4-23}$$

The matching condition (4-23) is required to ensure that the controller has access to the uncertainty to reduce its destabilizing effect [66].

Taking these properties and assumptions in to account we will have *Theorem 1* (in Appendix B) which is an improved Lyapunov-Razumikhin type theorem.

There are three methods to obtain H_0 as the key matrix in output feedback control:

1- In our case as the rows of C_0 are linearly independent so $(C_0 C_0^T)^{-1}$ does exist, and hence $(C_0 C_0^{+}) = 1$ [68], so we can obtain H_0 as follows:

$$H_0 = B_0^T P_0 C_0^{+} \tag{4-24}$$

It should be mentioned that we can obtain H_0 only if the matching condition (4-23) has a feasible solution.

2- Defining a constrained linear matrix equality (LME) as follows:

$$P_0 A_0 + A_0^T P_0 < 0 \tag{4-25}$$

subject to constraints

$$\begin{aligned} &H_0 C_0 = B_0^T P_0 \\ &P_0 = P_0^T > 0 \end{aligned} \tag{4-26}$$

to solve it with convex optimization tools, like YALMIP Toolbox, Matlab LMI Toolbox or LMITools, operating in Matlab environment. If (4-23) has a feasible solution we will obtain $P_0 > 0$ and H_0.

3- Using Kalman-Yacubovich-Popov or the *positive real lemma* [69] the following LMI will be proposed as the equivalent of (4-21) and (4-22)

$$P_0 = P_0^T > 0$$
$$\begin{pmatrix} -P_0A_0 - A_0^T P_0 & -P_0B_0 + (H_0C_0)^T \\ -B_0^T P_0 + H_0C_0 & 0 \end{pmatrix} > 0 \tag{4-27}$$

to be solved with convex optimization toolboxes. In case of feasible solutions we will obtain $P_0 > 0$ and H_0.

By proposing the second and the third methods, which we do not need Q_0, in fact we will *decrease* the number of the design parameters for the overall design procedure.

4.3.2 Robust Adaptive Stabilization

Before presenting the adaptive stabilization scheme, we present an output-feedback controller to stabilize the system provided that the bounding set is known. Take the following Lyapunov function candidate as $V(.):\Re^n \times \Re \to \Re_+$

$$V(x,t) = x^T(t)Px(t) + \int_{-\eta} x^T(\theta)Rx(\theta)d\theta; \quad P,R > 0 \tag{4-28}$$

The following theorem summarizes a preliminary stability result.

Lemma 1 is the lemma which helps the usability of the method for the delta wing application.

Lemma 1: The free nominal system (A_0, D_0) is asymptotically stable if, given positive definite symmetric matrices R in $\Re^{n\times n}$, there exist an inequality

$$\begin{bmatrix} PA_0 + A_0P + R & PD_0 \\ D_0P & -R \end{bmatrix} < 0 \tag{4-29}$$

which has a *p.d.s.* solution $P \in \Re^{n\times n}$.

Proof: The time derivative of Lyapunov function $\dot{V}(.)$ along any trajectory of the nominal system would be

$$\dot{V}(.) = \dot{x}^T(t)Px(t) + x^T(t)P\dot{x}(t) + x^T(t)Rx(t) - x^T(t-\eta)Rx(t-\eta)$$

Define $z(t) = [x^T(t), x^T(t-\eta)]^T$ and write $\dot{V}(.) = z^T(t)Hz(t)$ where

$$H = \begin{bmatrix} PA_0 + A_0^T P + R & PD_0 \\ D_0 P & -R \end{bmatrix}$$

a sufficient condition for asymptotic stability of the nominal system is the negative definiteness of H:

$$H < 0, P > 0 \tag{4-30}$$

This last inequality is an LMI in P and can be solved very efficiently by convex optimization algorithms.

Theorem 2: Assume that the bounding set is known and subject to assumption 1 and 2. Choose the scalar $\rho \in (1, \rho^*)$ where $\rho^* \triangleq \lambda_{\min}(Q_0) / \{2\lambda_{\max}(P_0)\|D_0\|\}$. Then the output feedback controller

$$u_\rho(x_t, t) = -\mu_0 H_0 y(t)$$
$$\mu_0 \geq \mu_M = \frac{1}{2}\left[\frac{\varsigma^2}{\Gamma_u} + \frac{\vartheta^2}{(1-\Delta)\lambda_{\min}(Q_0)}\right] \tag{4-31}$$

is globally practically stable where $\Delta \in (0,1)$ and $\Gamma_u \in \Re_+$ are *design parameters*.

Proof: Presented in Appendix B.

Remark: The major task of the controller in equation (4-31) is to suppress the

uncertainty by using its maximum possible bound. It is realized, however, that μ_0 is unknown when ς and ϑ are unknown. In order to implement equation (4-31) in the absence of knowledge of the bounds outside the uncertainties, it is desirable to design an adaptive scheme for μ_0.

For $g > 0$, consider the following adaptive scheme for μ_d where μ_0 is replaced by μ_d:

$$\begin{aligned} u_\rho^d(x_t,t) &= -\mu_d H_0 y(t) \\ \dot{\mu}_d &= -g\mu_d + \|H_0 y\|^2 \quad \mu_d(t_0) = \mu_d^+ \end{aligned} \tag{4-32}$$

the system in equation (4-14) can be robustly stabilized.

The practical stability property of the system considered in equations (4-12 - 4-14) combined with the proposed adaptive controller give the following theorem.

Theorem 3: Subject to structural Assumptions 1 and 2, there exists a constant ρ_m such that the closed-loop system consisting of the plant in equations (4-12 - 4-14) with the feedback controller in equation (4-32) is globally practically stable.

It can be shown that $u_\rho^d(.)$ is continuous, quasi-bounded and locally Lipschitz. Therefore a unique solution of the system:

$$\begin{aligned} \dot{x}(t) &= A_0 x(t) + D_0 x(t-\eta) + B_0[u_\rho^d(x_t,t) + L(x_t, Xvb, t)] \\ u_\rho^d(x_t,t) &= -\mu_d H_0 y(t) \\ \dot{\mu}_d &= -g\mu_d + \|H_0 y(t)\|^2 \qquad \mu_d(t_0) = \mu_d^+ \\ x_{t_0}(\theta) &= \nu(\theta) \quad \theta \in [-\eta, 0] \end{aligned} \tag{4-33}$$

exists on an interval $[t_0, t_0 + \upsilon), \upsilon > 0$, and thus Property 1 holds.

Proof: Presented in Appendix B.

These theorems (1, 2 and 3) in fact are similar to ones have been proposed in [66]; here we have justified them for delta wing application purpose.

Figure 41 shows a schematic illustration of this adaptive controller applied to the vortex-coupled delta wing dynamics.

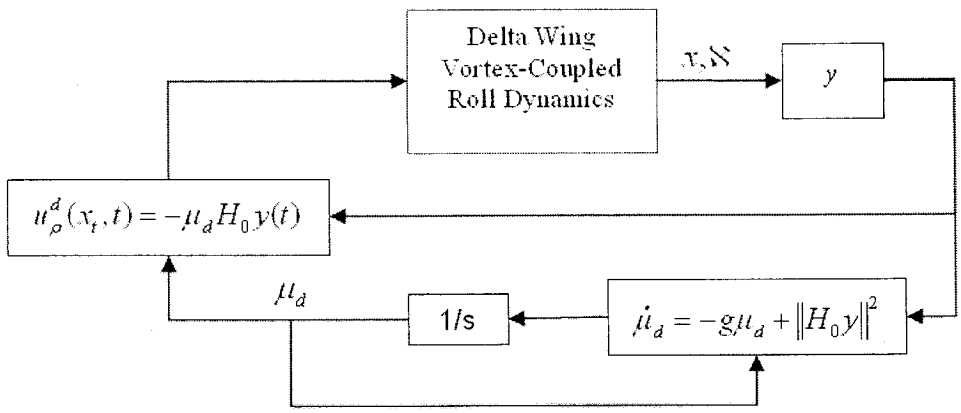

Figure 41. Schematic illustration of the adaptive stabilizing controller.

4.4 Control Design and Parameter Selection

This section is about optimising the performance, by presenting an algorithm of control design and parameter selection by doing a trade-off between the main parameters which we will discuss their impact on the performance.

Two practical algorithms of control design and parameter selection procedure for delta wing stabilization problem are presented. These algorithms are combination of *Trial and error*, *experience* and *heuristic*.

Algorithm 1:

1. Set the initial conditions: $x_{t0}(\theta) = [0, 0, x_3(\theta), x_4(\theta)]$;
2. Define the output matrix C_0, by setting d and e ;

3. Select a proper $Q_0 = \xi \times I;\ \xi > 0$, by setting ξ, so $\lambda_{\max}[Q_0] = \lambda_{\min}[Q_0] = \xi$;

4. Compute P_0 using $P_0 A_0 + A_0^T P_0 = -Q_0$, with the aid of MATLAB;

5. Compute H_0 as the main matrix in output feedback controller, using $H_0 = B_0^T P_0 C_0^+$.

Note: This matrix is the key matrix in matching condition and should satisfy the following two conditions: a) with this H_0, rational function $T(s)$ in equation (4-21) should be strictly positive real (SPR); b) the following inequality should hold during the simulation process: $\|H_0 y\| \le \delta_0 \|x\|$ where $\delta_0 \triangleq \|B_0^T P_0\|$;

6. Set μ_d^+ based on one of the following methods:

   I. Select $\Delta \in (0,1)$ and $\Gamma_u \in \Re_+$ as design parameters in equation (4-31); find proper ς and ϑ, by trial and error, to define the bounds of the uncertainties; then compute μ_M using equation (4-31), and select $\mu_0 > \mu_M$ as the initial value for the adaptation parameter ($\mu_d^+ = \mu_0$);

   II. Just make an initial guess for μ_d^+;

7. Select a proper $g > 0$, as a gain in adaptation law;

8. Compute adaptation law using equation (4-32), as the control gain;

9. Compute control input using equation (4-32);

10. Apply the control input to the delta wing vortex-coupled roll dynamics;

11. Check the performance, if it is acceptable using practical stability notion and the designer engineering sense, then the process is ended, if not go to step 1, and repeat the process to capture the required performance.

Algorithm 2:

1. Set the initial conditions: $x_{i0}(\theta)=[0,\ 0,\ x_3(\theta),\ x_4(\theta)]$;
2. Define the output matrix C_0, by setting d and e ;
3. Compute P_0 and H_0 using convex optimization toolboxes, with the aid of MATLAB. Define one of the following procedures to solve the constrained LMEs:
   I. Solving $P_0A_0 + A_0^T P_0 < 0$ as a LME subject to constraints $H_0C_0 = B_0{}^T P_0;\ P_0 = P_0{}^T > 0;$
   II. Solving the following LMI with convex optimization toolboxes:

$$P_0 = P_0{}^T > 0, \begin{pmatrix} -P_0A_0 - A_0^T P_0 & -P_0B_0 + (H_0C_0)^T \\ -B_0{}^T P_0 + H_0C_0 & 0 \end{pmatrix} > 0$$

4. Make an initial guess for μ_d^+;
5. Select a proper $g > 0$, as a gain in adaptation law;
6. Compute adaptation law using equation (4-32), as the control gain;
7. Compute control input using equation (4-32);
8. Apply the control input to the delta wing vortex-coupled roll dynamics;

9. Check the performance, if it is acceptable using practical stability notion and designer engineering sense, then the process is ended, if not go to step 1, and repeat the process to capture the required performance.

For required performance the designer should trade off among the main parameters, to be discussed here. The following notes are done based on various simulations to study the sensitivity of the control process to the selective design parameters and the effect of these parameters on control process:

Initial guesses for μ_d^+, does not affect the system performance, it simply influence the implementation of the control action. Therefore simulations should be used to determine a suitable initial guess for $\hat{\mu}_d$; as it has been stated in [66], and simulation studies show.

By increasing e, with a constant d, i.e. adding more proportion of roll rate to output, the output and control input reach to their steady-state level, faster. Roll angle and roll rate decay to their steady-state level slower. The extremum of roll rate will be pretty smaller, which is desirable, but the extremum of control input will be larger. The extremums in vortex breakdown related states, i.e. x_1 and x_2, will be smaller.

Changing ξ, results in changes in $\|Q_0\|$ and $\|P_0\|$ and hence in $\|H_0\|$; and because H_0 is not unique so we can optimise the performance via changing H_0, with regard to the fact that its variations won't change the stability.

With larger amounts of ξ, states and control input reach to their steady-state level faster, but with the cost of higher extremums in control input and roll rate. No difference observed in reaching time of controller gain (μ_d) to its steady-state level.

With smaller amount of g, the states reach faster to their steady-state level, but with the cost of more extremums in roll rate, and with regard to the fact that the control input (u) and controller gain (μ_d), decay to their steady-state level slower. No difference observed in control input extremums.

To have an acceptable performance, one should trade off between the discussed parameters as the main parameters, in a way to find the best combination of "*time to reach steady-state level*", "*extremums*" and "*oscillations*" of the states, output, control input and dynamic parameters. Figures 42 and 43 show comprehensive flowcharts of the proposed algorithms of control design and parameter selection for practical application of delta wing vortex-coupled roll stabilizing control.

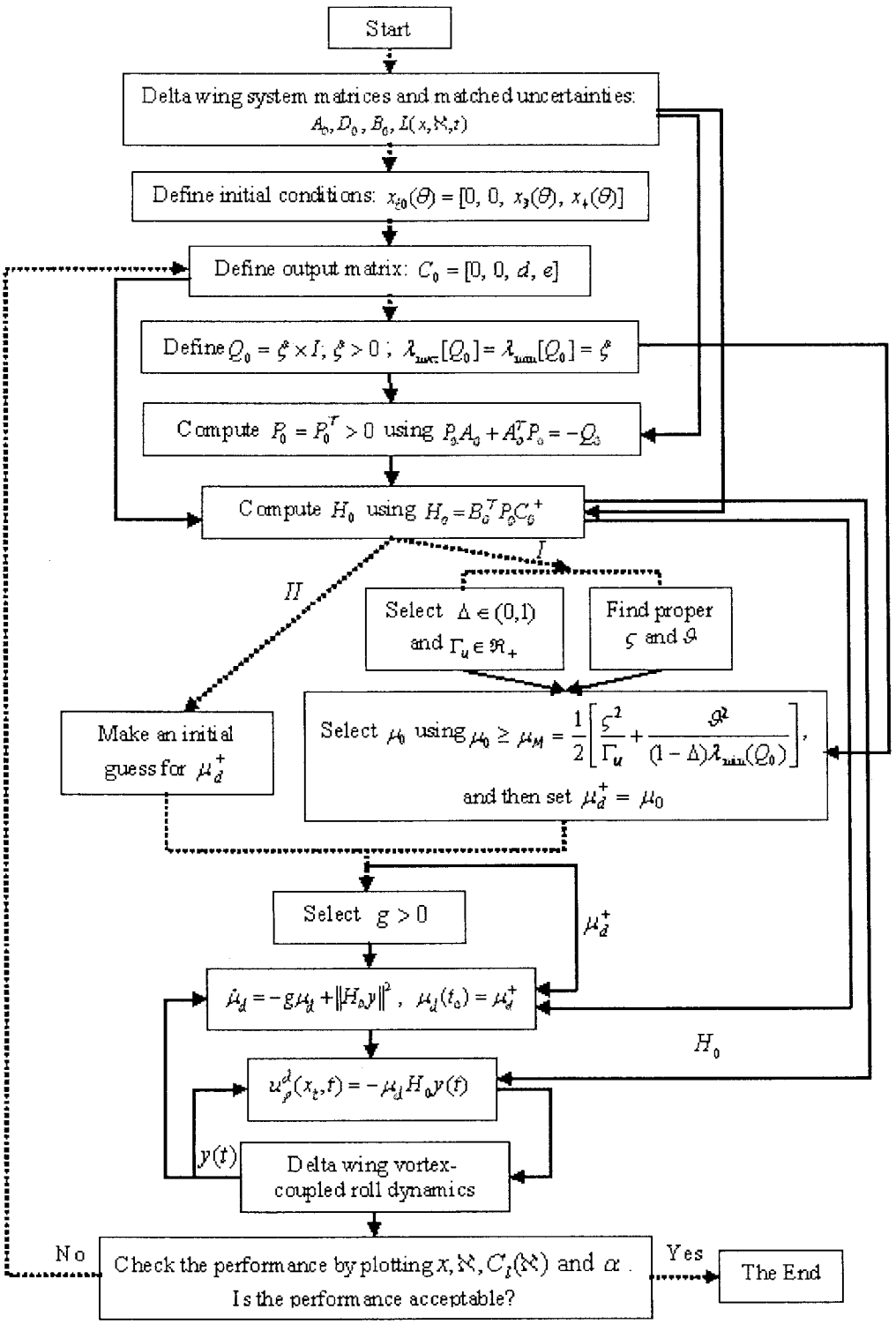

Figure 42. Flowchart of the first algorithm for delta wing stabilization control process application

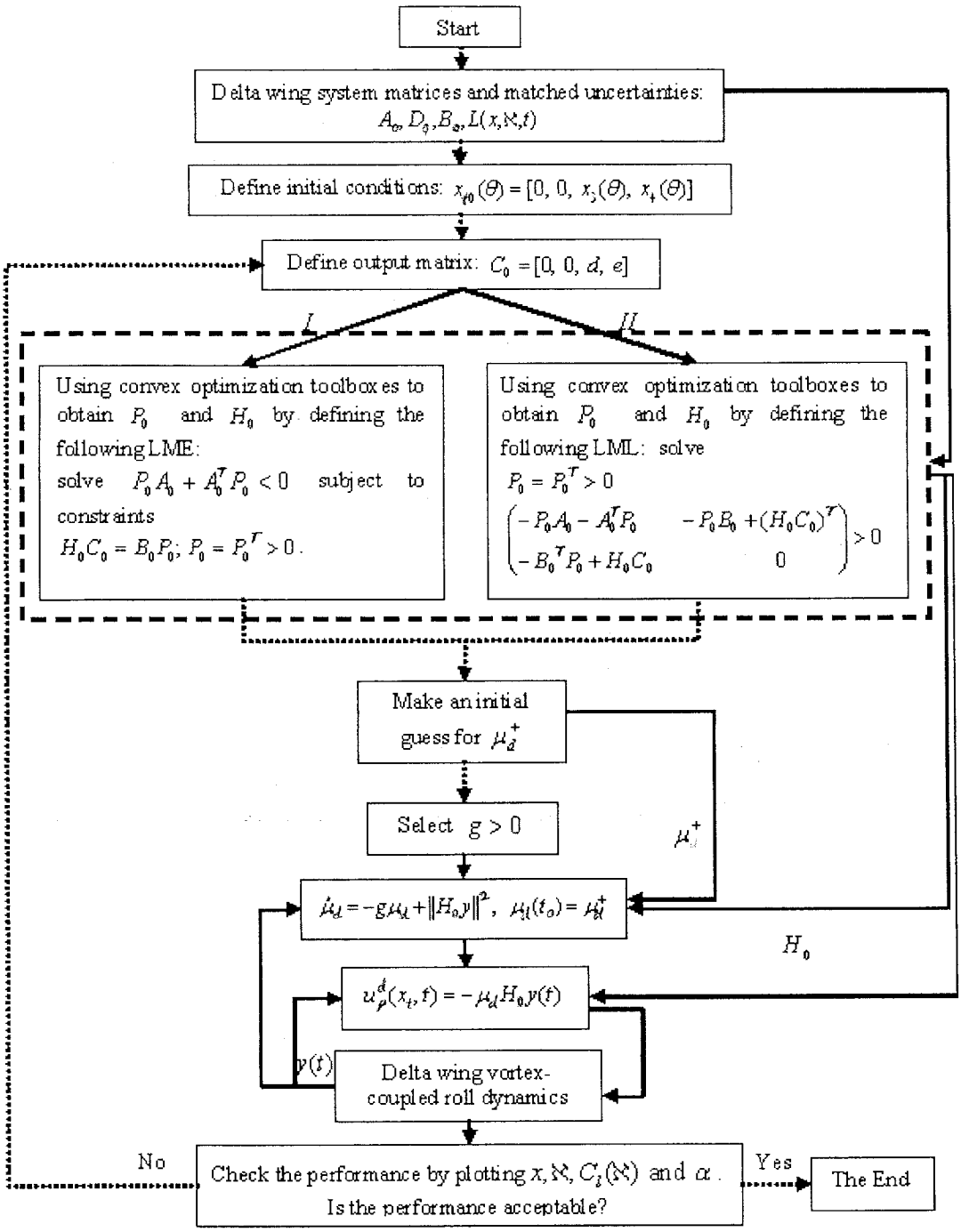

Figure 43. Flowchart of the second algorithm for delta wing stabilization control process application

4.5 Application to Delta Wing System

Two numerical simulations, has been done in MATLAB to show the applicability of the controller to the retarded vortex-coupled delta wing SISO model. The parameters

for both of this simulations has been chosen as follows: $\eta = 0.1, \xi = 0.1, d = 1, e = 0.1,\ g = 10, \hat{\mu}_0 = 80, h = 1$. The initial conditions (IC) for the first simulation are: $\nu(\theta): x_1(\theta) = x_2(\theta) = 0, x_3(\theta) = 60$ [deg], $x_4(\theta) = 80$[deg/sec]. Results of the first simulation with positive initial conditions have been shown in Figure 44 to 53. Figure 44, shows the time history of output as a combination of roll angle and roll rate, as it is apparent the output goes to its steady-state level pretty fast. Figure 45, shows the time history of x_3 state, which is in the vicinity of its equilibrium point. Figure 46, shows the time history of x_4 state. The delta wing is stabilized in a relatively short time period with aforementioned initial conditions. Figure 47, shows the time history of x_1 & x_2 states. Figure 48, shows the control input time history; as it is apparent the input control signal is well damped. Figure 49, shows the time history of the adaptive controller gain (μ_d); the controller gain decays smoothly to a steady-state level. Figure 50, shows angle of attack (AOA) time history, as it is apparent the delta wing does the manoeuvre in the 25° AOA. Figure 51 and 52 show the left and right vortex breakdown locations respectively. It is apparent that the vortex breakdowns are happening on the mid-chord of the wing, as we expect from a stabilized delta wing. Figure 53, shows the time history of rolling moment coefficient as a nonlinear function of left and right vortex breakdown locations ($C_l(\aleph)$). The oscillation is a result of oscillations in vortex breakdown locations.

For the second simulation the initial conditions: $\nu(\theta): x_1(\theta) = x_2(\theta) = 0, x_3(\theta) = -60$ [deg], $x_4(\theta) = -80$[deg/sec]. Results of the second simulation with negative initial conditions have been shown in Figure 54 to 63. Figure 54, shows the time history of output as a combination of roll angle and roll rate, as it is

apparent the output goes to its steady-state level pretty fast. Figure 55, shows the time history of x_3 state, which is in the vicinity of its equilibrium point. Figure 56, shows the time history of x_4 state. The delta wing is stabilized in a relatively short time period with aforementioned initial conditions. Figure 57, shows the time history of x_1 and x_2 states. Figure 58, shows the control input time history; as it is apparent the input control signal is well damped. Figure 59, shows the time history of the adaptive controller gain (μ_d); the controller gain decays smoothly to a steady-state level. Figure 60, shows angle of attack (AOA) time history, as it is apparent the delta wing does the manoeuvre in the 25° AOA. Figure 61 and 62 show the left and right vortex breakdown locations respectively. It is apparent that the vortex breakdowns are happening on the mid-chord of the wing, as we expect from a stabilized delta wing. Figure 63, shows the time history of rolling moment coefficient as a nonlinear function of left and right vortex breakdown locations ($C_l(\aleph)$). The oscillation is a result of oscillations in vortex breakdown locations.

Simulation results show that the controller has an acceptable performance, since roll angle has a practically stable convergence to the vicinity of its equilibrium point near zero. Roll rate also converges to zero in a practically stable manner. The extremum in roll rate simulations is acceptable since the delta wing dynamics is capable of doing high performance manoeuvres. The other two states (vortex breakdown location related states) also have stable convergence to the zero. Oscillations in the states and also vortex breakdown locations are acceptable as we are using practical stability notion in the presented controller. Both simulations show an acceptable combination of performance criteria, i.e. "time to reach steady-state level", "extremums" and "oscillations" in states, control input, output and dynamic parameters.

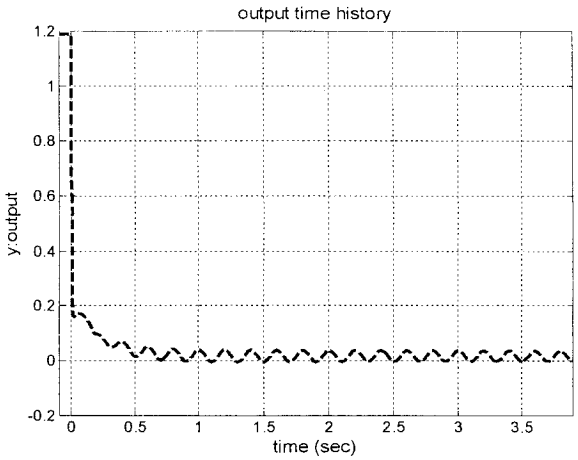

Figure 44. $y(t)$ time history (plant output), positive IC

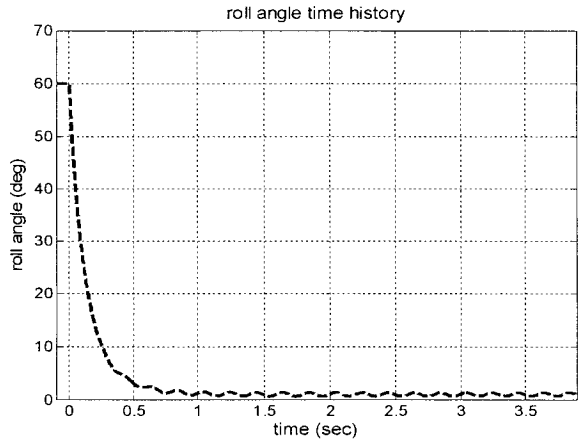

Figure 45. $x_3(t)$ time history, positive IC

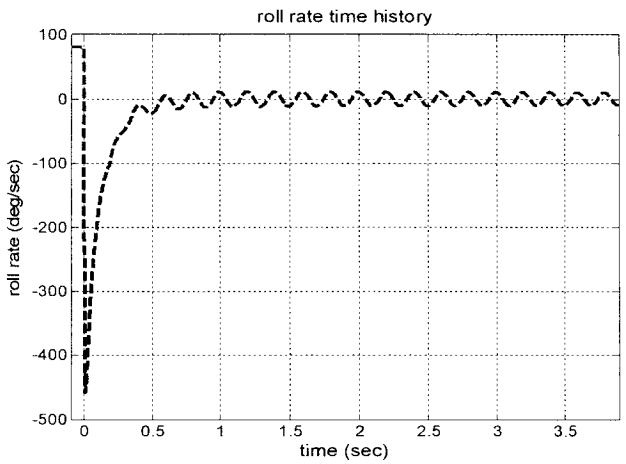

Figure 46. $x_4(t)$ time history, positive IC

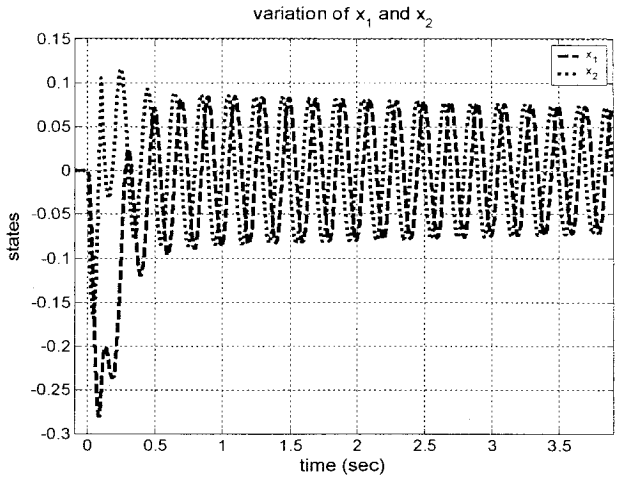

Figure 47. $x_1(t)$ and $x_2(t)$ time history, positive IC

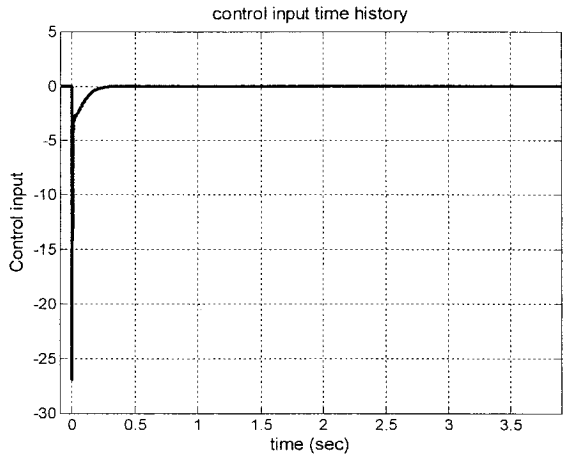

Figure 48. $u(t)$ (control input) time history, positive IC

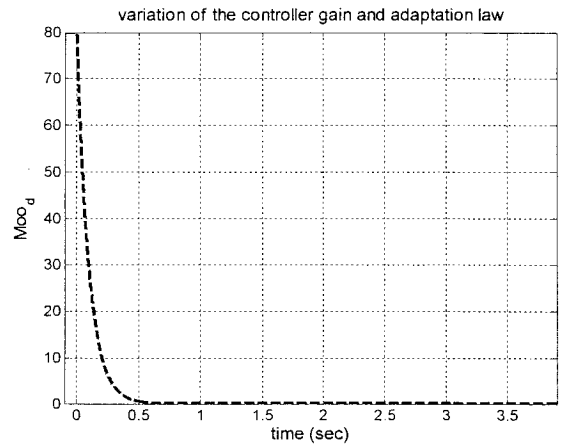

Figure 49. Variation of the controller gain μ_d, positive IC

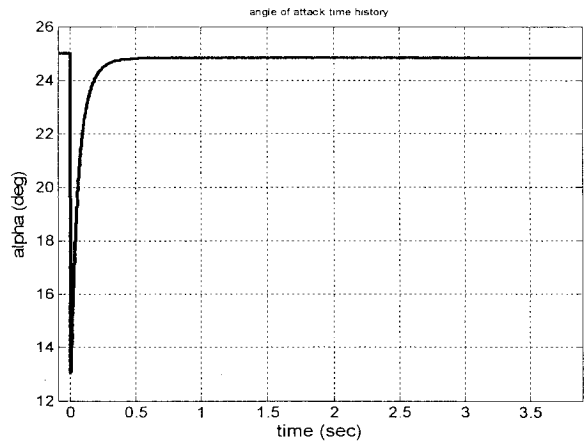

Figure 50. Angle of Attack time history, positive IC

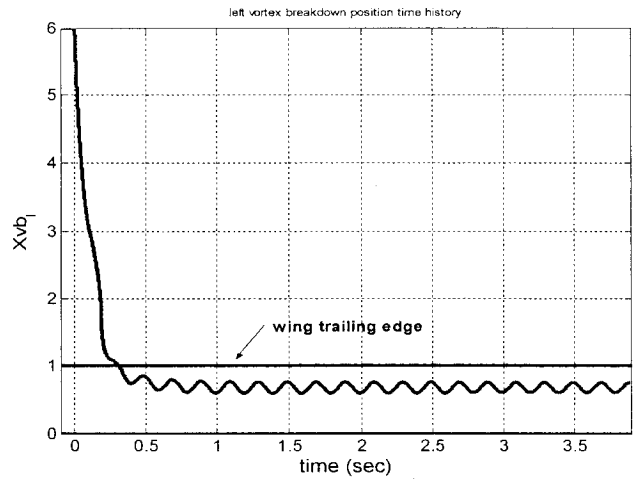

Figure 51. Left vortex breakdown position (X_{vbl}) time history, positive IC

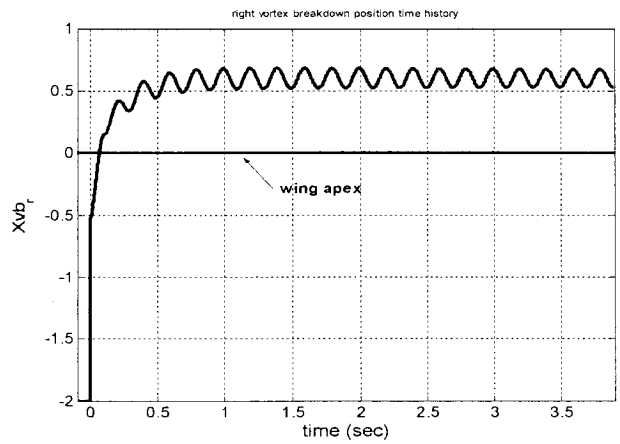

Figure 52. Right vortex breakdown position (X_{vbr}) time history, positive IC

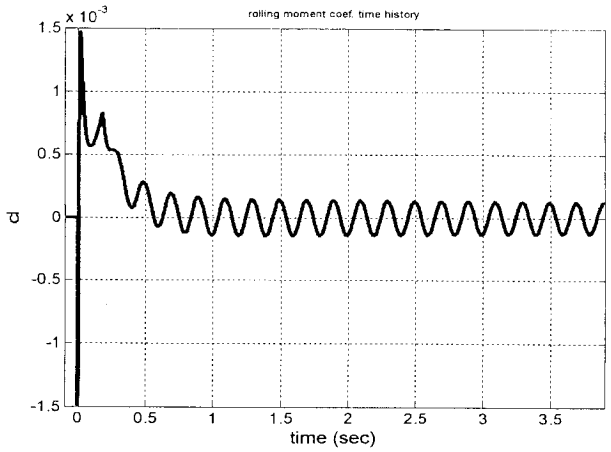

Figure 53. $C_l(\aleph)$ time history , positive IC

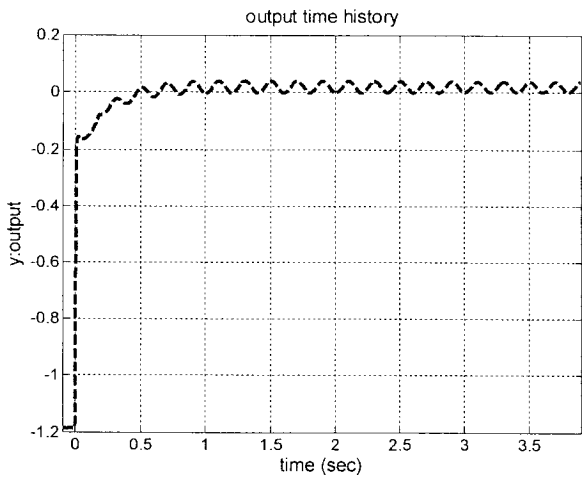

Figure 54. $y(t)$ time history (plant output), negative IC

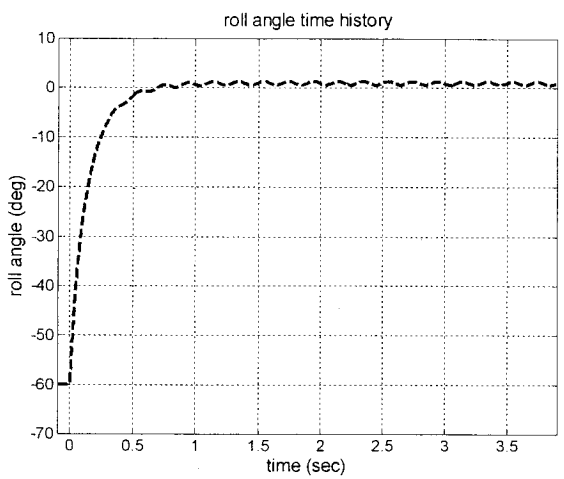

Figure 55. $x_3(t)$ time history, negative IC

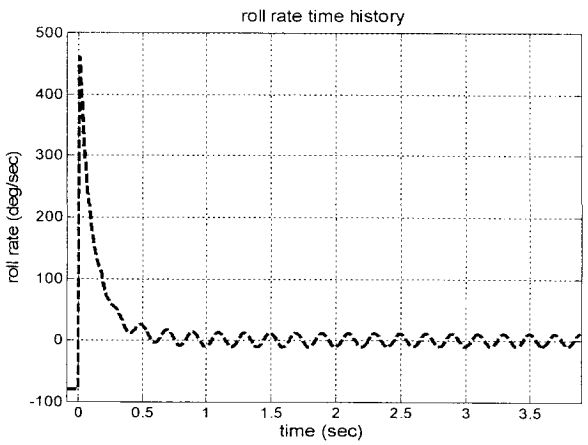

Figure 56. $x_4(t)$ time history , negative IC

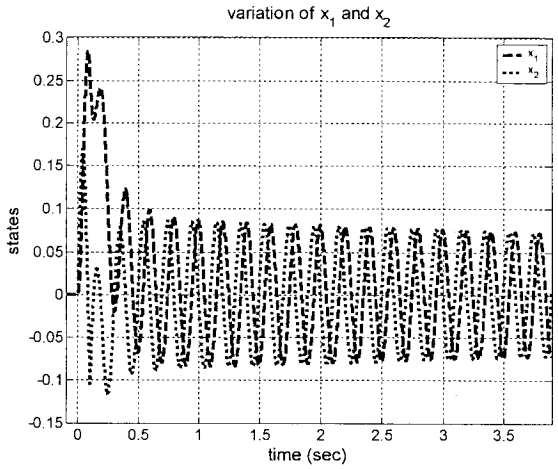

Figure 57. $x_1(t)$ and $x_2(t)$ time history, negative IC

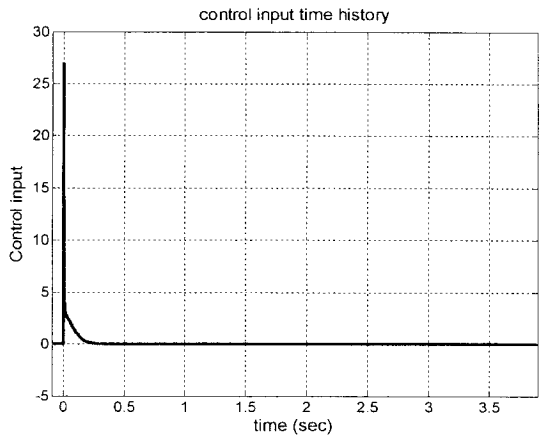

Figure 58. $u(t)$ (control input) time history, negative IC

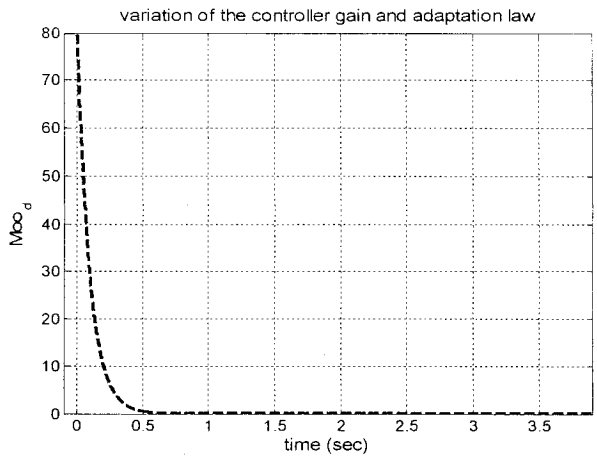

Figure 59. Variation of the controller gain μ_d , negative IC

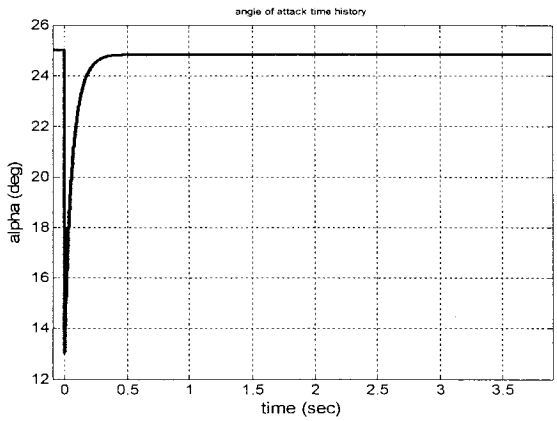

Figure 60. Angle of Attack time history, negative IC

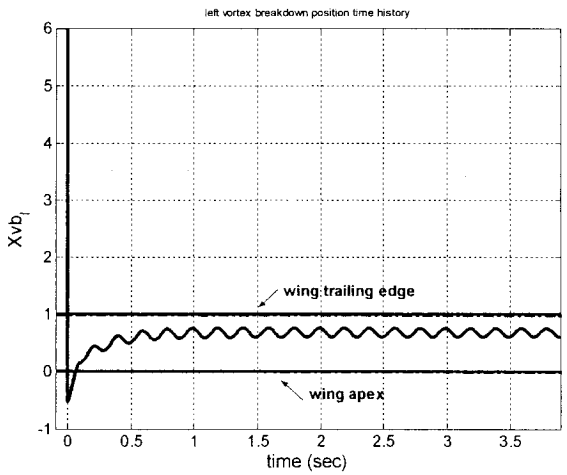

Figure 61. Left vortex breakdown position (X_{vbl}) time history, negative IC

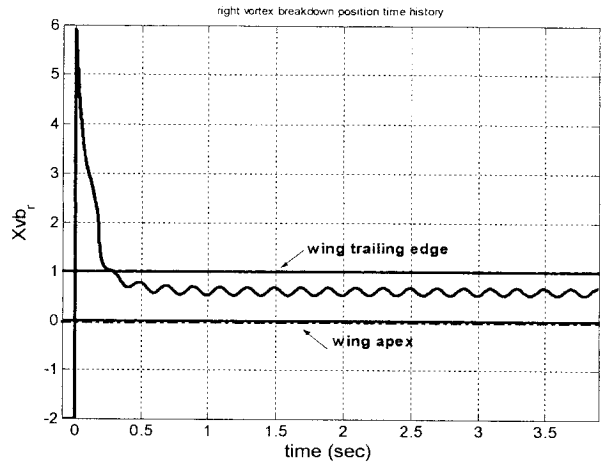

Figure 62. Right vortex breakdown position (X_{vbr}) time history, negative IC

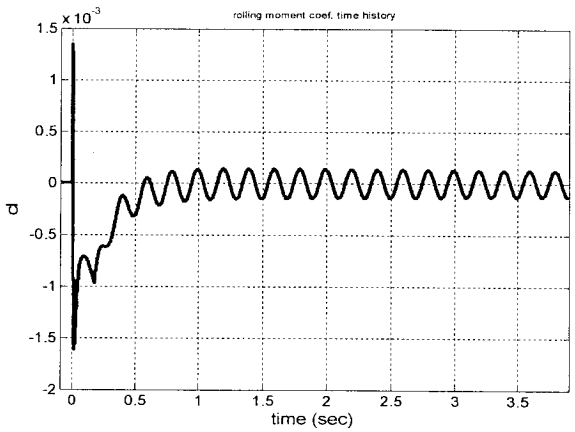

Figure 63. $C_l(\aleph)$ time history, negative IC

4.6 Summary

In this chapter we showed the applicability of an existing robust adaptive feedback stabilizing control strategy for the fast vortex-coupled roll dynamics of delta wing subject to state delay in a high AOA flight condition. The controller renders the closed-loop system globally practically stable. Simulations demonstrated the applicability of the controller for the fast and high performance delta wing dynamics. The heuristic design process and parameter selection methods have been proposed for easier implementation of this control scheme. This approach can be extended to multi-input,

multi-output (MIMO) model of delta wing vortex-coupled roll dynamics with state delay, and also to the model with variable delay.

5 . Robust Adaptive Tracking Control of Vortex-Coupled Delta Wing Systems Subject to State Delay

5.1 Introduction

In this chapter, we will propose a combinatory control structure to control the available high performance delta wing retarded dynamic system. The controller is a combination of robust state feedback controller as the internal loop of the combinatory controller and a sliding adaptive tracking controller which uses a special gaussian RBF neural network as the online estimator of the unknown nonlinearity. This controller will be applied to the vortex-coupled roll dynamics of the delta wing to track a complex reference trajectory. This complex trajectory is chosen to show the ability of the proposed combinatory controller to control the delta wing for complicated manoeuvres; since delta wings are high performance aerial vehicles which are flying in high angle of attack flight condition with subsonic or supersonic speeds.

The combinatory control input also will be applied to 4^{th} order delta wing vortex-coupled roll dynamics with state delay, and 6^{th} order delta wing vortex-coupled roll

dynamics with state delay and SMA micro-actuator dynamics, to check the effect of perturbations as inputs to the vortex breakdown dynamics. Heuristic design process and parameter selection methods will be proposed for easier implementation of the controllers with and without internal loop.

5.2 Delta Wing Vortex-Coupled Roll Dynamics

5.2.1 SISO Model

To implement the new control strategy, we repeat the modified state-space model of vortex-coupled delta wing roll dynamics presented in Chapter 4:

$$\begin{cases} \dot{x}_1(t) = c\, x_2(t) \\ \dot{x}_2(t) = -c\, x_1(t) - \varepsilon_d\, x_2(t) + x_4(t) + x_4(t-T) \\ \dot{x}_3(t) = -\varepsilon_d\, x_3(t) + x_4(t) \\ \dot{x}_4(t) = -C_l(\aleph) Q - f_c\, x_4(t) + (hu(t))/I_w \end{cases} \tag{5-1}$$

where $Q = qs_w b_w / I_w$, vortex breakdown vector is defined as follows:

$$\aleph = [X_{vbl}(t), X_{vbr}(t)]^T \tag{5-2}$$

Bearing friction has the following form:

$$f_c\, x_4(t) = (b_w / 2u_\infty)\, x_4(t) \tag{5-3}$$

Damping coefficient is selected as follows:

$$\varepsilon_d = 0.2 \tag{5-4}$$

Vortex breakdown locations in new form, without integral term and with state variables are as follows [40]:

$$X_{vbl}(t) = X_{sl}(x(t)) + X_{sl}(x(t))k_q(t)x_4(t) + a(t)x_1(t) \tag{5-5}$$

$$X_{vbr}(t) = X_{sr}(x(t)) + X_{sr}(x(t))k_q(t)x_4(t) - a(t)x_1(t) \tag{5-6}$$

where

$$k_q(t) = 0.91/\tan(\alpha(t)) \tag{5-7}$$

$$a(t) = 1.65/\tan(\alpha(t)) \tag{5-8}$$

Angle of attack is considered as follows [10]:

$$\alpha(t) = \arctan(\cos(\phi(t))\tan(\sigma)) \ [rad] \tag{5-9}$$

Release time (delay in the model):

$$T^* = T = 0.1 \text{ [sec]} \tag{5-10}$$

Rolling moment coefficient is a nonlinear function of vortex breakdown location [10], for now, we just assume it as a third order polynomial as follows [40]:

$$C_l(\aleph) = e_0 + e_1(X_{vbl} - X_{vbr}) + e_2(X_{vbl}^{\ 2} - X_{vbr}^{\ 2}) + e_3(X_{vbl}^{\ 3} - X_{vbr}^{\ 3}) \tag{5-11}$$

where X_{vbl} and X_{vbr} represent the breakdown locations for the left and right vortices, e_0, e_1, e_2 and e_3 are tuning parameters, which are obtained by third order least square estimation.

5.2.2 SISO Model with SMA Actuator Dynamics

To implement the dynamics of the SMA micro-actuator dynamics in the proposed model we will assume to first order filters as follows:

$$\begin{cases} \dot{x}_5(t) = (-x_5(t) + h_2\, u_2(t)) / \varepsilon_{SMA} \\ \dot{x}_6(t) = (-x_6(t) + h_3\, u_3(t)) / \varepsilon_{SMA} \end{cases} \tag{5-12}$$

Using the data presented in Ref. [43], we will assume ε_{SMA} is equal to the time the SMA micro-actuator flaps will react to their input commands. So its range will be:

$$[\min(t_{SMA})] \leq \varepsilon_{SMA} \leq [\max(t_{SMA})] \tag{5-13}$$

Implementing the model easily for control synthesis, the modified state-space model of vortex-coupled delta wing roll dynamics with delay and SMA actuator dynamics will be:

$$\begin{cases} \dot{x}_1(t) = c\, x_2(t) \\ \dot{x}_2(t) = -c\, x_1(t) - \varepsilon_d\, x_2(t) + x_4(t) + x_4(t-T) \\ \dot{x}_3(t) = -\varepsilon_d\, x_3(t) + x_4(t) \\ \dot{x}_4(t) = -C_l(\aleph) Q - f_c\, x_4(t) + h_1 u_1(t) / I_w \\ \dot{x}_5(t) = (-x_5(t) + h_2 u_2(t)) / \varepsilon_{SMA} \\ \dot{x}_6(t) = (-x_6(t) + h_3 u_3(t)) / \varepsilon_{SMA} \end{cases} \tag{5-14}$$

Vortex breakdown locations in new form, without integral term and coupled with SMA micro-actuators dynamics will be:

$$X_{vbl}(t) = X_{sl}(x(t)) + X_{sl}(x(t))\, k_q(t)\, x_4(t) + a(t)\, x_1(t) + x_5(t) \tag{5-15}$$

$$X_{vbr}(t) = X_{sr}(x(t)) + X_{sr}(x(t))\, k_q(t)\, x_4(t) - a(t)\, x_1(t) + x_6(t) \tag{5-16}$$

The two inputs $u_2(t)$ and $u_3(t)$ are associated with the left and right vortex breakdown locations X_{vbl} and X_{vbr} respectively. These two inputs can be considered as perturbation inputs. We will define these inputs in section 5.5.

5.3 State Feedback Stabilizing Controller

The state feedback controller has been presented in Theorem 2 in section 4.3.2. This control input in fact will be used as the internal loop of the final combined control structure which we are proposing in this chapter.

5.4 Tracking Controller Structure

We now design an adaptive sliding tracking controller. Rolling moment coefficient (C_l), as the main uncertain parameter, is estimated on-line in this controller. The sliding controller is designed as if the parameters to be estimated were known exactly, i.e. as if adaptation were successfully and exactly complete. Since this is initially not the case, the system first wanders outside the boundary layer, and the information thus generated is used to improve the parameters estimates. Conversely, the scheme recognizes that once in the boundary layer no advantage is gained by further adaptation, since even if the parameters of concern were exactly known, no improvement in tracking performance could be guaranteed formally.

5.4.1 Preliminaries

For this system $u(t)$ is the control input, C_l is an unknown non-linear function. The control objective is to force the state vector, $X = [x_3(t), x_4(t)]^T$ assumed available for measurement to follow a specified desired trajectory $X_d = [x_d(t), \dot{x}_d(t)]^T$. Defining the tracking error vector $\tilde{X}(t) = X(t) - X_d(t)$ the problem is thus to design a control law $u(t)$ which ensures that $\tilde{X}(t) \to 0$ as $t \to \infty$.

Reference model which has been applied to the controller is as follows:

$$\begin{cases} x_d(t) = x_d(t_0) + \sum_{i=1}^{M} A_i \sin(k_i t) \\ \dot{x}_d(t) = \sum_{i=1}^{M} A_i k_i \cos(k_i t) \\ \ddot{x}_d(t) = \sum_{i=1}^{M} -A_i k_i^2 \sin(k_i t) \end{cases} \qquad (5\text{-}17)$$

$$A_i = A, \; k_i = i, \; i = 1,2,..., M$$

Seeking agility and high maneuverability capabilities of delta wing in high angle of attack condition, a complex reference trajectory has been selected to show the controller capability to control high performance delta wing.

Using the approaches presented in Ref. [76] and [77], the proposed robust adaptive tracking controller structure is as follows:

$$u_{Track}(t) = u_{pd}(t) + m(t)\,u_{sl}(t) + (1 - m(t))\,u_{ad}(t) \qquad (5\text{-}18)$$

Here $u_{pd}(t)$ is a negative feedback term consisting of a weighted combination of both the measured tracking error states and a tracking metric $s(t)$ to be defined below. The term $u_{sl}(t)$, represents the sliding component of the tracking control law, and similarly the adaptive component is represented by $u_{ad}(t)$, which will attempt to recover and cancel the unknown function C_l. The function $m(t) = m(X)$ is a continuous, state dependent modulation which allows the controller for smooth transition between sliding and adaptive modes of operation, chosen so that $m(X) = 0$ on $\overline{A}_d$, $m(X) = 1$ on $\overline{A}_c$, and $0 < m(x) < 1$ on $\overline{A} - \overline{A}_d$.

$\overline{A}_d$ can be chosen so to correspond to a unit ball with respect to an appropriate weighted norm function. Thus, for example,

$$\bar{A}_d = \left\{X \mid \left\|X - X_0\right\|_{P,W} \le 1\right\} \text{ and } \bar{A} = \left\{X \mid \left\|X - X_0\right\|_{P,W} \le 1 + \Psi\right\} \tag{5-19}$$

Here Ψ is a positive constant representing the width of the transition region, X_0 fixes the absolute location of the sets in the state space of the plant, and $\|X\|_{P,W}$ is a weighted p-norm. In the limiting case

$$p = \infty \Rightarrow \|X\|_{\infty,W} = \max_{i=1}^{N}\left(\frac{x_i}{W_i}\right) \tag{5-20}$$

for a set of strictly positive weights $\{W_i\}_{i=1}^{N}$.

With these definitions, the modulation function can be taken as:

$$m(x(t)) = \max(0, sat(\frac{r(t)-1}{\Psi})) \tag{5-21}$$

where $r(t) = \|X(t) - X_0\|_{P,W}$ and *sat* is the saturation function. When $r(t) \le 1$, meaning that $X \in \bar{A}_d$, the output of the saturation function is negative, hence the maximum which defines $m(X)$ is zero, as desired. When $r(t) \ge 1 + \Psi$ corresponding to $X \in \bar{A}^c$ (where $\bar{A}^c$ is the complement of the set $\bar{A}$ in $\Re^n$, i.e., $\bar{A}^c = \Re^n - \bar{A}$) the saturation function is unity, hence $m(X) = 1$, again as desired. In between, for $X \in \bar{A} - \bar{A}_d$, it is easy to check that $0 < m(X) < 1$.

A useful tracking error metric for both sliding and adaptive control subsystems is defined by

$$s(t) = \Theta^T \tilde{X} = \dot{\tilde{x}}_3(t) + \lambda \tilde{x}_3(t) \tag{5-22}$$

where $\Theta^T = [\lambda\ 1]$ and $\lambda > 0$. The equation $s(t) = 0$ defines a time-varying hyperplane in $\Re^2$ on which the tracking error vector decays exponentially to zero [77]. If the

magnitude of S can be shown to be bounded by a constant ε (boundary layer), the actual tracking errors can be shown [77] to be asymptotically bounded by:

$$\left|\tilde{x}^{(i)}(t)\right| \le 2^i \lambda^{i-n+1}\varepsilon, \quad i = 0,1,...,n-1 \tag{5-23}$$

5.4.2 Gaussian Radial Basis Function Approximation

It is by now well known that three layer feed forward neural networks, i.e. networks with one hidden layer of nonlinear nodes, can uniformly approximate continuous functions over compact subsets of their domains. This holds both for networks with hidden nodes which output smoothly saturating functions of their argument, such as the standard "sigmoid" operating on the dot product of the input signals and feed-in weights, as well as the "radial basis function" nodes, which output nonlinear functions of the Euclidean distance from the network inputs to the corresponding set of feed-in weights [76].

In the proposed adaptive controller, the online C_l estimation will be implemented by a gaussian radial basis function (RBF) Neural Networks specially developed for our case using left and right vortex breakdown positions, which can be represented mathematically as:

$$\hat{C}_l(\aleph) = (\sum_{i=1}^{N} w_i \Delta g_i(X_{vbl\&r}, \xi_{l\&ri})) \tag{5-24}$$

inputs to the RBF NN:

$$X_{vbl} = (a_l, b_l) \subset R \;\&\; X_{vbr} = (a_r, b_r) \subset R \tag{5-25}$$

centers :

$$\xi_{li} = a_l + i\Delta_l,\ \Delta_l = (b_l - a_l)/N,\ \ \xi_{ri} = a_r + i\Delta_r,\ \Delta_r = (b_r - a_r)/N \tag{5-26}$$

gaussian RBFs :

$$g_{li} = \exp(-(X_{vbl} - \xi_{li})/(2\sigma_l^2)),\ \ g_{ri} = \exp(-(X_{vbr} - \xi_{ri})/(2\sigma_r^2)) \tag{5-27}$$

$$\Delta g_i = g_{li} - g_{ri}$$

widths:

$$\sigma_l = (b_l - a_l)/\sqrt{2N^2},\ \ \sigma_r = (b_r - a_r)/\sqrt{2N^2} \tag{5-28}$$

where g_{li} and g_{ri} are the nonlinear functions implemented by node i in two subcomponents of the first hidden layer and Δg_i is a linear combination of two subcomponents of the first hidden layer in second hidden layer; ξ_{li} and ξ_{ri} represent the input weights (or "center" in the radial basis function literature) of node i, and w_i represents the output weight for that node which is updated using the adaptation law.

Figure 64 shows conceptual illustration of RBF NN proposed for online estimation of uncertainty, which is used in adaptive control component of tracking controller. This figure shows two hidden layers of the network, first one is combined of two sub-layers and the second hidden layer is a linear combination of these two sub-layers.

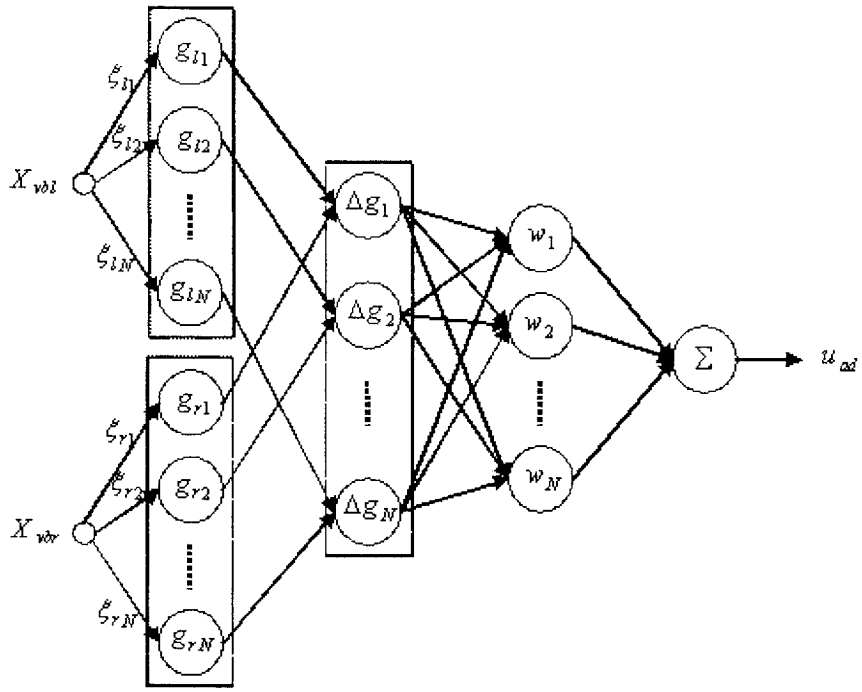

Figure 64. Radial Basis Function (RBF) neural network structure proposed for online estimation of rolling moment coefficient.

5.4.3 Tracking Controller Subsystems

Using the metric $s(t)$ and the saturation function, the control subsystems defined as follows:

$$a_r(t) = [0\ \lambda]\tilde{X}(t) - \ddot{x}_d(t) \tag{5-29}$$

$$u_{pd}(t) = -(k_d s(t) + a_r(t)) \tag{5-30}$$

$$u_{sl}(t) = -k_{sl}\ sat(s(t)/\varepsilon) \tag{5-31}$$

$$u_{ad}(t) = \hat{C}_{l\bar{A}}(\aleph)Q = (\sum_{i=1}^{N} \hat{w}_i(t)\Delta g_i) qs_w b_w \tag{5-32}$$

Deadzone adaptation requires discontinuously starting and stopping the parametric adjustment mechanism according to the magnitude of the error signal. These

discontinuities can be eliminated using the metric $s(t)$, by introducing the continuous function s_Δ defined as:

$$s_\Delta(t) = s(t) - \varepsilon \ sat(s(t)/\varepsilon) \tag{5-33}$$

Adaptation law:

$$\dot{\hat{w}}_i = -k_a(1-m(t))s_\Delta \Delta g(X_{vbl\&r}(X(t)), \xi_{l\&ri}) \tag{5-34}$$

$$\Delta g(X_{vbl\&r}(X(t)), \xi_{l\&rl}) = Y_{1*N} \tag{5-35}$$

where k_d, k_{sl} and k_a are positive constants which should be chosen for each of the control subsystems. k_{sl} should be selected sufficiently large for the sliding controller to overcome the uncertainties.

5.4.4 Tracking Controller Stability

To prove the stability of the controller introduced above for the case where there is no time delay a Lyapunov like function candidate has been proposed [76]. By using Barbalat's lemma [75] this establishes convergence of s_Δ to zero. Hence the inequality $|s(t)| \le \varepsilon$ holds asymptotically, and the asymptotic bounds on the individual tracking errors follow using (5-23). However, for the case where there is a time delay, such as the vortex coupled model, the internal dynamics must also be stable for this method to apply. Therefore, there is no firm stability guarantee for this case without some further analysis. The controller for this case is essentially a design approach with no rigorous stability proof.

Figure 65 shows a flowchart which proposes the heuristic process for control design and parameter selection sequence for easier application of this tracking controller to delta wing vortex-coupled dynamics. More explanations will be presented in section 5.6 about how to select parameters.

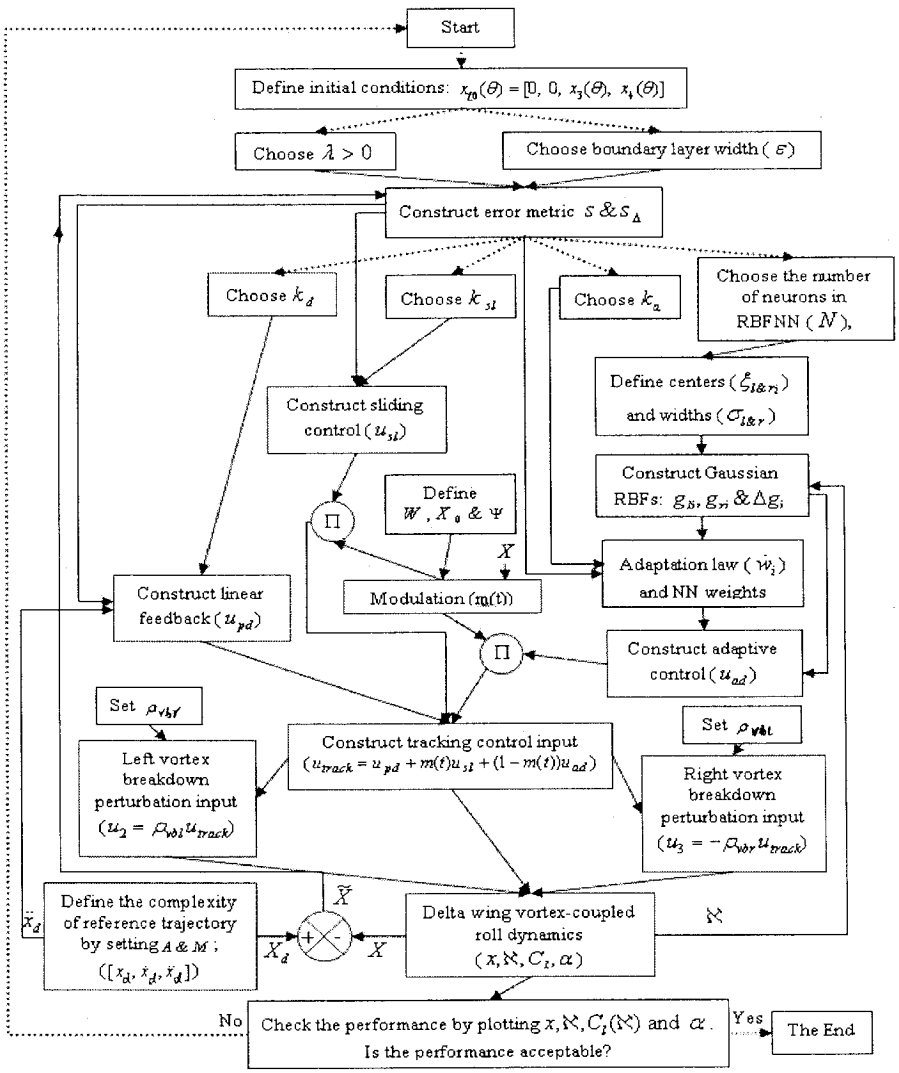

Figure 65. Flowchart for application of tracking control to the delta wing dynamics

To compare this controller with the adaptive controller presented in the Chapter 4, we have assumed zero reference trajectory and applied the controller to the retarded vortex-coupled delta wing SISO model. The simulation results of this controller for

stabilization purpose have been shown in figures 66 to 69. Comparing these figures with figures 45 to 48, we will notice that the performance of the adaptive stabilizer controller presented in Chapter 4 is better. This is one of the reasons which we will use the stabilizer controller presented in previous chapter as the internal loop of the final controller to be presented in this chapter.

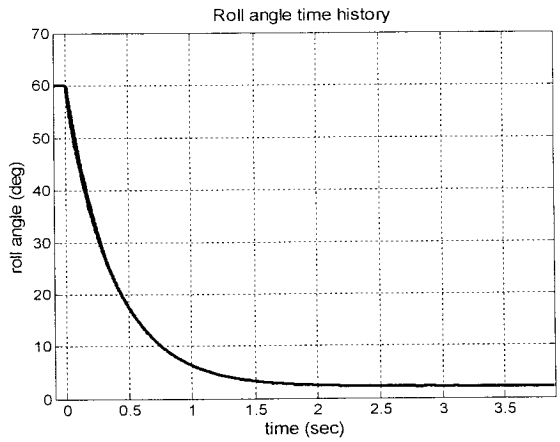

Figure 66. $x_3(t)$ time history, using NN adaptive controller, positive IC

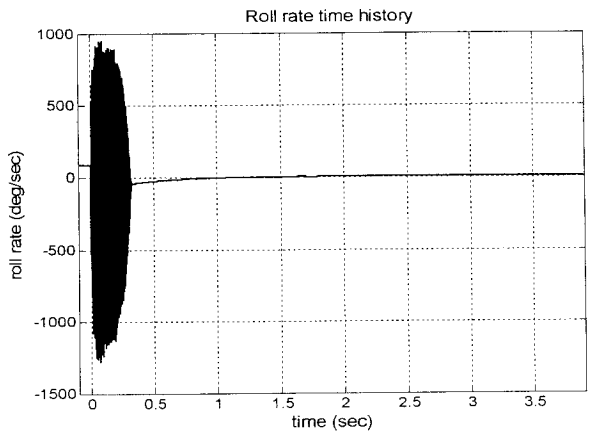

Figure 67. $x_4(t)$ time history, using NN adaptive controller, positive IC

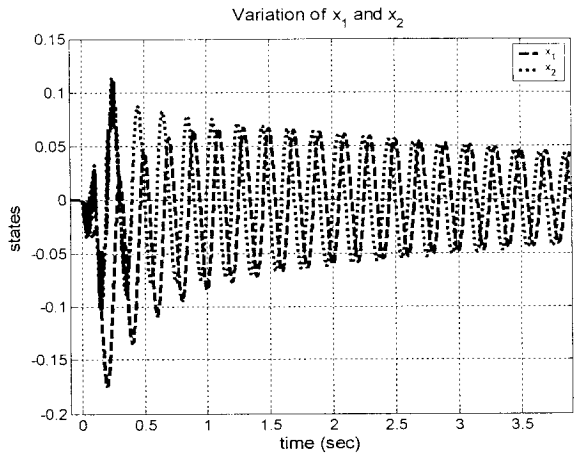

Figure 68. $x_1(t)$ and $x_2(t)$ time history, using NN adaptive controller, positive IC

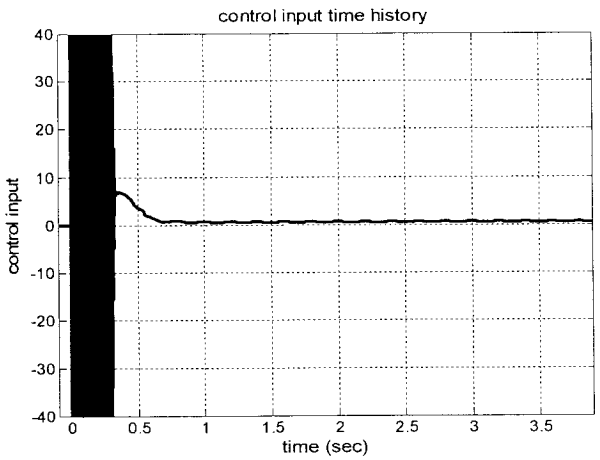

Figure 69. $u(t)$ (control input) time history, using NN adaptive controller, positive IC

Figures 72 to 82 show the results of the numerical simulation of tracking control applied to the delta wing SISO model coupled with SMA actuator dynamics to track the complex reference trajectory.

5.5 Final Controller Structure

The final robust adaptive tracking controller (combined controller) structure is presented as follows:

$$
\begin{aligned}
u(t) &= u_{Track}(t) + u_{Stab}(t) \\
&= u_{pd}(t) + m(t)u_{sl}(t) + (1 - m(t))u_{ad}(t) + u_{\rho}(x_t, t) \\
&= -(k_d s(t) + a_r(t)) - m(t)k_{sl}\, sat(s(t)/\varepsilon) \\
&\quad + (1 - m(t))(\sum_{i=1}^{N} \hat{w}_i(t)\Delta g_i)qs_w b_w - \mu_0 H_0 y(t)
\end{aligned}
\tag{5-36}
$$

The control inputs for the SISO model coupled with SMA actuator dynamics, are as follows:

$$u_1(t) = u(t) \tag{5-37}$$

$$u_2(t) = \rho_{vbl} u(t) \tag{5-38}$$

$$u_3(t) = -\rho_{vbr} u(t) \tag{5-39}$$

where ρ_{vbl} and ρ_{vbr} are defining the effect of perturbation inputs on the vortex breakdown location and also its effects on the control task.

Figure 70 is the illustration of the structure of proposed combinatory robust adaptive tracking controller with internal loop.

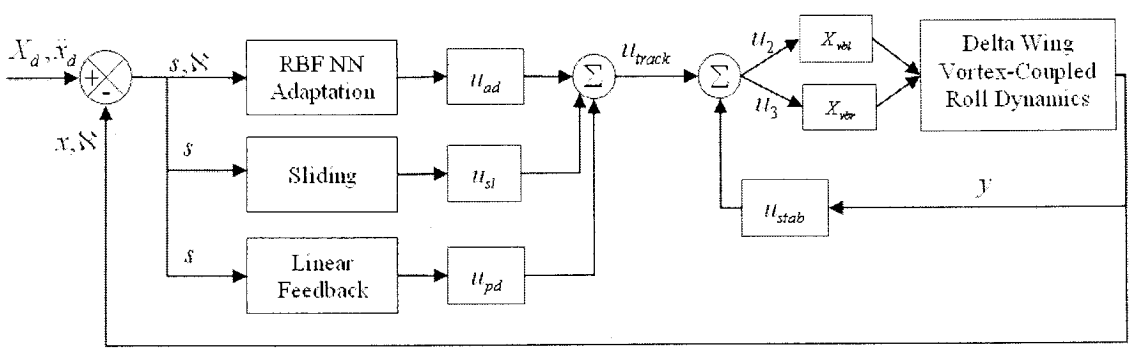

Figure 70. Conceptual illustration of the combinatory control structure.

5.6 Control Design and Parameter Selection

This section is about optimising the performance, by presenting an algorithm of the control design and parameter selection by doing a trade-off among the main parameters; we will discuss their impact on the performance later.

The practical algorithm of the control design and parameter selection procedure for tracking control of delta wing vortex-coupled dynamics, which is a combination of *Trial and error*, *experience* and *heuristic*, is as follows:

1. Set the initial conditions: $x_{t0}(\theta) = [0,\ 0,\ x_3(\theta),\ x_4(\theta)]$;
2. For the state feedback control component (internal loop):
   I. Define the output matrix C_0, by setting d and e ;
   II. Select a proper $Q_0 = \xi \times I;\ \xi > 0$, by setting ξ, so $\lambda_{\max}[Q_0] = \lambda_{\min}[Q_0] = \xi$;
   III. Compute P_0 and H_0 using one of the proposed methods, with the aid of MATLAB.
   IV. Select $\Delta \in (0,1)$ and $\Gamma_u \in \Re_+$ as the design parameters;
   V. Find proper ς and ϑ, by trial and error to define the bounds of the uncertainties;
   VI. Compute μ_M and select $\mu_0 > \mu_M$;
   VII. Compute state feedback control input: $u_\rho(x_t, t) = -\mu_0 H_0 y(t)$;
3. For the tracking control component:
   I. Define the complexity of reference trajectory by setting A and M; then compute $[x_d, \dot{x}_d, \ddot{x}_d]$;

II. Choose $\lambda > 0$ and ε;

III. Construct error metric s and also s_Δ;

IV. Choose k_d, k_{sl} and k_a which are positive real constants;

V. Choose the number of neurons in RBF neural network: N;

VI. Define centres and widths of gaussian RBFs;

VII. Construct gaussian RBFs: g_{li}, g_{ri} & Δg_i;

VIII. Compute adaptive parameter $\dot{w}_i$ which is the output weight of the RBFs;

IX. Define W, X_0 & Ψ to be used in modulation;

X. Compute modulation: $m(t) = \max(0, sat(\frac{r(t)-1}{\Psi}))$, $r(t) = \|X(t) - X0\|_{P,W}$;

XI. Compute linear feedback: $u_{pd}(t) = -(k_d s(t) + a_r(t))$;

XII. Compute sliding control: $u_{sl}(t) = -k_{sl}\, sat(s(t)/\varepsilon)$;

XIII. Compute adaptive control: $u_{ad}(t) = \hat{C}_{lA}(\aleph) = (\sum_{i=1}^{N} \hat{w}_i(t)\Delta g_i) q s_w b_w$, which is compensates for the unknown nonlinearity;

XIV. Compute tracking control input: $u_{track} = u_{pd}(t) + m(t)u_{sl}(t) + (1 - m(t))u_{ad}(t)$;

XV. Compute the overall control input:

$$u_1 = u_{pd}(t) + m(t)u_{sl}(t) + (1 - m(t))u_{ad}(t) + u_\rho(x_t, t)$$

4. Set ρ_{vbl} and ρ_{vbr}, which gives the perturbation intensity for left and right vortex breakdown locations;

5. Compute the left and right vortex breakdown perturbation inputs: $u_2(t) = \rho_{vbl} u_1(t)$, $u_3(t) = -\rho_{vbr} u_1(t)$;

6. Apply the control inputs to the delta wing vortex-coupled roll dynamics $(x, \aleph, C_l, \alpha)$;

7. Check the performance, if it is acceptable using practical stability notion and the designer engineering sense, then the process is ended, if not go to step 1, and repeat the process to capture the required performance.

For required performance the designer should trade-off among the main parameters, to be discussed here. The following notes are done based on various simulations to study the sensitivity of the control process to the selective design parameters and the effect of these parameters on the control process:

Initial guesses for μ_0 does not affect the system performance; it simply influences the implementation of the control action. Therefore simulations should be used to determine a suitable μ_0, as simulation studies prove it. By increasing e, with a constant d, i.e. adding more proportion of roll rate to output (in internal loop). The extremum of roll rate will be smaller, but the extremum of control input will be larger. The extremums in vortex breakdown related states, i.e. x_1 and x_2, will be smaller. Changing ξ, results in changes in $\|Q_0\|$ and $\|P_0\|$ and hence in $\|H_0\|$. H_0 is not unique so we can optimise the performance via changing H_0, with regard to the fact that its variations won't change the stability. With larger amounts of ξ, states and control input reach to their steady-state level faster, but with the cost of higher extremums in control input and roll rate.

λ is a positive coefficient in error metric; increasing this constant results in a better tracking performance, with the expense of increasing the control effort. ε defines the width of a boundary layer, which is used to prevent discontinuous control transitions.

For better performance of the controller, i.e. less tracking error, this parameter should be smaller. k_a, in fact, determines the adaptation rate, increasing this constant the controller adaptation rate increase; by increasing the complexity of the reference model, this constant should be increased. k_d is the linear feedback gain in tracker controller, increasing this gain will enhance the tracking performance. k_{sl} is the gain of the sliding controller; it should be selected large enough to overcome the uncertainties. N is the number of neurons in RBF neural network; increasing this number increases the ability of neural net for online estimation of unknown nonlinearity, but on the other hand, it will increase the computational effort. σ_l and σ_r are the widths of proposed RBFs; they can be set based on the speed of variation in nonlinearity. ρ_{vbl} and ρ_{vbr} are defining the amount of disturbances which are applying to the left and right vortex breakdowns to enhance the controllability, but it should not be very high, since it will cause the instability of the system. In the modulation function, Ψ is a positive constant, defines the width of the transition region between $\overline{A}$ and $\overline{A}_d$ sets; X_0 is the centers' vector to be defined using the reference model; W_i define the weights for computing the p-norms in the modulation function. These weights can be set using the range of change of the x_d and $\dot{x}_d$ in the reference model.

To have an acceptable performance, one should trade off between the discussed parameters as the main parameters in such a way to find the best combination of "*error and its rate*", "*control effort*" and "*computational effort*". Figure 71 shows a flowchart which proposes the process for the control design and parameter selection sequence. This

algorithm helps easier implementation of the proposed combinatory control structure for the delta wing vortex-coupled dynamics.

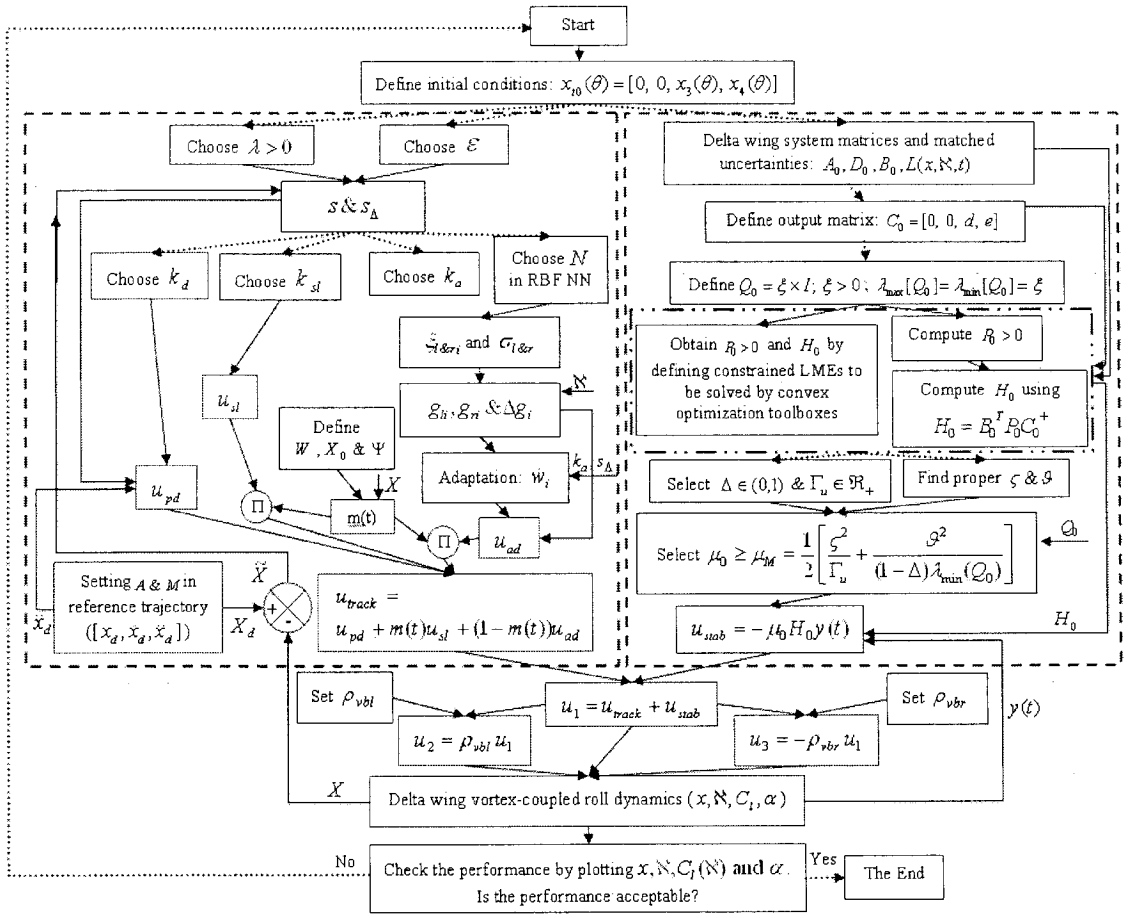

Figure 71. Flowchart for application of the combined control law to the delta wing vortex-coupled dynamics.

5.7 Numerical Simulation and Discussion

Different simulations have been done to show the controllers performance. The initial conditions for all of these simulations set as: $v(\theta): x_1(\theta)=x_2(\theta)=0, x_3(\theta)=30\,[\text{deg}], x_4(\theta)=100[\text{deg/sec}]$. The complexity of the reference trajectory has been defined by setting the related parameters to be $A=0.05,\ M=6$.

For numerical simulation of *tracking control* of the *delta wing SISO model coupled with SMA micro-actuator dynamics*, we chose $k_d = 1, k_{sl} = 1, k_a = 10$, $\lambda = 20$ and $\varepsilon = 0.01$ for the tracking controller; and also we assumed $\rho_{vbl} = \rho_{vbl} = 0.1$ and $\varepsilon_{SMA} = 0.1$. Simulation results for the controller have been shown in Figure 72 to 82. Figure 72, shows the time history of the $x_3(t)$ state and its reference; tracking performance is not good. Figure 73, shows the time history of $x_4(t)$ state and its reference. Figure 74, shows the time history of $x_1(t)$ and $x_2(t)$ states. Figure 75 and 76, show error and error derivative time histories. Figure 77, shows the control input time history. Figure 78, shows the control input components time history. Figure 79, show the sliding time history; as it is apparent variation is inside the proposed boundary layer but there are some big jumps. Figure 80, shows the time history of the left vortex breakdown location on the wing after implementing u_2 in the left vortex breakdown equation. Figure 81, shows the time history of the right vortex breakdown location on the wing after implementing u_3 in the right vortex breakdown equation. Figure 82, shows the time history of x_5 and x_6 states, which are the first order filters implemented for left and right vortex breakdown locations consequently. Figures show that the controller is stable but the tracking performance is not good enough.

The following two simulations are done by applying the proposed combinatory control law to show the superior performance of this controller in comparison to the sole tracker control. The output matrix for stabilizing controller is set as: $C_0 = [0\ 0\ 1\ 0\ 0\ 0]$.

For numerical simulation of controlling the *delta wing SISO model*, we chose $\eta = T = 0.1[\text{sec}], \Delta = 0.5, \Gamma_u = 15$ and $\mu_0 = 256$ for the stabilizing control, and

$k_d = 1, k_{sl} = 1, k_a = 10$, $\lambda = 20$ and $\varepsilon = 0.01$ for the tracking controller. Simulation results for the controller have been shown in Figure 83 to 93. Figure 83 shows the time history of the $x_3(t)$ state and its reference, which tracking performance is quite good Figure 84, shows the time history of $x_4(t)$ state and its reference. Figure 85, shows the time history of $x_1(t)$ and $x_2(t)$ states. Figure 86 and 87, show error and error derivative time histories. Figure 88, shows the control input time history. Figure 89, shows the control input components time history. Figure 90 and 91, show the sliding time history and its zoomed in figure; as it is apparent variation is inside the proposed boundary layer i.e. the inequality $|s(t)| \le \varepsilon$ holds asymptotically. Figure 92, shows the time history of the left vortex breakdown location on the wing. Figure 93, shows the time history of the right vortex breakdown location on the wing. Figures show that the controller is stable and has an acceptable and accurate tracking performance and also has enough robustness to parameter uncertainties.

For numerical simulation of controlling the *delta wing SISO model coupled with SMA micro-actuator dynamics*, we chose $\eta = T = 0.1[\text{sec}], \Delta = 0.5, \Gamma_u = 15$ and $\mu_0 = 256$ for the stabilizing control, and $k_d = 1, k_{sl} = 1, k_a = 10$, $\lambda = 20$ and $\varepsilon = 0.01$ for the tracking controller; and also we will assume $\rho_{vbl} = \rho_{vbl} = 0.1$ and $\varepsilon_{SMA} = 0.1$. Simulation results for the controller have been shown in Figure 94 to 105. Figure 94, shows the time history of the $x_3(t)$ state and its reference, which tracking performance is quite good. Figure 95 shows the time history of $x_4(t)$ state and its reference. Figure 96 shows the time history of $x_1(t)$ and $x_2(t)$ states. Figure 97 and 98, show error and error derivative time histories. This figure shows less tracking error in comparison to the case without perturbation

inputs. Figure 99, shows the control input time history. Figure 100 shows the control input components time history. Figure 101 and 102 show the sliding time history and it's zoomed in figure for better visibility; as it is apparent variation is inside the proposed boundary layer i.e. the inequality $|s(t)| \leq \varepsilon$ holds asymptotically. Figure 103 shows the time history of the left vortex breakdown location on the wing after implementing u_2 in the left vortex breakdown equation. Figure 104 shows the time history of the right vortex breakdown location on the wing after implementing u_3 in the right vortex breakdown equation. Figure 105 shows the time history of x_5 and x_6 states, which are the first order filters implemented for left and right vortex breakdown locations consequently. Figures show that the controller is stable and has an acceptable and accurate tracking performance and also has enough robustness to parameter uncertainties.

It is apparent from figures that the control scheme with perturbations applied in vortex breakdown locations i.e. choosing ρ_{vbl} and $\rho_{vbr} > 0$, via SMA micro-actuators performs better than the control scheme without perturbations i.e. $\rho_{vbl} = \rho_{vbr} = 0$. This has been demonstrated in better tracking performance and less control effort for the same numerical control simulation.

The figures which are relating to the simulation with combinatory control input (with internal control loop) show enhanced tracking performance in comparison to the simulations of the dynamic with tracking control (without internal control loop) as the control input, and this shows the advantage of the proposed combinatory control structure for vortex-coupled delta wing dynamics.

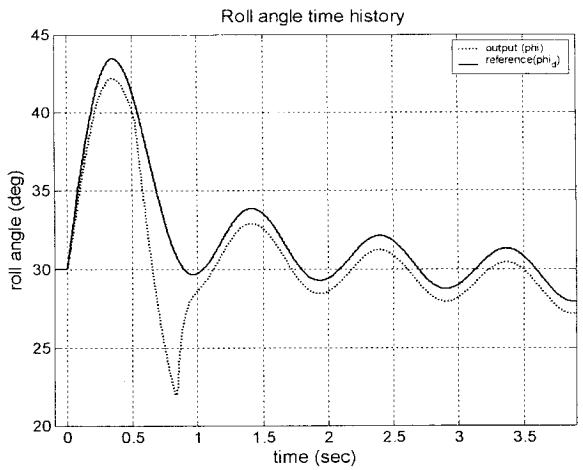

Figure 72. φ *and* φ_d time history

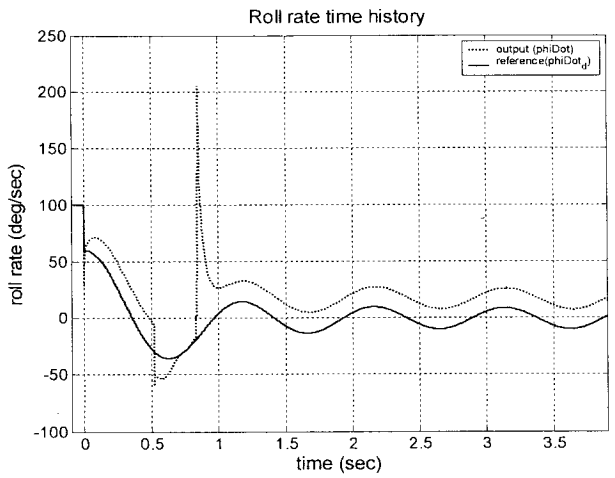

Figure 73. $\dot{\varphi}$ *and* $\dot{\varphi}_d$ time history

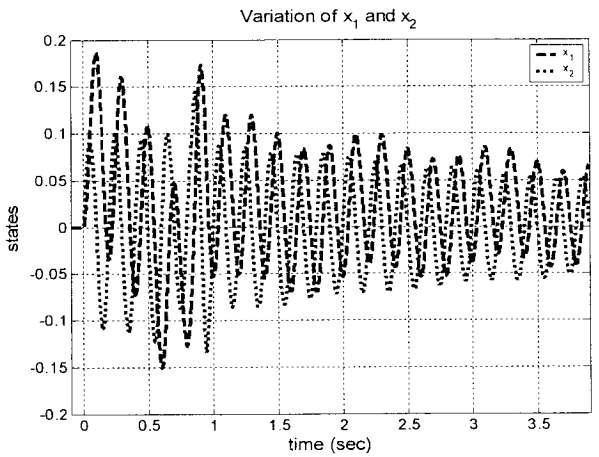

Figure 74. x_1 and x_2 time history

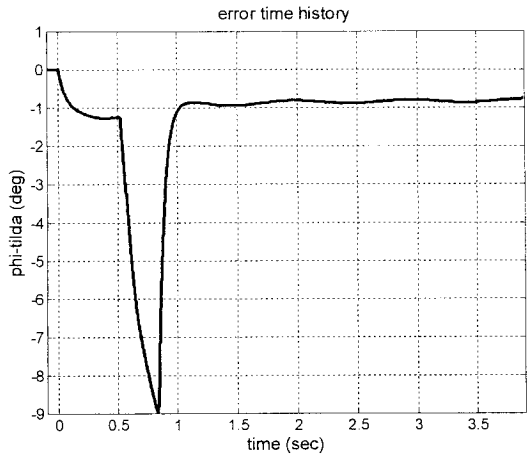

Figure 75. Error ($\tilde{\varphi} = \varphi - \varphi_d$) time history

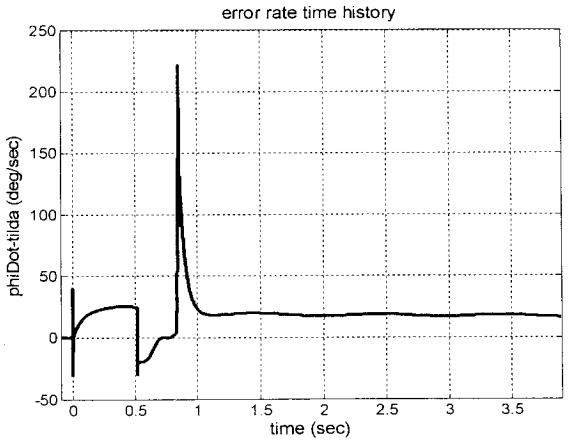

Figure 76. Error rate ($\dot{\tilde{\varphi}} = \dot{\varphi} - \dot{\varphi}_d$) time history

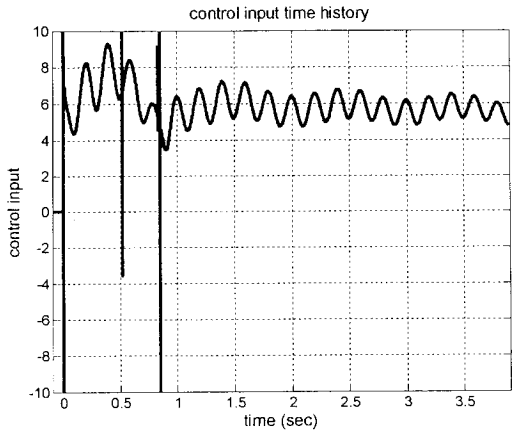

Figure 77. *u(t)* (overall control input) time history

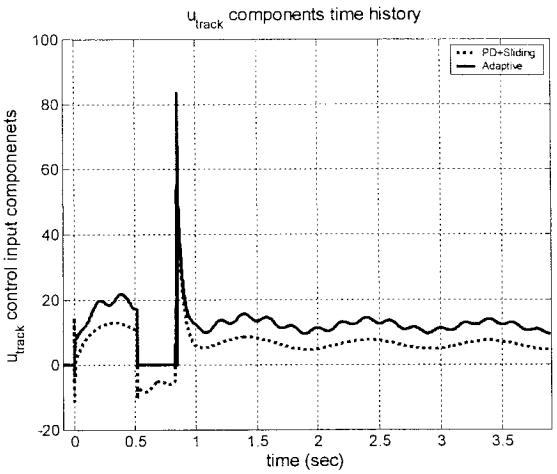

Figure 78. Control input components time history

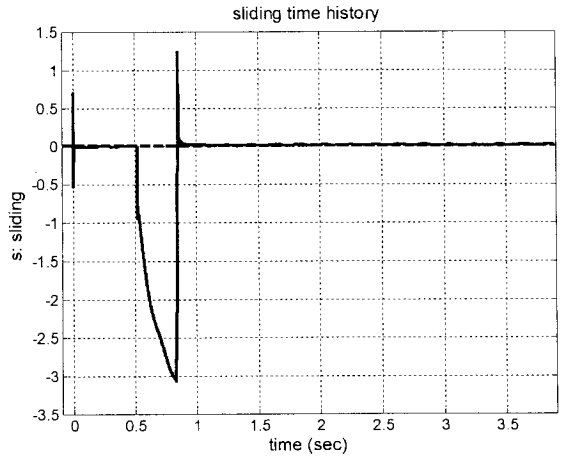

Figure 79. $s = \dot{\tilde{\varphi}} - \lambda\tilde{\varphi}$ (sliding) time history

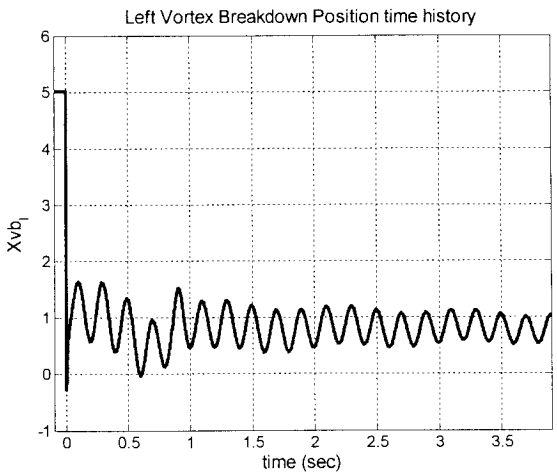

Figure 80. X_{vbl} time history with $u_2(t)$ control input

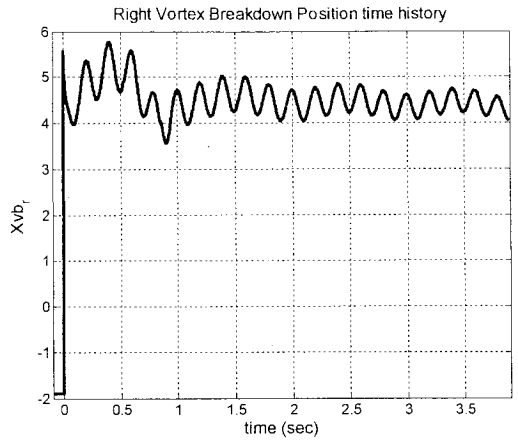

Figure 81. X_{vbr} time history with $u_3(t)$ control input

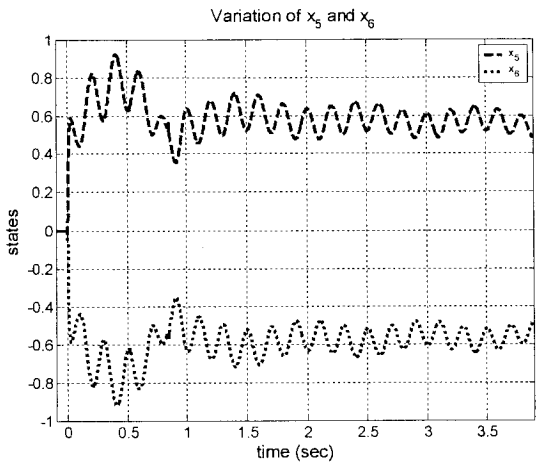

Figure 82. x_5 and x_6 time history

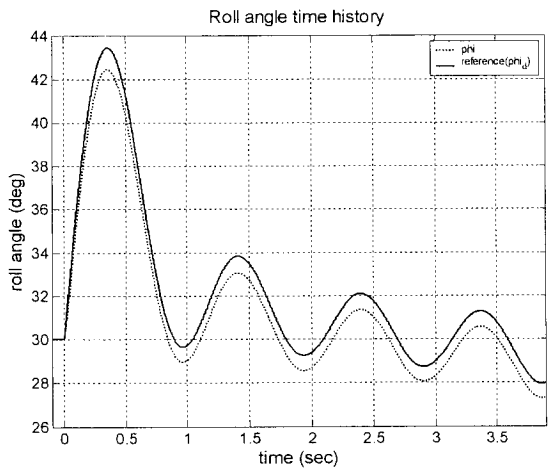

Figure 83. φ *and* φ_d time history - SISO case controlled by combinatory control input

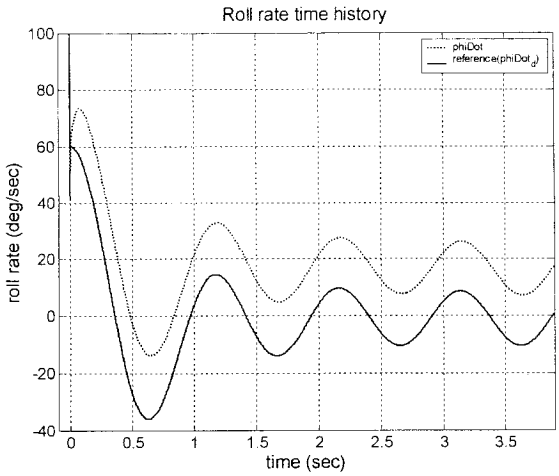

Figure 84. $\dot{\varphi}$ *and* $\dot{\varphi}_d$ time history - SISO case controlled by combinatory control input

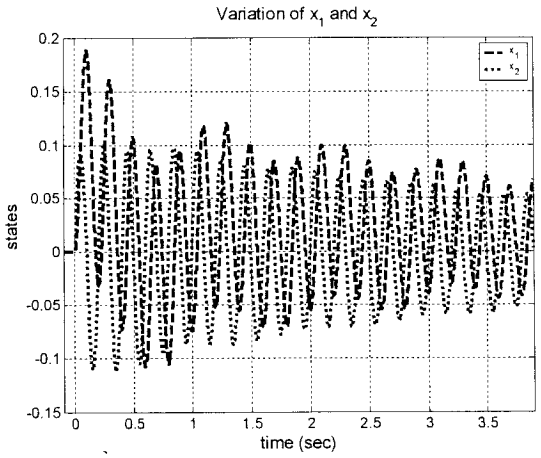

Figure 85. x_1 and x_2 time history- SISO case controlled by combinatory control input

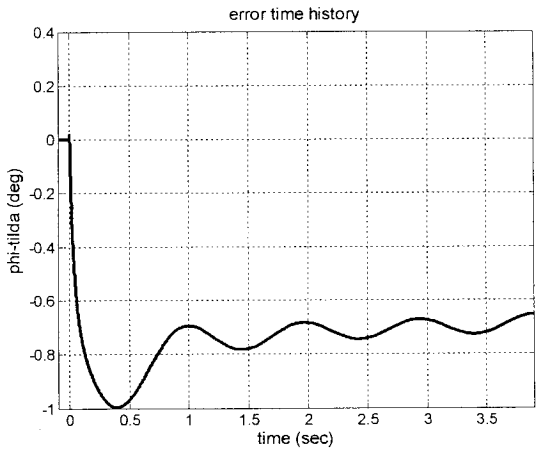

Figure 86. Error ($\tilde{\varphi} = \varphi - \varphi_d$) time history- SISO case controlled by combinatory control input

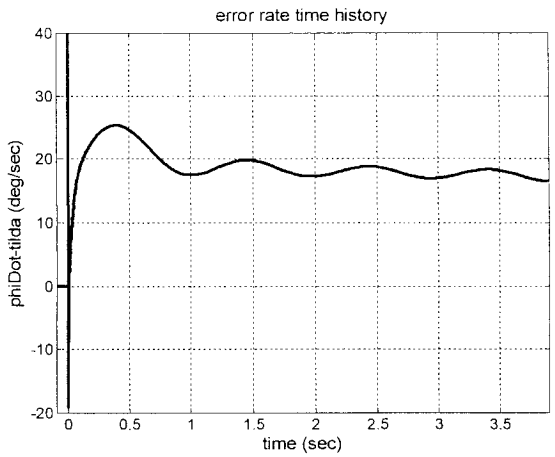

Figure 87. Error rate ($\dot{\tilde{\varphi}} = \dot{\varphi} - \dot{\varphi}_d$) time history- SISO case controlled by combinatory control input

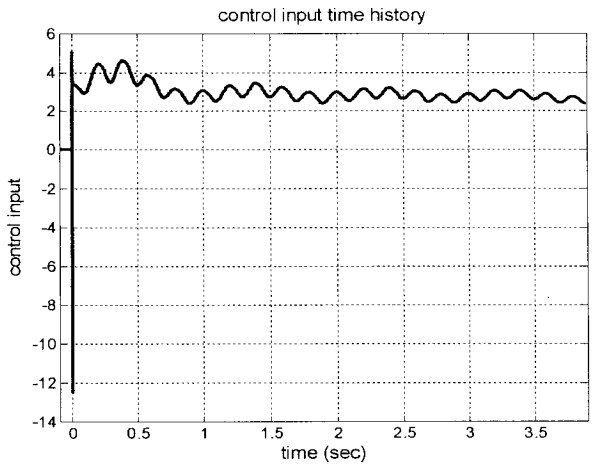

Figure 88. *u(t)* (overall control input) time history- SISO case controlled by combinatory control input

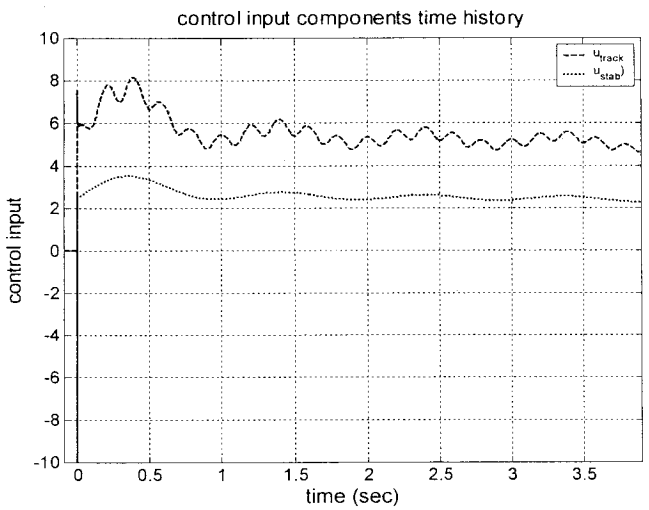

Figure 89. Control input components time history- SISO case controlled by combinatory control input

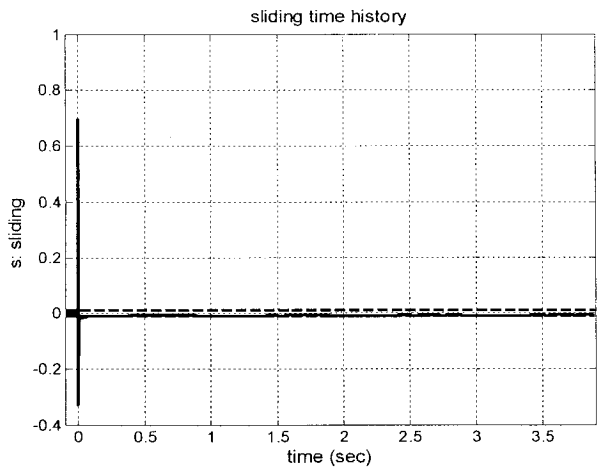

Figure 90. $s = \dot{\tilde{\varphi}} - \lambda\tilde{\varphi}$ (sliding) time history- SISO case controlled by combinatory control input

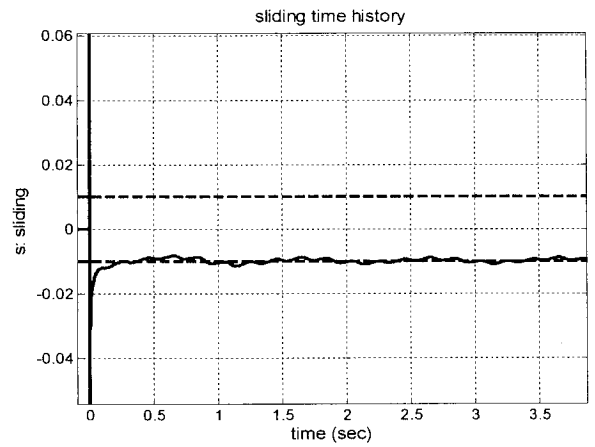

Figure 91. $s = \dot{\tilde{\varphi}} - \lambda\tilde{\varphi}$ (sliding) time history (zoomed in), showing the boundary layer- SISO case

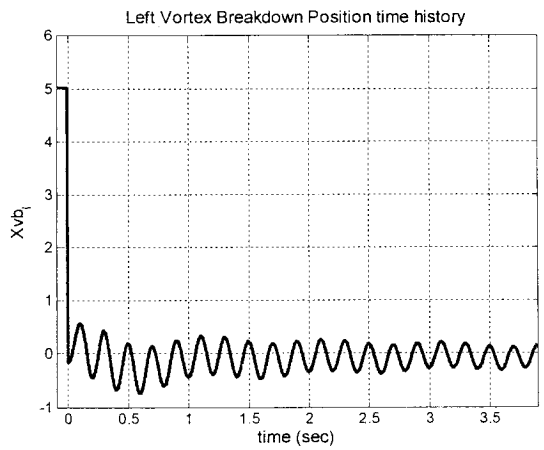

Figure 92. X_{vbl} time history- SISO case controlled by combinatory control input

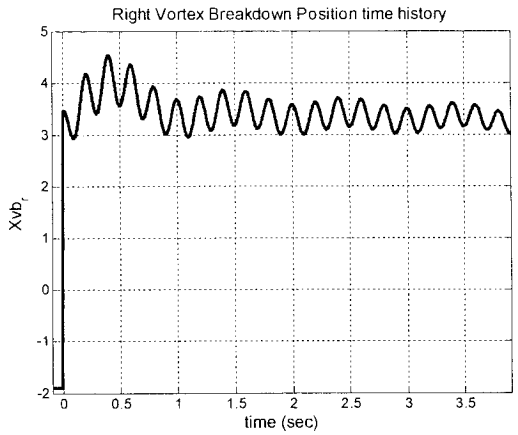

Figure 93. X_{vbr} time history- SISO case controlled by combinatory control input

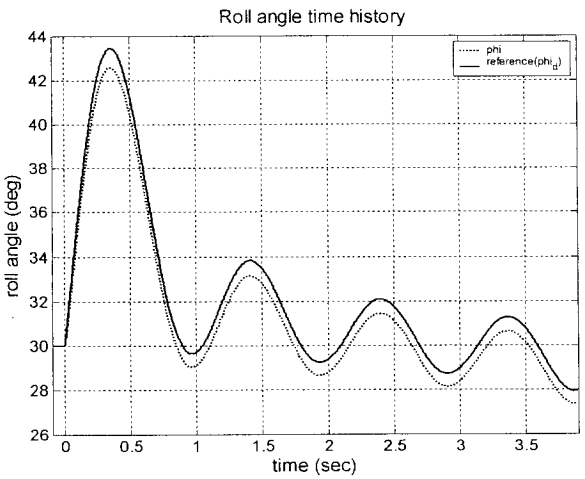

Figure 94. φ *and* φ_d time history - controlled by combinatory control input

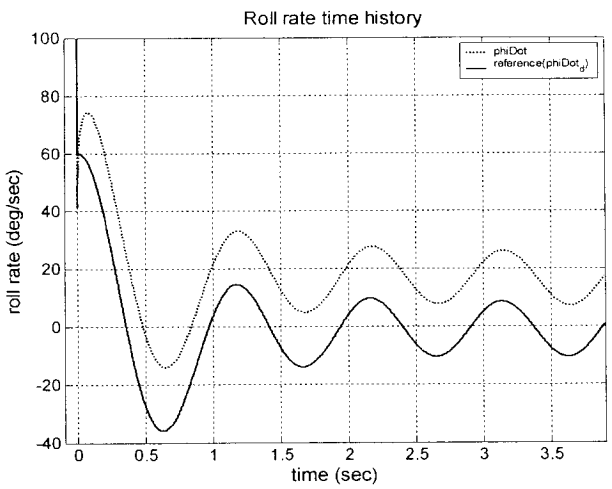

Figure 95. $\dot{\varphi}$ *and* $\dot{\varphi}_d$ time history - controlled by combinatory control input

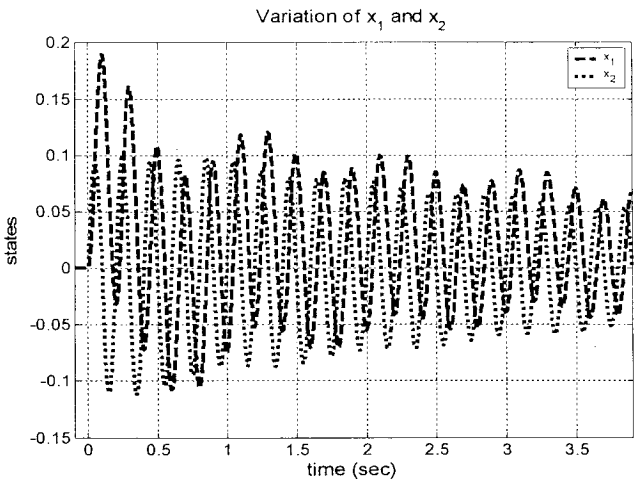

Figure 96. x_1 and x_2 time history- controlled by combinatory control input

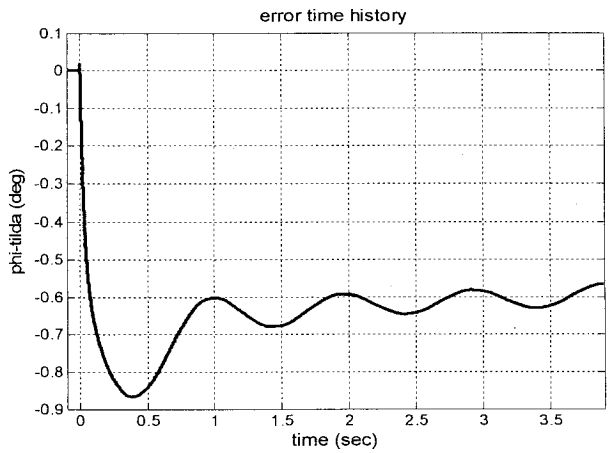

Figure 97. Error ($\tilde{\varphi} = \varphi - \varphi_d$) time history- controlled by combinatory control input

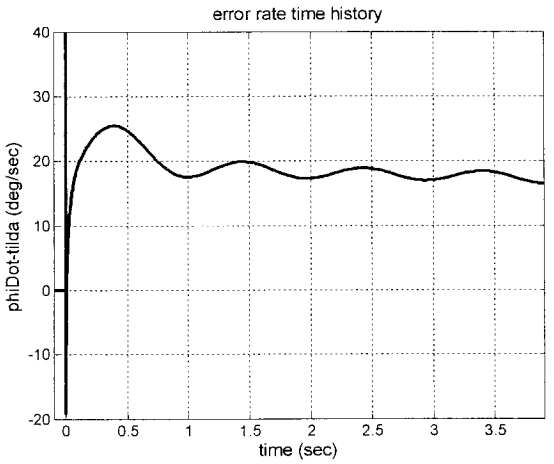

Figure 98. Error rate ($\dot{\tilde{\varphi}} = \dot{\varphi} - \dot{\varphi}_d$) time history- controlled by combinatory control input

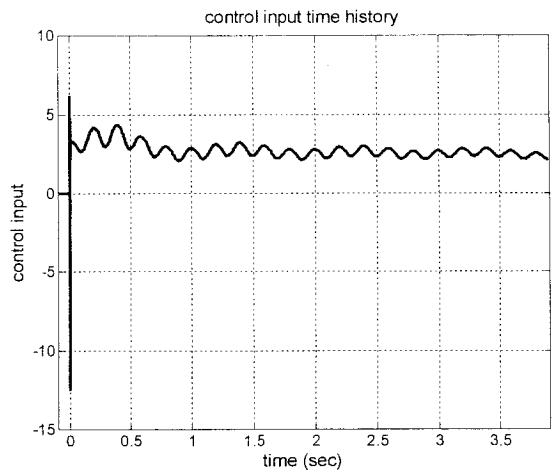

Figure 99. Overall control input ($u(t)$) time history- controlled by combinatory control input

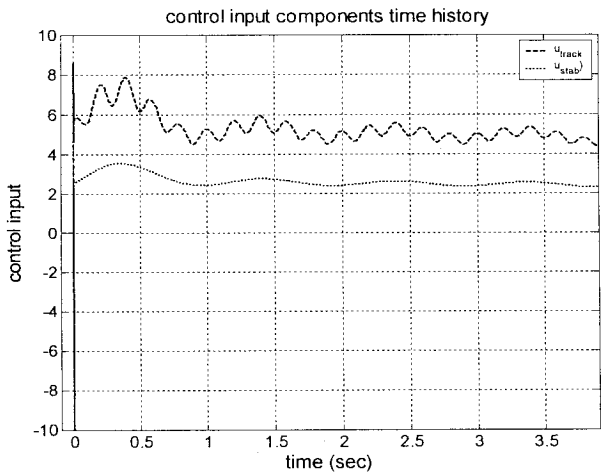

Figure 100. Control input components time history- controlled by combinatory control input

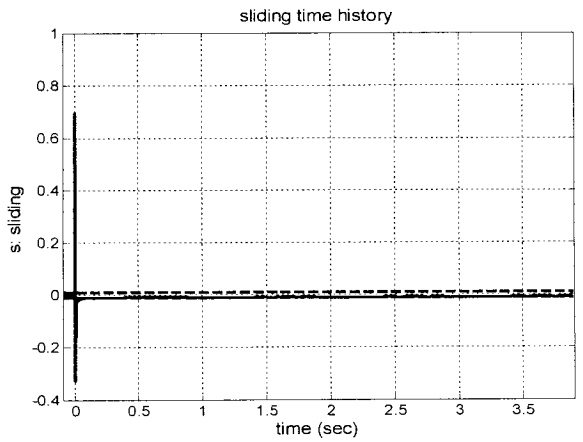

Figure 101. $s = \dot{\tilde{\varphi}} - \lambda\tilde{\varphi}$ (sliding) time history- controlled by combinatory control input

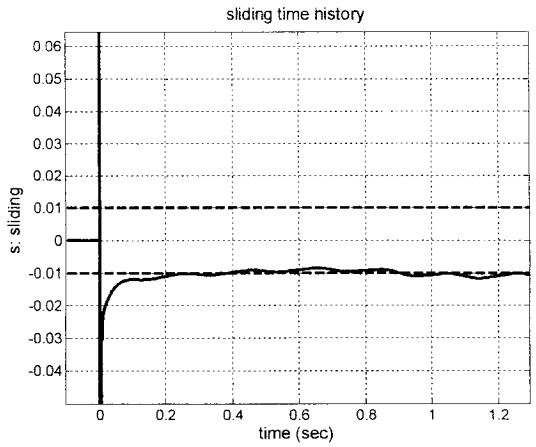

Figure 102. $s = \dot{\tilde{\varphi}} - \lambda\tilde{\varphi}$ (sliding) time history (zoomed in) , showing the boundary layer

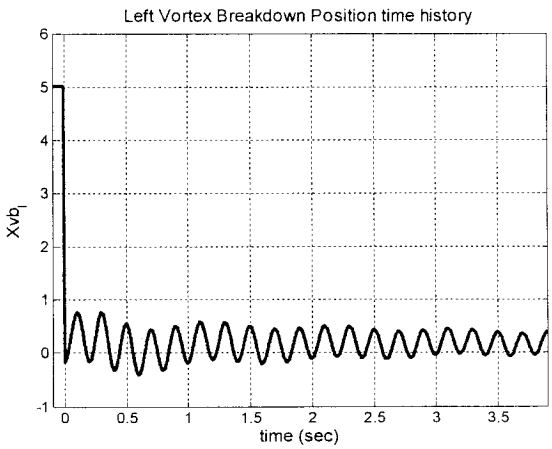

Figure 103. X_{vbl} time history with $u_2(t)$ control input- controlled by combinatory control input

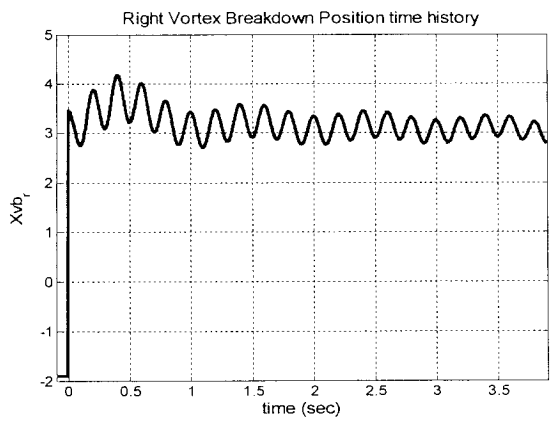

Figure 104. X_{vbr} time history with $u_3(t)$ control input- controlled by combinatory control input

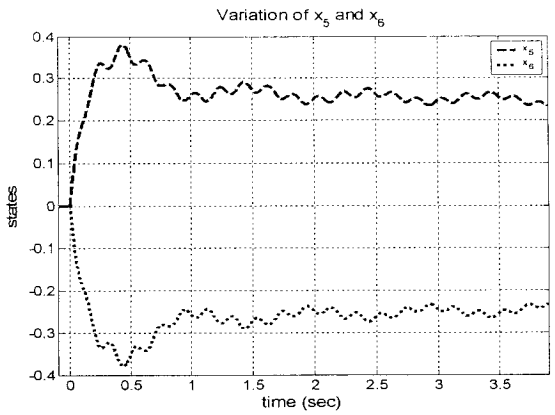

Figure 105. x_5 and x_6 time history- controlled by combinatory control input

5.8 Summary

In this chapter, a combinatory control strategy combined of a modified state feedback stabilizing controller, as the internal loop, and a robust adaptive sliding tracking controller has been proposed, to be applied to the vortex-coupled roll dynamics of delta wing subject to state delay. The first subcomponent renders the closed-loop system globally practically stable. The second one is a robust adaptive sliding tracking controller which utilizes a special gaussian RBF neural network for online estimation of rolling moment coefficient as the main uncertainty of the model. The RBF network designed for delta wing case is a four layer RBF neural network with two hidden layers, with left and right vortex breakdown positions as the input to the first hidden layer. The second hidden layer is a linear combination of the two sub-layers of the first hidden layer.

To show the ability of the proposed combinatory control structure we implement it to control the delta wing for following a complex reference trajectory, since delta wings are high performance aerial vehicles which are flying in high angle of attack flight condition with subsonic or supersonic speeds.

Implementing the proposed combinatory control structure (controller with internal loop) enhanced the tracking performance in comparison to the controller without internal loop.

Adding two more control inputs as a fraction of the first control input in the combinatory control structure (can be interpreted as perturbations in the vortex breakdown dynamics), i.e. choosing ρ_{vbl} and $\rho_{vbr} > 0$, enhanced the tracking controller performance in comparison with the case without perturbations, i.e. $\rho_{vbl} = \rho_{vbr} = 0$. The combinatory controller in both cases showed accurate tracking performance and fulfilled the related requirements, but the second one was better due to its better tracking performance and less control effort. Delta wing simulation study demonstrated good performance of the proposed combinatory control structure.

Heuristic design process and parameter selection methods have been proposed for easier implementation of tracking control (controller without internal loop) and combinatory control structure (controller with internal loop).

The presented approach can be extended to multi-input, multi-output model of the delta wing roll dynamics. More efficient control inputs also can be designed to be applied to left and right vortex breakdown locations.

6 . Conclusions and Future Work

6.1 Conclusions

In Chapter 3, a free-to-roll vortex based nonlinear retarded state-space modelling and simulation based on the work done in [10]-[11] has been proposed. The relationship among the vortex breakdown location, rolling moment coefficient and roll angle were described with state equations, which constitute a plant model in nonlinear state-space form enabling control synthesis for system with state delay. The proposed model was validated and verified with delta wing free-to-roll various experimental results. Three different methods were used for the approximation of the system uncertainty which was rolling moment coefficient ($C_l(\aleph)$). These methods are linear, nonlinear (5^{th} order polynomial) curve fitting and also Radial Basis Function Regularization Neural Networks (RBFNN). In the future, better parameter tuning is needed to increase the accuracy of the model, especially correlations for $C_l(\aleph)$. Other Neural networks (wavelet or MLP) can be utilized for this purpose. Model can be extended for the system with time-varying state delay.

In Chapter 4, the applicability of an existing robust adaptive feedback stabilizing control strategy for the fast vortex-coupled roll dynamics of delta wing subject to state delay in a high AOA flight condition has been shown. The controller renders the closed-loop system globally practically stable. Simulations demonstrated the applicability of the controller for the fast and high performance delta wing dynamics. The heuristic design

process and parameter selection methods have been proposed for easier implementation of this control scheme. This approach can be extended to multi-input, multi-output model of delta wing vortex-coupled roll dynamics with state delay.

In Chapter 5, a combinatory control strategy combined of a modified state feedback stabilizing controller, as the internal loop, and a robust adaptive sliding tracking controller has been proposed, to be applied to the vortex-coupled roll dynamics of delta wing subject to state delay. The first subcomponent renders the closed-loop system globally practically stable. The second one is a robust adaptive sliding tracking controller which utilizes a special gaussian RBF neural network for online estimation of rolling moment coefficient as the main uncertainty of the model. The RBF network designed for delta wing case is a four layer RBF neural network with two hidden layers, with left and right vortex breakdown positions as the input to the first hidden layer. The second hidden layer is a linear combination of the two sub-layers of the first hidden layer.

To show the ability of the proposed combinatory control structure we implement it to control the delta wing for following a complex reference trajectory, since delta wings are high performance aerial vehicles which are flying in high angle of attack flight condition with subsonic or supersonic speeds.

Implementing the proposed combinatory control structure (controller with internal loop) enhanced the tracking performance in comparison to the controller without internal loop. Adding two more control inputs as a fraction of the first control input in the combinatory control structure (can be interpreted as perturbations in the vortex breakdown dynamics), i.e. choosing ρ_{vbl} and $\rho_{vbr} > 0$, enhanced the tracking controller performance in comparison with the case without perturbations, i.e. $\rho_{vbl} = \rho_{vbr} = 0$. The

combinatory controller in both cases showed accurate tracking performance and fulfilled the related requirements, but the second one was better due to its better tracking performance and less control effort. Delta wing simulation study demonstrated good performance of the proposed combinatory control structure. The heuristic design process and parameter selection methods have been proposed for easier implementation of the tracking control (controller without internal loop) and the combined control structure (controller with internal loop). The presented approach can be extended to multi-input, multi-output model of the delta wing roll dynamics. More efficient control inputs also can be designed to be applied to left and right vortex breakdown locations.

6.2 Future Work

In this section, we state the possible future directions for the approaches proposed in this thesis. Future directions are as follows:

- Further analysis on the *stability* of the proposed combined control law.
- Analysis of the *internal dynamics (zero dynamics)* of the vortex-coupled delta wing system with combinatory control input.
- Developing control schemes for the *MIMO model* of vortex-coupled delta wing roll dynamics.
- Extending the developed control schemes for the model with *time-varying delay* in the states of the proposed model.
- Using *other neural networks*, i.e. wavelets and MLP, in modelling and also adaptive control of vortex-coupled delta wing roll dynamics.
- Extending artificial neural network (ANN) control to handle unmodelled dynamics and *multiple equilibria.*

- Integrating outer-loop flow control schemes with *inner-loop* shape memory alloy (SMA) actuators.
- *Experimental implementation and verification* of closed loop system with the proposed controllers.

7 . References

[1] Delta Wings, U.S. Centennials of Flight Commission, Centennial of Flight, http://www.centennialofflight.gov/essay/Evolution_of_Technology/delta_wing/Tech10.htm

[2] Filippone, A., Advanced Topics in Aerodynamics, Aerodyn, http://aerodyn.org/Wings/delta.html

[3] Chambers, J. B., Grafton, S. B., *Aerodynamic Characteristics of Airplanes at High Angles of Attack*, NASA TM 74097, December 1977.

[4] Huang, A., Folk, C., Silva, C., Christensen, B., Chen, Y., Ho, C. M., Jiang, F., Grosjean, C., Tai, Y.C., Lee, G.B., Chen, M., Newbern, S., "Application of MEMS Devices to Delta Wing Aircraft: From Concept Development to Transonic Flight Test", AIAA Paper 2001-0124, Jan. 2001.

[5] Sundararajan, N., Saratchanadran, P., Li, Y., *Fully Tuned Radial Basis Function Neural Networks for Flight Control*, Kluwer Academic Publishers, Boston, 2002.

[6] Agarwal, M., "A Systematic Classification of Neural-Network-Based Control", IEEE Control Systems Magazine, Vol.17, No.2, April, 1997, pp 75-93.

[7] Richard, J. P., "Time-Delay Systems: an Overview of Some Recent Advances and Open Problems", Automatica, Vol. 39, 2003, pp 1667-1694.

[8] Stepan, G., *Retarded Dynamical Systems: Stability and Characteristic Functions*, Pitman Research Notes in Mathematics Series, Longman Scientific & Technical, Essex, UK, 1989.

[9] Lakshmikantham, V., Leela, S., Martynyuk, A. A., *Practical Stability of Nonlinear Systems*, World Scientific Publishing, Singapore, 1990.

[10] Huang, X. Z., "Non-Linear Indicial Response and Internal State-Space (NIRISS) Representation and Its Application on Delta Wing Configurations", RTO Technical Report, RTO-TR-047, 2003.

[11] Huang, X. Z., Lou, H. Y., Hanff, E. S., "Non-Linear Indicial Response and Internal State-Space Representation for Free-to-Roll Trajectory Prediction of a 65^{o} Delta Wing at High Incidence", AIAA Paper 2002-4713, 2002.

[12] Huang, X. Z., Sun, Y.Z., Hanff, E.S., "Circulation Criterion to Predict Leading-Edge Vortex Breakdown Over Delta Wings", AIAA Paper 1997-2265, 1997.

[13] Huang, X. Z., Hanff, E. S., "Prediction of Normal Force on a Delta Wing Rolling at High Incidence", AIAA paper 93-3686, Aug. 1993.

[14] Chaderjian N. M., Schiff B., "Numerical Simulation of forced and Free-to-Roll Delta Wing Motions", *Journal of Aircraft*, Vol. 33, No. 1, 1996.

[15] Greenwell, D. I., "Simple Engineering Model for Delta-Wing Vortex Breakdown", *Journal of Aircraft*, Vol. 40, No. 2, 2003.

[16] Zamarreno, J. M., Vega, P., "State Space Neural Network, Properties and Application", *Neural Networks*, Vol. 11, 1998.

[17] Efe, M. O., Kaynak, O., "A Comparative Study of Neural Network Structures in Identification of Nonlinear Systems", *Mechatronics*, No. 9, 1999, pp 287-300

[18] Xu, J., Ho, D. W. C., "Adaptive Wavelet Networks for Nonlinear System Identification", Proceedings of the American Control Conference, June 1999.

[19] Yan, L., Sundararajan, N., Saratchandran, P., "Nonlinear System Identification Using Lyapunov Based Fully Tuned Dynamic RBF Networks", *Neural Processing Letters*, No. 12, 2000, pp 291-303.

[20] Ahmad, S. M., Shaheed, M. H., Chipperfield, A. J., Tokhi, M. O., "Non-linear Modelling of a One-Degree-of-Freedom Twin-Rotor Multi-Input Multi-Output System Using Radial Basis Function Networks", *Proc Instn Mech Engrs, Part G: J Aerospace Engineering*, Vol. 216, Sep. 2002.

[21] Reisenthel, P. H., "Development of a Nonlinear Indicial Model for Maneuvering Fighter Aircraft", AIAA 96-0896, 1996.

[22] Reisenthel, P. H., "Application of Nonlinear Indicial Modeling to the Prediction of a Dynamically Stalling Wing", AIAA 96-2493, 1996.

[23] Reisenthel, P. H., "Development of a Nonlinear Indicial Model Using Response Functions Generated by a Neural Network", AIAA 97-0337, 1997.

[24] Reisenthel, P. H., Bettencourt, M. T., "A Nonlinear Indicial Prediction Tool for Unsteady Aerodynamic Modeling", AIAA 98-4350, 1998.

[25] Reisenthel, P. H., Xie, W., Gursul, I., Bettencourt, M. T., "An Analysis of Fin Motion Induced Vortex Breakdown", AIAA 99-0136, 1999.

[26] Reisenthel, P. H., Bettencourt, M. T., "Data-Based Aerodynamic Modeling Using Nonlinear Indicial Theory", AIAA 99-0763, 1999.

[27] Reisenthel, P. H., Bettencourt, M. T., "Extraction of Nonlinear Indicial and Critical State Response from Experimental Data", AIAA 99-0764, 1999.

[28] Pamadi, B. N., Murphy, P. C., Klein, V., Brandon, J. M., "Prediction of Unsteady Aerodynamic Coefficients at High Angles of Attack", NASA Center for AeroSpace Information (CASI), AIAA Paper 2001-4077 , Aug. 2001.

[29] Reisenthel, P. H., "Prediction of Unsteady Aerodynamic Forces via Nonlinear Kernel Identification", CEAS / AIAA / ICASE / NASA Langley International Forum on Aeroelasticity and Structural Dynamics, Williamsburg, VA, June 22-25, 1999.

[30] Goman, M., Khrabrov, A., "State-Space Representation of Aerodynamic Characteristics at High Angles of Attack", *Journal of Aircraft*, Vol. 31, No. 5, Sep.-Oct. 1994, pp 1109-1115.

[31] Smith, T. A., Hakanson, J. W., , Nair, S. S., Yurkovich, R. N., "State-Space Model Generation for Flexible Aircraft", *Journal of Aircraft*, Vol. 41, No. 6, Nov.-Dec. 2004, pp 1473-1481.

[32] Juang, J. N., Kholodar, D., Dowell, E. H., "System Identification of a Vortex Lattice Aerodynamic Model", NASA/TM-2001-211229, Oct. 2001.

[33] Murphy, P. C., Klein, V., "Estimation of Aircraft Unsteady Aerodynamic Parameters from Dynamic Wind Tunnel Testing", AIAA Paper 2001-4016, 2001.

[34] Klein, V., Noderer, K. D., "Modeling of Aircraft Unsteady Aerodynamic Characteristics, Part 1 - Postulated Models", NASA Technical Memorandum 109120, May 1994.

[35] Tobak, M., Chapman, G. T., Schiff, L. B., "Mathematical Modeling of the Aerodynamic Characteristics in Flight Dynamics", NASA-TM-85880, 1984.

[36] Tobak, M., Schiff, L. B., "Aerodynamic Mathematical Modeling - Basic Concepts", NASA Center for AeroSpace Information (CASI), 1981.

[37] Schiff, L. B., Tobak, M., Malcolm, G. N., "Mathematical Modeling of the Aerodynamics of High-Angle-of-Attack Maneuvers", AIAA Paper 80-1583, Atmospheric Flight Mechanics Conference, Danvers, MA, Aug. 1980.

[38] Jenkins, J. E., Myatt, J. H., , Hanff, E. S., "Body-Axis Rolling Motion Critical States of a 65-Degree Delta Wing", *Journal of Aircraft*, Vol. 33, No. 2, Mar.-Apr. 1996, pp 268-278.

[39] Grismer D. S., Jenkins, J. E., "Critical States Transients for a Rolling 65-Degree Delta Wing", *Journal of Aircraft*, Vol. 34, No. 3, May-Jun. 1997, pp 380-386.

[40] Pakmehr, M., Gordon, B. W., and Rabbath, C. A., "Control-Oriented Modeling and Identification of Delta Wing Vortex-Coupled Roll Dynamics", Proceedings of the American Control Conference 2005 (ACC05), Portland, Oregon, June 2005, pp 1521-1526.

[41] Ericsson, L. S., Hanff, E. S., "Further Analysis of High-Rate Rolling Experiments of a 65-Deg Delta Wing", *Journal of Aircraft*, Vol. 31, No. 6, Nov.-Dec. 1994, pp 1350-1357.

[42] Lee, G. B., Shih, C., Tai, Y. C., Tsao, T., Liu, C., Huang, A., Ho, C. M., "Robust Vortex Control of a Delta Wing by Distributed Microelectromechanical-Systems Actuators", *Journal of Aircraft*, Vol. 37, No. 4, Jul.-Aug. 2000, pp 697-705.

[43] Lechevin, N., Rabbath, C. A., "Quasipassivity-based Robust Nonlinear Control synthesis for Flap Positioning Using Shape Memory Alloy Micro-Actuators",

Proceedings of the American Control Conference 2005 (ACC05), Portland, Oregon, June 8-10, 2005, pp 3019 - 3024.

[44] Eykhoff, P., *System Identification, Parameter and State Estimation*, John Wiley & Sons Ltd., New York, 1974.

[45] Ericsson, L. S., "Difficulties in Predicting Vortex Breakdown effect on a Rolling Delta Wing", *Journal of Aircraft*, Vol. 33, No. 3, May-Jun. 1996, pp 380-386.

[46] Haykin, S., *Neural Networks a Comprehensive Foundation,* Second Edition, Prentice Hall, Upper Saddle River, NJ, 1999.

[47] Huang, X. Z., "Experimental Investigation of Leading-Edge Vortex Control via Microactuators", presentation in 'Missile Flight Control using Micro-actuated Flow Effectors' meeting, DRDC Valcartier TN 2004-066, May 2004.

[48] Rule, J. A., Richard, R. E., Clark, R. L., "Design of an Aeroelastic Delta Wing Model for Active Flutter Control", *Journal of Guidance, Control and Dynamics*, Vol. 24, No. 5, Sep.–Oct. 2001, pp 918-924.

[49] Araujo, A. D., Singh, S. N., "Variable Structure Adaptive Control of Wing-Rock Motion of Slender Delta Wings", *Journal of Guidance, Control and Dynamics*, Vol. 21, No. 2, March-April 1998, pp 251-256.

[50] Monahemi, M. M., Krstic, M., "Control of Wing Rock Motion Using Adaptive Feedback Linearization", *Journal of Guidance, Control and Dynamics*, Vol. 19, No. 4, Jul.-Aug. 1996, pp 905-912.

[51] Singh, S. N., Yim, W., Wells, W. R., "Direct Adaptive and Neural Control of Wing-Rock Motion of Slender Delta Wings", *Journal of Guidance, Control and Dynamics*, Vol. 18, No. 1, Jan.-Feb. 1995, pp 25-30.

[52] Shue, S. P., Agarwal, R. K., Shi, P., "Nonlinear H $_{infinity}$ Method for Control of Wing Rock Motions", *Journal of Guidance, Control and Dynamics*, Vol. 23, No. 1, Jan. 2000, pp 60-68.

[53] Luo, J., Lan, C. E., "Control of Wing-Rock Motion of Slender Delta Wings", *Journal of Guidance, Control and Dynamics*, Vol. 16, No. 2, Mar.-Apr. 1993, pp 225-231.

[54] Crassidis, J. L., "Robust Control of Nonlinear Systems Using Model-Error Control Synthesis", *Journal of Guidance, Control and Dynamics*, Vol. 22, No. 4, 1999, pp 595-601.

[55] Tarn, J. H., and Hsu, F. Y., "Fuzzy Control of Wing Rock for Slender Delta Wings", IEEE Region 10 Conference, Tencon, IEEE paper 0-7803-0849-2/92, Nov. 1992, pp 715-719.

[56] Liu, Z. L., Su, C. Y., and Svoboda, J., "Control of Wing Rock Phenomenon with a Variable Universe Fuzzy Controller", Proceeding of the 2004 American Control Conference (ACC 04), June 30 - July 2, 2004, pp 1719-1724.

[57] Lin, C. M., and Hsu, C. F., "Recurrent Neural Network Adaptive Control of Wing-Rock Motion", *Journal of Guidance, Control and Dynamics*, Vol. 25, No. 6, 2002, pp 1163-1165.

[58] Kooi, S. B. L., "Dynamic Recurrent Neural Networks for Stable Adaptive Control of Wing Rock Motion", Ph.D. Dissertation, Mechanical Engineering Department, Concordia University, Montreal, Canada, 1999.

[59] Xin, M., Balakrishnan, S. N., "Control of the Wing Rock Motion using a New Suboptimal Control Method", *Proc. Instn Mech. Engrs Part G: J. Aerospace Engineering*, Vol. 218, May 2004, pp 257-266.

[60] Pakmehr, M., Gordon, B. W., Rabbath, C. A., "Robust Adaptive Control of Delta Wing Vortex-Coupled Roll Dynamics Using RBF Neural Networks", Proceedings of the 2005 IEEE Conference on Control Applications (CCA05), Toronto, Canada, Aug. 2005, pp 1039-1043.

[61] Kolmanovskii, V. B., Niculescu, S.-I., Gu, K., "Delay effects on stability: a survey", Proceedings of the 38th IEEE Conference on Decision and Control, Volume 2, Dec. 1999, pp 1993-1998.

[62] Pepe, P., "Adaptive Output Tracking for a Class of Nonlinear Time-Delay Systems", International Journal of Adaptive Control and Signal Processing, Vol. 18, April 2004, pp 489-503.

[63] Germani, A., Manes, C., Pepe, P., "Input-Output Linearization with Delay Cancellation for Nonlinear Delay Systems: the Problem of the Internal Stability", International Journal of Robust and Nonlinear Control, Vol. 13, 2003, pp 909-937.

[64] Couaisbaut, F., Dambrine, M., Richard, J. P., "Robust Control of Delay Systems: a Sliding Mode Control Design via LMI", Systems & Control Letters, Vol. 46, July 2002, pp 219-230.

[65] Pakmehr, M., Gordon, B. W., Rabbath, C. A., "Robust Adaptive Tracking Control of Delta Wing Vortex-Coupled Roll Dynamics Subject to Delay", Accepted to be presented at the 2005 ASME International Mechanical Engineering Congress and Exposition, Orlando, Florida USA, November 5-11, 2005 (to be published).

[66] Foda, S. G., Mahmoud, M. S., "Adaptive Stabilization of Delay Differential Systems with Unknown Uncertainty Bounds", *International Journal of Control*, Vol. 71, No. 2, 1998, pp 259-275.

[67] Khalil, H., *Nonlinear Systems*, 3rd edition, Prentice Hall, Upper Saddle River, New Jersey, 2002.

[68] Ben-Israel, A., Grenville, T. N. E., *Generalized Inverses: Theory and Applications*, 2nd edition, Springer, New York, 2003.

[69] Scherer, C., Weiland, S., Lecture Notes DISC Course on Linear Matrix Inequalities (LMI) in Control, Version 2, Apr. 1999, pp 48, http://www.dcsc.tudelft.nl/~cscherer/2416/lmi.pdf

[70] Li, Y., Sundararajan N., and Saratchandran P., "Neuro-Controller Design for Nonlinear Fighter Aircraft Maneuver Using Fully Tuned RBF Networks", *Automatica*, Vol. 37, 2001, pp 1293-1301.

[71] Gonzalez, A. E., "Adaptive Control Scheme for Plants with Time-Varying Structure Using On-Line Parameter Estimation", PhD Thesis, Electrical Engineering Department, University of Dayton, Dayton, Ohio, Dec. 2003.

[72] Eberhardt, R. L., and Ward, D. G., "Indirect Adaptive Flight Control System Interactions", *Int. J. Robust Nonlinear Control*, Vol. 9, 1999, pp 1013-103.

[73] Wise, K. A., Brinker, J. S., Calise, A. J., Enns, D. F., Elgersma, M. R., and Voulgaris, P., "Direct Adaptive Reconfigurable Flight Control for a Tailless Advanced Fighter Aircraft", *Int. J. Robust Nonlinear Control*, Vol. 9, 1999, pp 999-1012.

[74] Calise, A. J., Johnson, E. N., Johnson, M. D., and Corban, J. E., "Applications of Adaptive Neural-Network Control to Unmanned Aerial Vehicles", AIAA/ICAS International Air and Space Symposium and Exposition: The Next 100 Years, Dayton, OH, July 2003.

[75] Slotine, J. -J. E., Li, W., *Applied Nonlinear Control*, Prentice Hall, Englewood Cliffs, New jersey, 1991.

[76] Sanner, R. M., Slotine, J. -J. E., "Gaussian Networks for Direct Adaptive Control", *IEEE Transactions on Neural Networks*, Vol. 3, No. 6, Nov. 1992, pp 837-863.

[77] Slotine, J. -J. E., Coetsee, J. A., "Adaptive Sliding Controller Synthesis for Nonlinear Systems", *International Journal of Control*, Vol. 43, No. 6, 1986, pp 1631-1651.

Appendices

7.1 APPENDIX A

Definitions and properties from Ref. [66] which are used in Chapters 4 and 5 are summarized below:

Definition 1: The solutions $x(t_0,\nu)(t)$ of equation (4-19), are said to be uniformly ultimately bounded if there exist $\sigma > 0$ and $T = T(\sigma,\delta) > 0$, independent of t, such that $x_t(t_0,\nu) \le \sigma$ for all $t \ge t_0 + T(\sigma,\delta)$ $\forall \nu \in c_1, |\nu| \le \delta$.

Definition 2: The retarded system in equation (4-19), is said to be *globally practically stabilizable* with respect to the closed ball $G(\rho_m)$ if and only if given any $\rho_m \in (0,\infty)$, there exists a feedback control $\Psi(.): c_1 \times \Re \to \Re^m$ for which the following properties hold:

Property 1: Given $t_0 \in \Re$ and $\nu(t_0) \in c_1$ the closed-loop system

$$x(t) = f(x_t(t), \Psi(x_t,t), t)$$

has a solution $x(t_0,\nu)(t) \in \Re^n$ for all $\nu(t_0) \in c_1, t > t_0$.

Property 2: Given $l \in (0,\infty)$ there exist $\rho \in (0,\infty)$ such that for all solutions $x(t_0,\nu)(t) \in \Re^n$, $\nu(t_0) \in c_1, t > t_0$,

$$\|\nu(t_0)\| \le l \Rightarrow \|x(t)\| \le \rho(l), \quad \forall t \in [t_0,t)$$

Property 3: Every solution $x(t_0,v)(t) \in \Re^n$, $v(t_0) \in c_1, t > t_0$, can be continued over $[t_0,\infty)$.

Property 4: Given any $\rho_M > \rho_m$, there exists a $\sigma(\rho_M) > 0$ such that for every solutions $x(t_0,v)(t) \in \Re^n$, $v(t_0) \in c_1, t > t_0$,

$$\|v(t_0)\| \le l \Rightarrow x(t) \in G(\rho_M), \quad \forall t \ge t_0 + T(\rho_M, l)$$

Property 5: Given any $\rho_M > \rho_m$, there exists a $\sigma(\rho_M) > 0$ such that for every solutions $x(t_0,v)(t) \in \Re^n$, $v(t_0) \in c_1, t > t_0$,

$$v(t_0) \in G(\sigma(\rho_M)) \Rightarrow x(t) \in G(\rho_M), \quad \forall t \ge t_0$$

7.2 APPENDIX B

Theories and proofs which are used in Chapters 4 and 5 are as follows:

Theorem 1 [66]: Let $q_1 > 1$ be a constant scalar. Assume that there exist a continuously differentiable function $V_c(x,t): \Re^n \times \Re \to \Re_+$ and strictly increasing continuous functions $\gamma_i(.): \Re^+ \to \Re^+, i = 1,2,3$, vanishing identically at the origin, i.e. class κ_∞ functions [67], such that

(1) $\lim_{\|x\| \to \infty} \gamma_i(\|x\|) = \infty, \quad i = 1,2,3$

$$\gamma_1(\|x\|) \le V(x,t) \le \gamma_2(\|x\|), \quad \forall (x,t) \in \Re^n \times \Re \tag{1}$$

(2) There is a scalar $q_2 \ge 1/q_1$ such that

$$\overline{V}_t = \sup_{\theta \in [-\tau, 0]} V[t+\theta, x(t+\theta)] < q_1 V[t, x(t)] \tag{2}$$

At any $t \geq t_0$ implies

$$\bar{x}_t = \sup_{\theta \in [-\eta, 0]} \|x(t+\theta)\| < q_1 q_2 \|x(t)\| < \gamma_1^{-1}\{q_1 \gamma_2(\|x(t)\|)\} \tag{3}$$

(3) The derivative of the Lyapunov function $\dot{V}(x,t): \Re^n \times \Re \to \Re$ along the trajectories of the retarded uncontrolled system satisfies

$$\dot{V}(x,t) \leq -\gamma_3(\|x\|) \tag{4}$$

whenever

$$\bar{x}_t = \sup_{\theta \in [-\eta, 0]} \|x(t+\theta)\| < \rho \|x(t)\|, \quad \rho = q_1 q_2 \geq 1; \quad t \geq t_0 \tag{5}$$

Then the zero solution of equation (4-19) is uniformly asymptotically stable.

Proof of Theorem 2:

$u_\rho(.)$, which is continuous, quasi-bounded and locally Lipschitz is a unique solution of the system [66]:

$$\begin{aligned} &\dot{x}(t) = A_0 x(t) + D_0 x(t-\eta) + B_0[u_\rho(t) + L(x, \aleph, t)] \\ &x_{t_0}(\theta) = \nu(\theta); \quad \theta \in [-\eta, 0] \end{aligned} \tag{6}$$

The following Lyapunov function candidate ($V_0(.): \Re^n \times \Re_+ \to \Re_+$) has been presented:

$$V_0(x,t) = x^T(t) P_0 x(t) \tag{7}$$

Considering the stabilization of the nominal free system

$$\dot{x} = A_0 x(t) + D_0 x(t-\eta); \; x_{t_0}(\theta) = \nu(\theta); \; \theta \in [-\eta, 0] \tag{8}$$

The Lyapunov derivative $\dot{V}_0(.)$ along the solutions of equation (8), satisfies

$$\dot{V}_0(x,t) = x^T(t)(P_0A_0 + A_0^T P_0)x(t) + 2x^T(t)P_0D_0x(t-\eta) \tag{9}$$

which has been shown in [66] that

$$\dot{V}_0(x,t) \le -\lambda_{\min}(Q_0)\rho_1\|x\|^2 \tag{10}$$

where $\rho_1 \in (0,1)$. This guarantees the desired uniform asymptotic stability of the nominal uncontrolled system.

Now, for a given $\rho_m > 0$, the Lyapunov derivative for the system in equation (6) satisfies [66]

$$\dot{V}_{stab}(x,t) = \dot{V}_0(x,t) + 2x^T(t)P_0B_0u_\rho + 2x^T(t)P_0B_0L \tag{11}$$

It has been shown in [66], that $\dot{V}_{stab}(x,t) \le 0$, and hence using uniform boundedness property, Property 5 will be established.

Proof of Theorem 3:

Consider the composite Lyapunov function candidate $V_c(.):\Re^n \times \Re \times \Re_+ \to \Re_+$:

$$\begin{aligned} V_c(x,\mu_d,t) &\hat{=} V_0(x,t) + V_\mu(\mu_d,t) \\ &= x^T(t)P_0x(t) + (\mu_d(t) + \hat{\mu}_0)^2 \end{aligned} \tag{12}$$

Define $\tilde{z} = [x^T(t), \mu_d(t) - \hat{\mu}_0]^T$ and choose

$\gamma_1(\|\tilde{z}\|) = \min\left\{[\lambda_{\min}(P_0),1]\|\tilde{z}\|^T\right\}, \gamma_2(\|\tilde{z}\|) = \min\left\{[\lambda_{\max}(P_0),1]\|\tilde{z}\|^T\right\}$. So that $V_c(x,\mu_d,t)$ satisfies Theorem 1.

For a given $\rho_m > 0$ and a realization of $\sigma \in \Gamma$, the Lyapunov derivative $V_c(.):\Re^n \times \Re \times \Re_+ \to \Re_+$ for the system described by the equation (4-33), is given by

$$\dot{V}_c(x,\mu_d,t) = 2x^T(t)P_0\dot{x}(t) + 2(\mu_d(t) - \mu_0(t))\dot{\mu}_d(t) \tag{13}$$

Using equations (4-31), (4-32), and (22) presented in [66], it can be shown that

$$\begin{aligned} u_\rho^d(t) - u_\rho(t) &= -(\mu_d - \hat{\mu}_0)H_0 y(t) \\ &= -(\mu_d - \hat{\mu}_0)H_0[C_0 x] \\ \|H_0 y\| &\le \delta_0 \|x\| \end{aligned} \tag{14}$$

where $\delta_0 \triangleq \|B_0^T P_0\|$

Using equations (14) with the aid of Theorem 2, algebraic manipulation of equation (13) leads to

$$\dot{V}_c(x,\mu_d,t) \le -\Phi^T \Omega \Phi + \Psi^T \Phi + \Gamma \tag{15}$$

where $\Phi \triangleq \left[\|B_0^T P_0\|, \|\mu_d - \hat{\mu}_0\|\right]^T$, $\Omega \triangleq \begin{bmatrix} (1-\Delta)\lambda_{\min}(Q_0) & 0 \\ 0 & g \end{bmatrix}$ and $\Psi \triangleq [0 \;\; 2\hat{\mu}_0 g]$, since $(1-\Delta)\lambda_{\min}(Q_0) > 0$, choosing $g > 0$, guarantees that $\Omega > 0$. It directly follows that $\dot{V}_c(x,\mu_d,t)$ is negative definite for all $(x,\mu_d,t) \in \Re^n \times \Re \times \Re_+$ such that

$$\lambda_{\min}(\Omega)\|\Phi\|^2 - 2g\hat{\mu}_0\delta_0\|\Phi\| - \Gamma > 0 \tag{16}$$

Thus the uniform boundedness in property 2 is satisfied by selecting

$$\rho(l) = \begin{cases} \sqrt{\alpha_2/\alpha_1\Lambda_d} & \text{if } l \le \Lambda_d \\ \sqrt{\alpha_2/\alpha_1 l} & \text{if } l > \Lambda_d \end{cases} \tag{17}$$

where $\alpha_1 \triangleq g\hat{\mu}_d / \lambda_{\min}(\Omega)$, $\alpha_2 \triangleq \Gamma / \lambda_{\min}(\Omega)$ and $\Lambda_d \triangleq \alpha_1\sqrt{\alpha_1^2 + \alpha_2}$. The remaining part of the proof is very similar to that of Theorem 2 presented in [66].